NTNU

Norwegian University of
Science and Technology

Application of Optical Current Transformers in Digital Substations

Ingvill Urdal Rian

Master of Energy and Environmental Engineering
Submission date: June 2018
Supervisor: Hans Kristian Høidalen, IEL
Co-supervisor: Magnus Kolgrov, Statnett SF
Rannveig Løken, Statnett SF

Norwegian University of Science and Technology
Department of Electric Power Engineering

Problem Description

Digitalization of substations will substantially reduce the required size of buildings and the amount of copper wiring. The required space is reduced because digital relays can contain more functions and the copper wiring is replaced by a process bus where a fiber optical ring contains all signals. The engineering time can also be reduced, and faster upgrade and renewal could be possible with more plug & play capabilities of the relays or intelligent electronic devices (IEDs). Digital substations also open up for the application of non-conventional instrument transformers (NCITs), such as optical current transformers (OCTs), were current and voltages are measured with other principles than traditional magnetic coupling. In order to integrate conventional instrument transformers into digital substations, stand-alone merging units (SAMUs) are required, which digitize the currents and voltages according to the IEC 61850 standard.

The following tasks are given:

- Describe a digital substation environment and the involved components.
- Study the technology used in optical current transformers and discuss error mechanisms, accuracy and specifications.
- Discuss benefits and drawbacks of applying optical current transformers in digital substations compared with conventional technologies.
- Evaluate whether optical current transformers are suitable for application in digital transmission substations.
- Study the response of the stand-alone merging unit SAM600 in the lab in terms of steady state behavior and transient capabilities. Study possible implications on relay response.

Preface

This thesis finalizes my master's degree in Energy and Environmental Engineering at the Norwegian University of Science and Technology (NTNU), Department of Electric Power Engineering. The master's thesis is a continuation of a specialization project on digital substations, which was carried out in the fall semester of 2017. The master's thesis has been realized in cooperation with Statnett and with the guidance of Professor Hans Kristian Høidalen at NTNU. The rapport is the result of work which was conducted during the spring semester of 2018.

Trondheim, 22 Juni 2017

Ingvill Urdal Rian

Acknowledgement

I would like to thank the following persons:

- My supervisor at NTNU, Hans Kristian Høidalen, for good guidance during the work on this master's thesis.
- My co-supervisors at Statnett, Magnus Kolgrov and Rannveig Løken, for their co-operation and for answering questions.
- PhD students, Maciej Grebla and Jaya Raghavendra Arun Yellajosula, for helping with the practical work and for giving good advice during the work process.

Abstract

In this master's thesis optical current transformers are studied in order to evaluate whether such sensors are suitable for application in digital transmission substations. The analysis includes a discussion of benefits and drawbacks and an evaluation of performance, maturity and fulfillment of substation application requirements as well as the digital substation concept. Experimental testing of a stand-alone merging unit is also performed with the objective of investigating its performance and comparing it to the performance of a conventional analog acquisition system. Potential impacts on the performance of transformer differential protection is also investigated.

The laboratory tests show that the stand-alone merging unit has a steady state performance which is comparable to that of a conventional analog acquisition system and a significantly better transient performance. As a result of the differing transient performances, fundamental frequency differential currents arise when these two technologies are combined in a hybrid mode configuration of a transformer differential protection. The resulting fundamental frequency differential currents are not big enough to affect the performance of the transformer differential protection in the tested cases.

Optical current transformers offer many benefits compared to conventional current transformers. Some of these are improved safety, reduced environmental impact, reduced need for maintenance and improvements in steady state and transient performance. The low weight facilitates integration with other primary equipment, which allows space to be saved in the substation yard. The combination of optical current transformers and a process bus makes the design of digital substations flexible and facilitates cost reductions.

The standards which apply to non-conventional instrument transformers and digital substations often leave some room for interpretation. This may lead to lack of interoperability between devices from different vendors in a digital substation. Competence building will also be required, and digital substations may be expected to become more vulnerable than the present day conventional substations due to outdoor placement of electronics and stringent time synchronization requirements.

It is concluded that optical current transformers seems to be suitable for application in digital transmission substations. However, there are several signs that the products and solutions are not completely mature yet. There are several investigations to be made, questions to be answered and issues to be solved before a migration from the present day conventional substations with conventional current transformers to digital substations with optical current transformers can take place.

Sammendrag

I denne masteroppgaven studeres optiske transformatorer for å vurdere hvorvidt slike sensorer egner seg til bruk i digitale transmisjonsstasjoner. Analysen omfatter en diskusjon av fordeler og ulemper og en evaluering av oppførsel, modenhet og oppfyllelse av applikasjonskrav samt digital stasjon-konseptet. Testing av en stand-alone merging unit utføres også for å undersøke enhetens oppførsel og sammenligne den med oppførselen til et konvensjonelt analogt system. Potensiell innvirkning på responsen til et transformer-differensialvern blir også undersøkt.

Laboratorietestene viser at stand-alone merging unit-en har en stasjonær oppførsel som er sammenlignbar med den stasjonære oppførselen til et konvensjonelt analogt system og en betydelig bedre transient oppførsel. Som et resultat av ulikhetene i de transiente oppførselene, oppstår differensialstrømmer når disse to teknologiene kombineres i en hybrid konfigurasjon av et transformatordifferensialvern. De resulterende differensialstrømmene er ikke store nok til å påvirke responsen til transformatordifferensialvernet i de testede tilfellene.

Optiske strømtransformatorer gir mange fordeler sammenlignet med konvensjonelle strømtransformatorer. Noen av disse er forbedret sikkerhet, redusert miljøpåvirkning, redusert behov for vedlikehold og forbedringer i stasjonær og transient oppførsel. Den lave vekten legger til rette for integrasjon med annet primært utstyr, noe som fører til at plass kan spares i anlegget. Kombinasjonen av optiske strømtransformatorer og prosessbuss gjør utformingen av digitale stasjoner fleksibel og legger til rette for kostnadsreduksjoner.

Standardene som gjelder for ikke-konvensjonelle måletransformatorer og digitale stasjoner gir ofte noe rom for tolkning. Dette kan føre til mangel på interoperabilitet mellom enheter fra forskjellige leverandører i en digital stasjon. Kompetansebygging vil også kreves, og digitale stasjoner kan forventes å bli mer sårbare enn dagens konvensjonelle stasjoner på grunn av utendørs plassering av elektronikk og strenge tidssynkroniseringskrav.

Det konkluderes med at optiske strømtransformatorer synes å være egnet til bruk i digitale transmisjonsstasjoner. Det er imidlertid flere tegn på at produktene og løsningene ikke er helt modne ennå. Det er flere undersøkelser som skal gjøres, spørsmål som skal besvares og problemer som skal løses før en overgang fra dagens konvensjonelle stasjoner med konvensjonelle strømtransformatorer til digitale stasjoner med optiske strømtransformatorer kan finne sted.

Contents

List of Figures

List of Tables

List of Abbreviations

ALF Accuracy Limit Factor

CCT Conventional Current Transformer

CIT Conventional Instrument Transformer

CT Current Transformer

CVT Conventional Voltage Transformer

DFT Discrete Fourier Transform

EMI Electromagnetic Interference

EMP Electromagnetic Pulse

GNSS Global Navigation Satellite System

GOOSE Generic Object Oriented Substation Event

HMI Human Machine Interface

HR High Remanence

HSR High-Availability Seamless Redundancy

HV High Voltage

I/O Input/Output

IED Intelligent Electronic Device

LR Low Remanence

LV Low Voltage

MMS Manufacturing Message Specification

MU Merging Unit

NCC Network Control Center

NCCT Non-Conventional Current Transformer

NCIT Non-Conventional Instrument Transformer

NCVT Non-Conventional Voltage Transformer

NR Non Remanence

NTNU Norwegian University of Science and Technology

NTP Network Time Protocol

OCT Optical Current Transformer

PPS Pulse Per Second

PRP Parallel Redundancy Protocol

PTP Precision Time Protocol

RMS Root-Mean-Square

SAMU Stand-Alone Merging Unit

SAS Substation Automation System

SCU Switchgear Control Unit

SLED Superluminescent Diode

SNR Signal-to-Noise Ratio

SV Sampled Values

TSO Transmission System Operator

Chapter 1

Introduction

1.1 Motivation

There is a growing interest in digitalization within almost every industry, including the electric power industry. Several Transmission System Operators (TSOs) in different countries have initiated the work to digitize their substations and are presently working on or have already implemented pilot digital substations [1], [2], [3], [4]. This includes the Norwegian TSO, Statnett, which has an ongoing research and development project where a small scale digital substation has been implemented as a part of an existing substation for testing purposes [4]. The main goal is to achieve a substation solution with improved safety, reduced costs and a reduction in the time spent on the building and upgrading process [5].

The migration from the present day substations to digital substations opens up the possibility to integrate Non-Conventional Instrument Transformers (NCITs), which are based on other measuring principles than the conventional iron core transformer principle [6], [7]. One type of NCIT is the Optical Current Transformer (OCT), which is promised to bring significant improvements compared to Conventional Current Transformers (CCTs). This applies to, among other things, the accuracy, dynamic range, transient performance, safety and size of such sensors [8].

Statnett has installed an OCT in their pilot digital substation in addition to a Stand-Alone Merging Unit (SAMU) [4], which allow existing Conventional Instrument Transformers (CITs) to be integrated into digital substations [6]. It is thus of interest to gain a deeper understanding of OCTs in order to evaluate whether such sensors are suitable for application in digital substations in the transmission network. Since SAMUs are likely to be applied in future digital substations, it is also relevant to perform experimental testing of such a device in order to investigate its performance and potential issues related to its application in digital substations.

1.2 Objectives

The main objective of this thesis is to evaluate whether OCTs are suitable for application in digital substations in the transmission network. This includes answering the following main research questions.

- What are the benefits and drawbacks of applying OCTs in digital transmission substations compared to the use of CCTs in conventional transmission substations?
- Are there any limitations in terms of performance which may prevent the application of OCTs in digital transmission substations?
- Are the products and solutions mature enough?
- Do OCTs meet the requirements of transmission substation applications?
- Will the overall solution fulfill the digital substation concept?

In addition to the investigations on OCTs, a SAMU shall be tested in the laboratory at the Norwegian University of Science and Technology (NTNU). The objectives of the laboratory tests are as follows.

- Investigate the steady state and transient performance of a SAMU.
- Compare the steady state and transient performance of a SAMU to those of a conventional analog acquisition system.
- Investigate whether a hybrid mode configuration could have an impact on the performance of transformer differential protection.

1.3 Limitations

This thesis has been conducted in cooperation with Statnett. The focus is therefore put on the application of OCTs in digital substations in the transmission network. Other types of Non-Conventional Current Transformer (NCCT) have not been considered, nor Non-Conventional Voltage Transformers (NCVTs). The author has chosen to go deeper into OCTs instead of treating different types of NCITs briefly. There was no OCT present to be tested. Thus, the study on OCTs was limited to a literature review. Experimental tests of an actual OCT would indeed have enriched this thesis.

There were also limitations in time and in the laboratory test setup, which limited the experimental testing of the SAMU. The phase accuracy of the SAMU could not be investigated due to lack of time synchronization between the output from the test set and the output from the SAMU. In addition, the highest current which could be applied to the

SAMU was limited by the maximum current output of the test set. This was 6.4 times the rated input current of the SAMU.

Only the current module of the SAMU was tested in the laboratory. The SAMU also incorporates a voltage module, which could have been tested. In the laboratory test setup, the SAMU was directly connected to the protection IED by a single fiber optic link, representing an ideal process bus without any significant time delays or other impacts on the digital output from the SAMU. The effects of an actual process bus incorporating switches and other connected devices was thus not investigated.

1.4 Approach

This thesis may be divided into two parts: a literature review and product survey on OCTs, and experimental testing of a SAMU.

The first part of this thesis is based on a literature review on the technology and application of OCTs in digital substations in addition to a product survey of four commercially available OCTs. The product survey was conducted by studying the available technical documentation of the different products as well as contacting the vendors in order to get answers to questions which were not covered by the technical documentation. During the fall semester of 2017, the author visited one one Statnett's transmission substations and Statnett's pilot digital substation. Experiences from these two visits and information obtained from contact with Statnett have also provided a basis for the content of this thesis.

The second part of this thesis is based on laboratory work which was performed in the ProSmart lab at NTNU during the spring semester of 2018. The steady state and transient performance of a SAMU was experimentally tested. In order to test the transient performance of the SAMU, simulations were created in ATPDraw to generate different transient current waveforms.

1.5 Structure of the Report

The rest of this thesis is structured as follows.

Chapter 2 introduces background information on conventional substations, CCTs, digital substations and relevant standards and regulations. This chapter is partially based on the specialization project report, "Digital Substations in Transmission Networks" [9], which was written by the same author during the fall semester of 2017.

Chapter 3 treats OCTs. This chapter starts with an introduction of some basic concepts and continues with descriptions of common detection methods, different types of OCTs and the associated Merging Unit (MU). The main sources of error and the characteristics of OCTs in terms of performance and other attributes are also described.

Chapter 4 presents the results of the product survey on OCTs. In this chapter the attributes of some of the OCTs which are commercially available at the present time are presented and compared.

In Chapter 5 the working principle and performance of SAMUs are described.

In Chapter 6 some considerations regarding the use of OCTs and other NCITs as well as SAMUs in digital substations are presented.

Chapter 7 describes the test setup and method which was used during the laboratory tests of the SAMU.

Chapter 8 presents the most important results from the laboratory tests.

In Chapter 9 the results of the laboratory tests which are given in Chapter 8 are discussed.

In Chapter 10 some preliminary conclusions are drawn from the discussion of the laboratory tests in Chapter 9. This chapter also includes some suggestions for future laboratory testing of SAMUs.

Chapter 11 provides a discussion of the benefits and drawbacks of applying OCTs in digital substations compared to the use of CCTs in conventional substations. It is also discussed whether OCTs are suitable for application in digital transmission substations.

In Chapter 12 the main research questions, which were presented in Section 1.2, are answered, and final conclusions are drawn. This chapter also includes some suggestions for future work.

Chapter 2

Background

In this chapter relevant background information is presented. Section 2.1 describes present day transmission substations, hereafter referred to as conventional substations. Section 2.2 treats CCTs and Section 2.3 describes digital substations. In Section 2.4 and Section 2.5 some relevant standards and regulations are presented, respectively.

The text in Section 2.1, Section 2.3 and Subsection 2.4.2 is taken from the specialization project report, "Digital Substations in Transmission Networks" [9], written by the same author during the fall semester of 2017. Some adaptions have been made. Section 2.2 is also partially based on the same specialization project report. However, additional parts have been added.

2.1 Conventional Substations

Transmission substations play an important role in transmission networks by connecting transmission lines and providing important functions, such as transformation of voltage levels, voltage control, reactive power control and power flow control [10]. In "Energiloven" § 1-5, the transmission network is defined as follows.

> *"The transmission network comprises of facilities for the transmission of electrical energy at voltage levels of at least 200 kV, and facilities at 132 kV which are of major importance for the operation of these facilities. The transmission network also includes facilities for electrical energy conversion, when the conversion facility is directly connected to facilities for transmission as mentioned in the first paragraph and transforms to a voltage level of at least 33 kV. ..."* [11] (Translated from Norwegian)

Transmission substations generally comprise of a lot of different equipment, which may be divided into two categories: primary equipment and secondary equipment. The primary equipment is high voltage equipment, such as switching equipment, instrument transform-

ers, power transformers, reactors, capacitor banks, busbars, power cables and power lines. The primary equipment is located in the substation yard and is typically organized in high voltage bays. The secondary equipment comprises of low voltage devices for protection, control and monitoring [12], [13], [14]. These devices are typically located in the control room of a control building. Together with the communication systems, these secondary devices constitute the Substation Automation System (SAS) [15]. SASs have three basic functions: to monitor, protect and control the primary equipment in the substation [16], [12].

The architecture of a SAS can be divided into three levels: the process level, the bay level and the station level [17]. The process level represents the interface to the primary process [15]. At this level, data is acquired and operations are executed in order to control the primary process [16]. The process level includes equipment such as CITs and different types of switching equipment [15].

The bay level comprises of Intelligent Electronic Devices (IEDs), such as protection IEDs and bay controllers, which perform protection and control functions, respectively [17]. Other bay level devices are disturbance recorders, electrical energy meters and devices used for quality metering. The station level incorporates the substation Human Machine Interface (HMI) and gateways which enable the communication between the substation and the Network Control Center (NCC). The station level provides the operators with status data from the substation equipment for the purpose of monitoring and control [17].

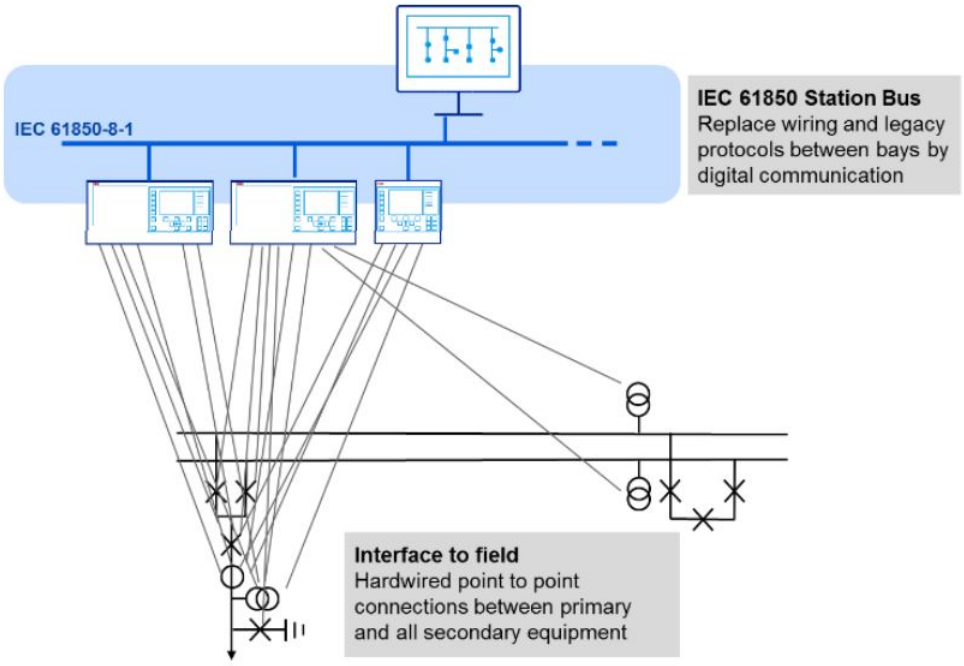

Figure 2.1: Layout of a conventional substation [18]. © 2017 IEEE

The interface between the station level and the bay level is a communication network referred to as the station bus, as shown i Figure 2.1. The station bus connects the bay level devices to the station level devices, thereby enabling the communication between the two levels as well as the communication between different bay level devices [12]. The connections between the process level equipment and the bay level devices, on the other hand, are still hardwired, as shown in Figure 2.1. There is thus a large number of copper cables running from the control building to the individual high voltage bays in conventional substations [4]. These are typically laid in large concrete cable trenches. The hardwired circuits comprise of the following [14].

- Analog circuits for currents and voltages acquired by CITs.
- Binary circuits for status information, such as position of switching equipment.
- Binary circuits for protection and control signals.
- AC and DC power supply circuits.

The primary process data is not digitized before it reaches the bay level. The secondary devices perform the conversion from analog or binary signals to digital and vice versa.

2.2 Conventional Current Transformers

CCTs scale the primary power circuit currents down to a level which is safe and practical to use as an input for protection, control and measuring devices and create a galvanic separation between the primary power circuit and the secondary devices [19], [20]. CCTs have a standard rated secondary current of 1 A or 5 A, as defined in IEC 61869-2 [21]. The standardization facilitates the use and interchange of CCTs and secondary devices from different vendors in a substation [20].

High voltage CCTs are inductive transformers with a conductive bar as the primary winding and one or more secondary windings, which are wound around iron cores encircling the primary bar [22]. A single Current Transformer (CT) core cannot satisfy the requirements of all of the applications which are needed in a substation. Due to the conflicting requirements of various applications, such as measuring and protection, different types of transformer cores have been designed specifically to meet the accuracy, dynamic range and bandwidth requirements of these applications [23]. The performance of a CCT is determined by the area and diameter of the core cross section as well as the magnetic properties [24]. The iron core causes measurement inaccuracies, which arise as a consequence of magnetizing current, flux leakage, magnetic saturation, eddy current losses and hysteresis losses. By designing different types of cores for specific applications, the measurement inaccuracies can be reduced to a minimum [25], [26].

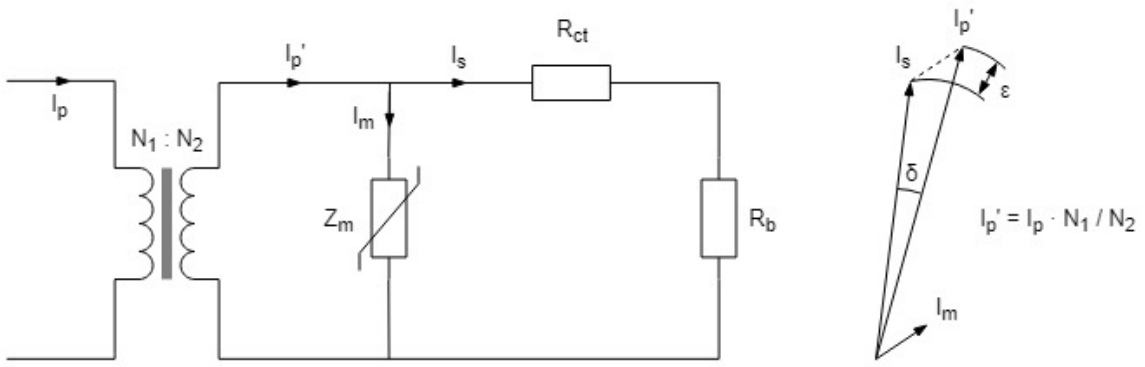

Figure 2.2: Simplified equivalent circuit and phasor diagram of a CCT. The figure is adapted from [27] and [28].

A simplified equivalent circuit of a CCT and the associated phasor diagram is shown in Figure 2.2. As shown in the figure, the primary current reffered to the secondary side (I_p') comprises of two components: the magnetizing current (I_m) and the secondary current (I_s). Since the magnetizing current is not transformed to the secondary side of the CT, the primary current (I_p) will be transformed with some errors in the amplitude and phase. These are referred to as the ratio error (ε) and the phase displacement (δ), respectively [26].

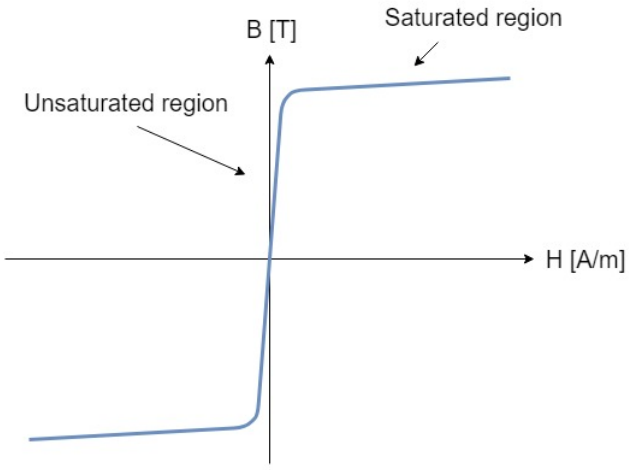

Figure 2.3: Simplified magnetization curve for a CCT. The figure is adapted from [27].

A simplified magnetization curve for a CCT is shown in Figure 2.3. The value of the magnetizing impedance (Z_m) in the equivalent circuit shown in Figure 2.2 is proportional to the slope of the magnetization curve [27]. Under normal load conditions CCTs typically operate in the unsaturated region of the magnetization curve. In this region the

magnetizing impedance has a much higher value than the secondary circuit impedance (R_{ct} + R_b). Hence, most of the secondary current flows through the secondary circuit. Under faulted conditions, on the other hand, CCTs may go into saturation due to high primary currents. In the saturated region of the magnetization curve, the value of the magnetizing impedance is much smaller than in the unsaturated region. Most of the secondary current will flow through the magnetizing impedance for a period of time each cycle. The result is a saturated secondary current, as shown by the blue current waveform in Figure 2.4. The saturation causes a high transformation error [27], [29]. CT saturation may for instance result in incorrect operation of differential protection functions or differential protection functions not operating when required to [30].

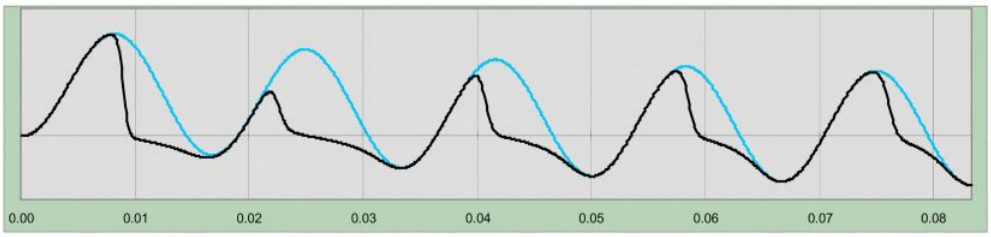

Figure 2.4: Current transformer saturation [31]. © 2002 IEEE

Measuring applications require high accuracy for currents up to the nominal primary current [32], [26]. In order to make the measurements as accurate as possible, measuring CT cores are designed with smaller cross sections. The magnetizing current is thereby minimized. At high current levels the measuring cores may saturate, which is beneficial in order to protect the measuring devices from high current levels [24] [26]. Protective applications, on the other hand, require a wide dynamic range and accurate measurements of fault currents [32], [26]. In order to avoid saturation at high current levels, protection CT cores are designed with larger cross sections [24].

CCTs for protection can roughly be divided into three types based on how the iron core is designed, if there are air gaps in the core and if so, how big the air gaps are. The three types are High Remanence (HR), Low Remanence (LR) and Non Remanence (NR). These have no air gaps in the core, small air gaps in the core and large air gaps in the core, respectively. For HR type CTs there is no limit specified for the remanent flux. The remanent flux of LR type CTs can be up to 10 % of the saturation flux, and the remanent flux limit for NR type CTs is set to zero [27]. CCTs with air gaps in the core are less prone to saturation since the air gaps reduce the magnetizing inductance and the remanence. However, the phase displacement and the ratio error will increase because a larger fraction of the secondary current will flow through the magnetizing impedance. In

addition, such CTs cannot reproduce the DC component in transient primary currents properly. The bigger the air gaps, the faster the DC component will be damped out [27], [33].

CCTs may be equipped with up to eight CT cores. The CCTs in present day transmission substations typically have protection cores which are assigned to separate protective applications in addition to separate measuring cores for energy metering and measuring. The secondary circuits of CCTs are connected in series with the input elements of secondary devices, as shown in Figure 2.5 [32].

In conventional transmission substations the secondary CT circuits are connected to the back of the protection and control panels in the control room. With one multiple cored CCT per phase of each feeder, there is a great number of copper cables running from the high voltage bays to the control building [34]. There is also a risk that one of these secondary CT circuits can be inadvertently opened. If this happens, the CT will saturate due to the infinite secondary impedance. A very high voltage is induced across the primary winding, which in turn causes a very high voltage across the secondary winding. As a result, arcing and possibly explosion of the CT can occur [35], [26]

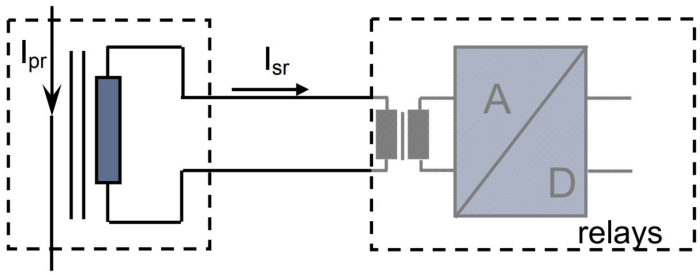

Figure 2.5: Connection of a CCT to a protection IED [36]. © 2011 IEEE

High voltage CCT typically have oil-paper or SF_6 insulation. In the Norwegian transmission grid, oil-paper insulated CTs are often used. Since these CTs contain oil, inspections have to be performed regularly were the oil level is checked. Instrument readings may also be performed. At Statnett this inspection is carried out each month. It is estimated that such an inspection takes about half an hour per CT [Appendix A].

CCT are quite heavy devices. As an example, for a system voltage of 420 kV, one vendor offers a top-core oil-paper insulated CT with a weight of 920 kg and a top-core SF_6 gas insulated CT with a weight of 1700 kg [37]. CCTs have been in wide use for a long time and have proven to be reliable and show a good stability over time [38], [39]. The expected lifetime is typically 25-40 years [7]. When it comes to the price, a CCT rated for

a maximum system voltage of 420 kV, which has three protection cores and two measuring cores, is estimated to cost up to 8 500 € [Appendix A].

2.3 Digital Substations

The term digital substation has no standard definition. However, in general, the term refers to substations where most of the primary process data is converted to digital form already in the substation yard, close to where it is measured. The exchange of those measured values as well as commands and signals between the secondary and the primary devices takes place via a communication network in accordance with the IEC 61850 standard. The communication network is referred to as the process bus [40], [4]. The process bus replaces the copper cables used for measuring and control circuits, which run from the control building to the separate high voltage bays in conventional substations. In digital substations the only copper cables left between the control building and the high voltage bays will be those used for AC and DC power supply circuits [41]. The layout of a digital substation is shown in Figure 2.6, with the station bus and process bus marked in dark and light blue, respectively.

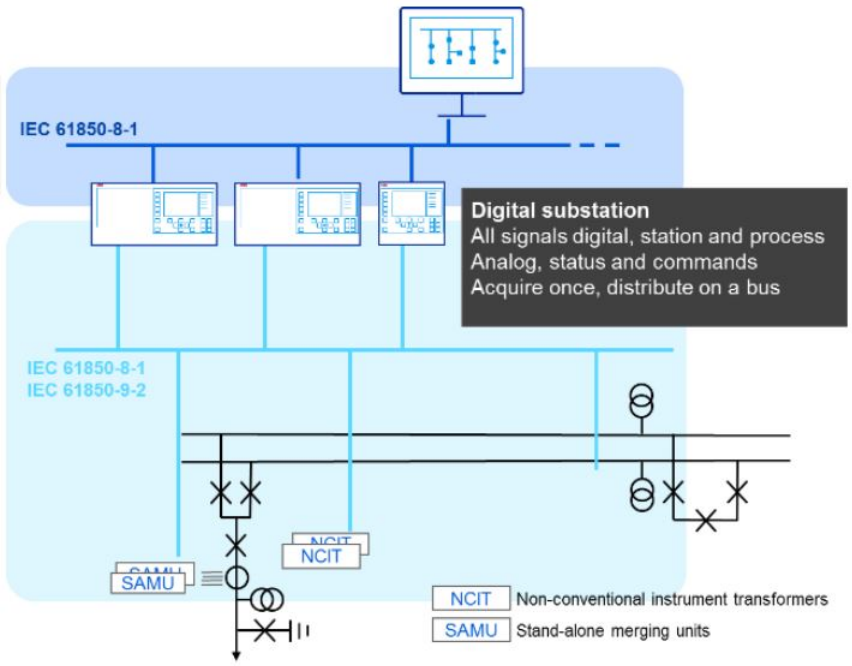

Figure 2.6: Layout of a digital substation [18]. © 2017 IEEE

2.3.1 Non-Conventional Instrument Transformers

The use of NCITs in substations has so far been limited. Typically, NCITs do not provide the standard analog 1 A/5 A or 110 V output required by conventional protection, control and monitoring devices. The introduction of a standardized process bus simplifies the integration of NCITs into substations [6]. Since NCITs typically require digital signal processing, a digital signal is a natural choice of output from such sensors [7].

Unlike CITs, NCITs are not based on the iron core transformer principle. The limitations of CITs due to the iron core can thus be overcome [7]. NCITs are based on electrical or non-electrical measuring principles. Examples of NCITs which employ electrical measuring principles are Rogowski coil current sensors and capacitive voltage dividers. OCTs use a non-electrical measuring principle based on the Faraday effect [42]. In Chapter 3 OCTs will be treated in further detail.

2.3.2 Merging Units and Stand-Alone Merging Units

Merging units provide an interface for the connection of NCITs or CITs to the process bus [43]. Merging units sample the current and voltage measurements from instrument transformers and distribute the digital output as Sampled Values (SV) on the process bus in accordance with IEC 61850-9-2 LE. The secondary devices which are connected to the process bus can subsequently subscribe to these SV [44]. In order for the secondary devices to be able to align SV from different merging units, the SV have to be time stamped by the merging units and synchronized in time [45], [33]. In general, there are two types of merging units. These are referred to as Merging Unit (MU) and Stand-Alone Merging Unit (SAMU), respectively. MUs are applied in conjunction with NCITs and are typically integrated with the associated sensor electronics. SAMUs, on the other hand, are used to interface CITs [4]. In Section 3.4 and Chapter 5, the associated MU of OCTs and SAMUs, will be treated in further detail, respectively.

There are several reasons why SAMUs are likely to be used in future digital substations. First of all, as described in Section 2.1, transmission networks also include voltage levels which are lower than 200 kV. In the lower voltage parts of transmission substations, a continuous use of CITs may be desirable due to lack of commercially available OCTs rated for these voltage levels. This could for instance be on the Low Voltage (LV) side of a power transformer. In this thesis OCTs from four different vendors are considered. At the present time, the OCTs offered by these vendors do not cover the lowest voltage levels which are included in the transmission network [46], [47], [48], [49]. In addition, the migration from the present day conventional substations to digital substations will be

a gradual process, and CITs are likely to be replaced on a step-wise basis [50]. SAMUs allow existing CITs to be integrated into digital substations [6], thereby enabling a gradual transition to digital substations.

2.3.3 Switchgear Control Units

Conventional switching equipment is integrated into digital substations by the use of Switchgear Control Units (SCUs). SCUs provide a binary interface for the connection of conventional switching equipment to the process bus in such a way that the switchgear can be monitored and controlled [43]. SCUs acquire information regarding the position and status of the switching equipment and distribute this information on the process bus according to IEC 61850-8-1. In addition, SCUs actuate the switchgear based on commands and signals which are received from the protection and control IEDs over the process bus [1].

2.3.4 Process Bus

The process bus is the communication network which replaces the traditional hardwired point-to-point connections between the primary equipment and the secondary devices in conventional substations. The communication network allows process level devices to exchange time-critical information with bay level devices and vice versa [17]. The process bus is realized by the use of fiber optic cables, in contrast to the copper cables which are used for the measuring and control circuits in conventional substations [4]. The primary process data is distributed on the process bus and may be accessed by all of the secondary devices which are connected to this communication network [40], [4].

Process bus communication is primarily of three types: SV streams, Generic Object Oriented Substation Event (GOOSE) messages and client-server communication based on the Manufacturing Message Specification (MMS) protocol [51]. Sampled current and voltage measurements from SAMUs and the associated MUs of NCITs are published to the process bus and sent to subscribing secondary devices as SV in accordance with IEC 61850-9-2 [52]. By the use of multicast messages, the same SV can be sent to several secondary devices simultaneously [41]. Status data and alarm information from the primary process are also transmitted to the secondary devices, typically as GOOSE messages in accordance with IEC 61850-8-1. Trip signals and open/close commands are sent from the protection and control IEDs to the SCUs as GOOSE messages, also in accordance with IEC 61850-8-1 [52].

2.3.5 Motivations Behind Digital Substations

There are several motivations behind digital substations. Some of them are as follows. First of all, the process bus can be realized by a much smaller number of fiber optic cables than the large number of copper cables which are required for the measuring and control circuits in conventional substations. The costs associated with cabling can thus be reduced [4]. Digital substations also allow the space which is required in the control building to be reduced. The secondary devices can be made smaller than today since the analog and binary Input/Output (I/O) boards are no longer needed in these devices [53]. In addition, the exchange of primary process data, commands and signals over the process bus facilitates the integration of several functions into the same IED, which in turn can lead to a reduced number of IEDs in the control room [4]. The reduction in cabling and number of devices in the control building also allows the time spent on engineering, installing, testing and replacing secondary systems to be significantly reduced [18], [53].

2.4 Standards and Implementation Guidelines

In this section, some of the standards and implementation guidelines which are relevant to the application of OCTs in digital substations are presented. This includes IEC 61850-9-2, IEC 61850-9-2 LE, IEC 61869 and IEC 60044-8.

2.4.1 IEC 61850-9-2

IEC 61850-9-2 is one of several parts of the IEC 61850 standard, "Communication networks and systems for power utility automation", which is the international standard for substation communication based on Ethernet [7]. IEC 61850-9-2 is called "Specific communication service mapping (SCSM) - Sampled values over ISO/IEC 8802-3" [54]. This part of the IEC 61850 standard concerns the transmission of SV over Ethernet. However, the standard leaves too much room for interpretation for actual systems to be implemented. For instance, the standard does not specify what the dataset of SV should include nor what the sample rate should be [55]. The solution came with the implementation guideline IEC 61850-9-2 LE, which will be described in the next subsection.

2.4.2 IEC 61850-9-2 LE

IEC 61850-9-2 LE, short for "IEC 61850-9-2 Light Edition", is an implementation guideline made by the UCA International Users Group [55]. The implementation guideline was created to ease the implementation of IEC 61850-9-2 and to facilitate interoperability

between different devices [55], [56]. IEC 61850-9-2 LE specifies two sample rates, one for protection and metering applications and one for power quality applications. For protection and metering applications a sample rate of 80 samples per cycle is defined and for power quality applications a sample rate of 256 samples per cycle. The resulting sample rates in a 50 Hz network are thus 4 000 Hz and 12 800 Hz, respectively. IEC 61850-9-2 LE defines the content of the SV dataset to be one sample of each of the three phase currents and three phase voltages from one network node in addition to neutral current and neutral voltage [55]. The neutral values can either be measured by CITs or calculated by the merging unit [56].

2.4.3 IEC 61869

The IEC 61869 standard, "Instrument transformers", applies to both CITs and NCITs. This standard comprises of several parts. Part 1, Part 6 and Part 9 are product family standards which define general requirements applying to all types of instrument transformers, additional general requirements applying to NCITs and additional requirements applying to instrument transformers with a digital output, respectively [57], [29], [33]. In addition to the product family standards, IEC 61869 comprises of several product standards. The product standards define additional requirements applying to specific types of instrument transformers [57]. IEC 61869 gradually replaces the old standard for instrument transformers, IEC 60044 [18]. At the present time, only Part 7 and Part 8 of IEC 60044, which apply to electronic voltage and current transformers, respectively, are still active [58].

IEC 61869-2

IEC 61869-2, "Additional requirements for current transformers", is a product standard which applies to inductive current transformers. In this part of IEC 61869, standard accuracy classes and corresponding error limits are defined for measuring current transformers and protective current transformers, respectively. IEC 61869-2 has defined the following standard measuring accuracy classes: 0.1, 0.2, 0,2 S, 0.5, 0,5 S, 1, 3 and 5. Measuring accuracy class 0,2 S is specified by limits of ratio error and phase displacement at 1 % to 120 % of the rated current. The standard accuracy classes for protective current transformers are divided into different groups based on how the classes are specified. For class P protective current transformers, the following standard accuracy classes are defined: 5P and 10P. Protective accuracy class P is specified by limits of ratio error and phase displacement at the rated primary current in addition to limits of composite error at the rated accuracy limit primary current. The rated accuracy limit primary current

is a multiple of the rated primary current. The multiplier is called the Accuracy Limit Factor (ALF), and its standard value is 5, 10, 15, 20 or 30 [21].

IEC 61869-6

IEC 61869-6, "Additional general requirements for low-power instrument transformers", specifies additional requirements concerning NCITs. In this part of IEC 61869, the analog and digital output errors of NCITs are defined. IEC 61869-6 also covers additional bandwidth requirements for NCITs [29].

IEC 61869-9

Part 9 of IEC 61869 is called "Digital interface for instrument transformers". IEC 61869-9 concerns instrument transformers which have a digital output and gives requirements for the digital communication of measurements from such instrument transformers. IEC 61850-9-2 LE partially formed the basis of this standard. However, additions and improvements have been made [33]. For instance, instead of defining the sample rate of the digital output in terms of samples per cycle, IEC 61869-9 defines sample rates which are not dependent of the rated frequency of the power system. The preferred sample rates are 4800 Hz for measuring and protective applications and 14 400 Hz for quality metering applications. The same publishing rate of 2400 frames per second is defined for both sample rates and is attained by packing 2 and 6 samples in each frame, respectively [55], [33].

According to IEC 61869-9, the specifications of the accuracy classes for NCITs with a digital output apply to the digital output from the MU. In other words, all errors which occur in the current measurement between the primary side of the NCIT and the digital output are included. This includes errors caused by inaccuracies in the time synchronization [33].

IEC 61869-13

Part 13 of IEC 61869, "Stand-Alone Merging Unit", has not been released yet. According to IEC's website, the forecasted publishing date is September 2019 [59]. This part of IEC 61869 will apply to SAMUs, as the name suggests. Among other things, this standard will define requirements for the transient performance of SAMUs. IEC 61869-13 will recommend making use of input elements which cannot saturate [60].

2.4.4 IEC 60044-8

IEC 60044-8 has partially been replaced by Part 6, 9 and 10 of IEC 61869. However, IEC 61869-8 is missing. This part has been planned for the future, but has not been developed yet [59]. Thus, IEC 60044-8 is still applicable to OCTs [18]. The same standard measuring accuracy classes are defined in IEC 60044-8 as for CITs in IEC 61869-2. The limits of error are also equivalent. For protective current transformers three standard accuracy classes are defined: 5 P, 10 P and 5TPE. The error limits for class 5 P and 10 P are equivalent to those specified for CITs in IEC 61869-2. In addition to the error limits specified for class 5 P, 5TPE also has a limit for the maximum peak instantaneous error at accuracy limit conditions [61].

2.5 Regulations and Guidelines

Transmission substations in Norway, both conventional substations with CITs and digital substations with NCITs, must conform to the requirements of certain regulations, including the ones listed below.

- "Forskrift om elektriske forsyningsanlegg" [62]
- "Forskrift om leveringskvalitet i kraftsystemet" [63]
- "Forskrift om forebyggende sikkerhet og beredskap i energiforsyningen (Beredskapsforskriften)" [64]
- "Forskrift om systemansvaret i kraftsystemet" [65]

In addition to the requirements specified in regulations, the owner may have their own requirements for the design of the substation.

§ 14 of "Forskrift om systemansvaret i kraftsystemet" states the following.

> *"**§ 14. Planning and commissioning of technical facilities in the power system***
> *The concessionaire shall inform the system operator about plans for new facilities or alteration of its own facilities in or connected to the regional or central grid, when other concessionaires are affected by this. The system operator shall issue a decision on approval of new facilities or alterations of existing facilities before these can be commissioned. ..."* [65] (Translated from Norwegian)

The decision of the system operator is normally based on conditions which are indicated by the guideline "Funksjonskrav i kraftsystemet" [66]. This guideline has been developed by

the system operator. Digital substations with OCTs must therefore meet the specifications in this guideline.

Given below are some excerpts from "Beredskapsforskriften", which the author finds particularly relevant when considering digital substations with OCTs.

§ 7-13 of "Beredskapsforskriften" states the following.

> *"**§ 7-13. Protection against electromagnetic pulse and interference***
> *The company must assess the vulnerability of the operational control system to electromagnetic pulse (EMP) or electromagnetic interference (EMI). If vulnerabilities are identified, security or emergency measures shall be implemented according to the operational control system's significance for safe operation and restoration of its function in the power supply."* [64] (Translated from Norwegian)

In "Beredskapsforskriften" facilities are classified based on the voltage level and the power rating. There are three classes: Class 1, Class 2 and Class 3. The requirements for Class 3 facilities are the strictest. These are facilities which have the greatest importance for the power supply [64].

> *"Class 3 includes:*
> *...*
> *b. Transformer station with overall main transformer rating of more than 100 MVA and built for a maximum voltage level of at least 200 kV and transformation to a secondary voltage level in networks of at least 30 kV.*
> *c. Independent switching station in the power system built for a voltage level of at least 200 kV.*
> *..."* [64] (Translated from Norwegian)

Substations in the transmission network are thus typically classified in class 3, based on the definition of the transmission network which was given in Section 2.1. There are some special requirements for the protection of facilities which are classified in Class 3. One of the requirements applying to Class 3 transformer stations and switching stations is the following [64].

> *"3.2.7 The facility shall have duplicated and physically independent routing of cables for control and communication, emergency and station power and high voltage, respectively, so that a single error or event cannot knock out vital functions."* [64] (Translated from Norwegian)

Chapter 3

Optical Current Transformers

This chapter treats OCTs whose measuring principle is based on the Faraday effect. In Section 3.1 basic concepts which are important for the understanding of the working principle of OCTs are described. Section 3.2 presents two common detection methods, and Section 3.3 describes some types of OCTs and their working principle. In Section 3.4 the associated MU of OCTs is shortly described. Section 3.5 treats the main sources of error in OCTs and some solutions to how these can be mitigated. In Section 3.6 important performance characteristics of OCTs are described, and in Section 3.7 other characteristics are presented.

3.1 Basic Concepts

In order to understand the operating principle and the error sources of OCTs, familiarity with the concepts of polarized light, birefringence and the Faraday effect is essential. The purpose of this section is to provide the necessary knowledge.

3.1.1 Polarized Light

Polarized light has an electrical field which oscillates in an orderly manner [67]. Depending on how the orientation of the electrical field vector evolves as the light wave propagates, polarized light can be characterized as being linearly, circularly or elliptically polarized. As shown in Figure 3.1a, the electric field vector of a linearly polarized light wave draws a line in a plane which is perpendicular to the propagation direction of the light. The electric field vector of a circularly polarized light wave, on the other hand, draws a circle, as seen in Figure 3.1b, while the electric field vector of elliptically polarized light draws an ellipse [68], [69]. Depending on the rotational direction of the electric field vector, circularly and elliptically polarized light may further be characterized as being right-hand or left-hand polarized [70].

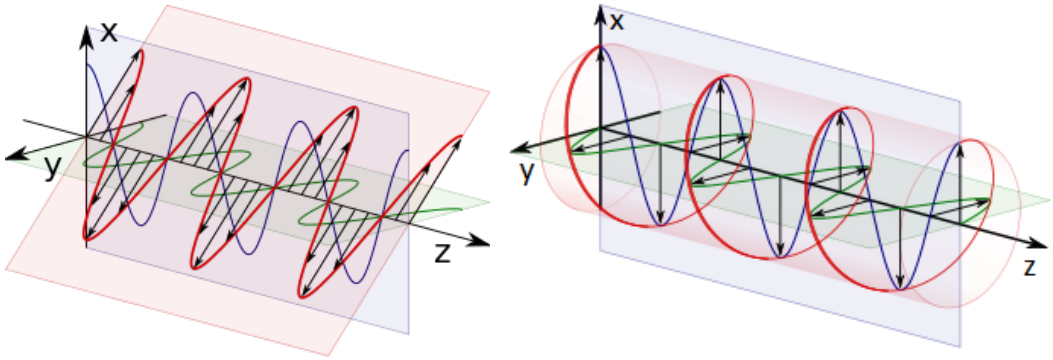

(a) Linearly polarized light [71]. **(b)** Circularly polarized light [72].

Figure 3.1: Polarized light.

Any type of polarized light can be decomposed into two orthogonal linearly polarized components [73]. Assuming that a polarized light wave is propagating along the z-axis, as in Figure 3.1a and Figure 3.1b, the light wave can be decomposed into a component polarized along the x-axis and a component polarized along the y-axis. In Figure 3.1 these two components are drawn in blue and green, respectively. The resulting light waves are drawn in red. Linearly, circularly and elliptically polarized light result from different magnitudes and relative phase shifts between the two orthogonal components. If the x and y components are in phase, as seen in Figure 3.1a, the resulting light will be linearly polarized. Circularly polarized light, on the other hand, results if the x and y components have the same amplitude and are 90° out of phase, as shown in Figure 3.1b. Any other mix of amplitudes and relative phase shifts gives elliptically polarized light [70]. Linearly polarized light can also be decomposed into two orthogonal circularly polarized components. Left-hand and right-hand circularly polarized light waves are orthogonal. Hence, a linearly polarized light wave can be seen as a superposition of a right-hand and a left-hand circularly polarized light wave [68].

3.1.2 Birefringence

A medium is said to be birefringent if the value of its refractive index is dependent on the propagation direction and the polarization of light [73]. The refractive index of a light wave in a medium determines the speed of the light through the medium, as shown by Equation (3.1),

$$v = \frac{c}{n} \tag{3.1}$$

where c is the speed of light in vacuum and n is the refractive index of light in a medium [69]. Birefringence may be divided into linear and circular birefringence. Depending on the propagation direction and the polarization of an incident light wave, a birefringent medium will either maintain or change the polarization of the light [68].

In a linearly birefringent medium, there are two orthogonal birefringence axes with different refractive indexes, commonly referred to as the fast axis and the slow axis. In Figure 3.1a, the fast and the slow axes could be the x-axis and the y-axis, respectively. The polarization of incident light which is linearly polarized along the fast or the slow axis of a linearly birefringent medium will remain unchanged as the light wave propagates through the medium. In Figure 3.1a this applies to the blue and the green linearly polarized light waves. However, these two light waves will experience different refractive indexes and thus travel at different speeds through the medium. If a linearly polarized light wave enters a linearly birefringent medium at an angle to the fast and the slow axes, the light wave will be split into two components due two the different refractive indexes of the fast and the slow axes. In Figure 3.1a this applies to the red wave, which will be split into the blue and the green linearly polarized components. Since the two components travel at different speeds through the medium, a phase shift will develop between them. As a result, the incident linearly polarized light is transformed into elliptically or circularly polarized light, depending on the value of the differential phase shift which develops [74], [75].

From the above-given explanation, it can be concluded that a linearly birefringent medium will maintain the polarization state of linearly polarized light which is polarized along the medium's fast axis or slow axis, and change the polarization state of linearly polarized light which is polarized at an angle to the fast and the slow axes [74], [75]. A circularly birefringent medium maintains the polarization states of right-hand and left-hand circularly polarized light [75]. However, these two polarization states will experience different refractive indexes in the medium and thus travel at different speeds [74]. The polarization state of linearly polarized light, on the other hand, will be rotated. This phenomena can be explained by considering the linearly polarized light wave as a superposition of a right-hand and a left-hand circularly polarized light wave. Due to the relative phase shift which develops between these two components in a circularly birefringent medium, the plane of polarization of the linearly polarized light wave will be rotated [75].

3.1.3 The Faraday Effect

The plane of polarization of a linearly polarized light wave will be rotated when the wave propagates through a magneto-optical medium which is placed in a magnetic field. This effect is known as the Faraday effect and is illustrated in Figure 3.2. The angle of rotation of the polarization plane is given by Equation (3.2),

$$\theta = VHL \tag{3.2}$$

where V is the Verdet constant of the medium, H is the magnetic field strength parallel to the propagation direction of the light and L is the distance which is travelled by the light in the medium [76]. The Verdet constant is dependent on the properties of the medium and varies with temperature and the wavelength of the light [69].

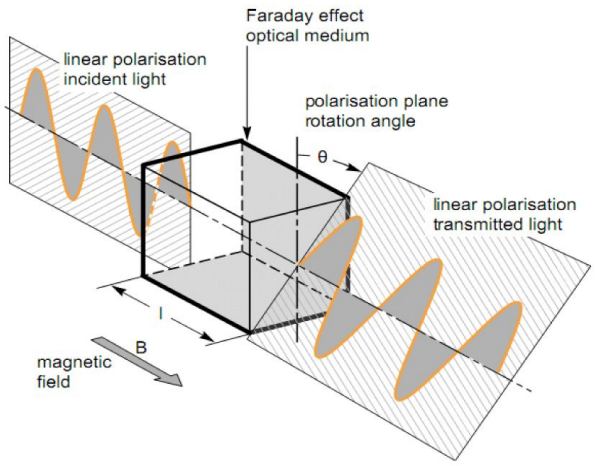

Figure 3.2: The Faraday effect [77]. © 2017 IEEE

The Faraday effect is actually circular birefringence induced by a magnetic field [74]. As already explained, a linearly polarized light wave can be considered as a superposition of a right-hand and a left-hand circularly polarized light wave. These two components will experience different refractive indexes in a magneto-optical medium which is subjected to a magnetic field. The result is a difference in the speeds of the two components through the medium. The polarization plane of the resultant linearly polarized light will thus be rotated [76]. If right-hand circularly polarized light propagates in the direction of the magnetic field, the speed of the light will be decreased. The speed of right-hand circularly polarized light which is propagating in the opposite direction of the magnetic field, on the other hand, will be increased. The opposite applies to left-hand circularly polarized light [68].

3.2 Detection Methods

OCTs make use of the Faraday effect to measure the current in the primary conductor [78]. Polarized light is sent through the sensing element, which is typically placed around the primary conductor. The light will thus propagate along the magnetic field which is produced by the primary current [74]. Two principal detection methods can be applied to measure the Faraday rotation of the light due to the magnetic field. These are polarimetric detection and interferometric detection [79].

3.2.1 Polarimetric Detection

Polarimetric detection is based on measuring the Faraday rotation angle of linearly polarized light which is propagating through the sensing element of the OCT. If the sensing element encloses the primary conductor, Equation (3.2) can be combined with Ampere's law by expressing the equation as a line integral. The Faraday rotation angle can then be expressed as in Equation (3.3),

$$\theta = V \oint_C \vec{H} d\vec{l} = VNI \tag{3.3}$$

where V is the Verdet constant of the sensing element, H is the magnetic field strength parallel to the propagation direction of the light, N is the number of turns of the sensing element around the primary conductor and I is the current in the primary conductor [76]. If the sensing element encloses the primary conductor, the Faraday rotation angle will thus be proportional to the current to be measured. The Faraday rotation angle cannot be detected directly. Instead it is transformed into a light intensity, which can be detected [76].

3.2.2 Interferometric Detection

An alternative to measuring the Faraday rotation angle of linearly polarized light is to measure the differential phase shift which accumulates between right-hand and left-hand circularly polarized light propagating through the sensing element, due to the Faraday effect. This is known as interferometric detection. As with polarimetric detection, the phase shift must be converted into a light intensity in order to be detectable [76].

3.3 Types of Optical Current Transformers

OCTs comprise of the following parts: the sensor heads housing the sensing elements, the sensor electronics and the fiber optic cables connecting the sensor electronics to the sensor heads [80]. The MUs is typically integrated with the sensor electronics [36]. OCTs may be divided into two groups based on the material which is used for the sensing element: optical fiber current sensors and bulk glass optical current sensors [81]. These two types of sensors will be described in further detail in the following subsections. The main focus will be on optical fiber current sensors since most of the commercially available OCTs which are considered in this thesis use this technology. This technology is also considered as a better solution for new OCTs [80].

3.3.1 Optical Fiber Current Sensors

The sensing element of optical fiber current sensors comprises of an optical fiber which is wound around the primary conductor one or several times [38]. One of the benefits of this type of OCT is that the sensitivity of the sensor can easily be adapted by choosing a different number of sensing fiber coil turns [79]. Optical fiber current sensors may use either polarimetric or interferometric detection methods [68]. In the rest of this subsection, some types of polarimetric and interferometric optical fiber current sensors will be presented and their working principles explained.

Polarimetric Optical Fiber Current Sensors

Figure 3.3 shows the schematic of an optical fiber current sensor with a basic polarimetric detection scheme. The working principle of the sensor is as follows. A light beam is emitted from a light source and transformed into linearly polarized light by a polarizer before it enters the sensing fiber coil. As the linearly polarized light beam propagates through the sensing fiber coil, the polarization plane of the linearly polarized light is rotated due to the Faraday effect [76]. At the end of the sensing fiber coil, the polarization plane of the light has been rotated by an angle which is given by Equation (3.3) [68].

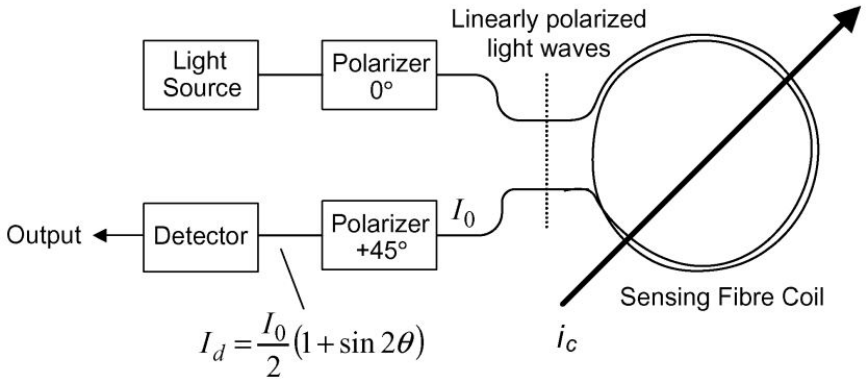

Figure 3.3: Basic polarimetric optical fiber current sensor [68]. © 2009 IEEE

When exiting the sensing fiber coil, the light beam passes through a second polarizer with a transmission axis which is oriented at 45° with respect to the transmission axis of the first polarizer. The intensity of the output light is detected by a photodetector and is given by Equation (3.4),

$$I_d = \frac{I_0}{2}(1 + \sin 2\theta) \tag{3.4}$$

where I_0 is the intensity of the input light and θ is the angle of rotation of the plane of polarization due to the Faraday effect [68]. For sufficiently small values of θ, the transfer function of the sensor is approximately linear. However, since the output light intensity is dependent on the intensity of the input light, the sensor will be sensitive to fluctuations in the input light. A solution to this issue is to modify the configuration of the sensor to the schematic shown in Figure 3.4 [68], [79].

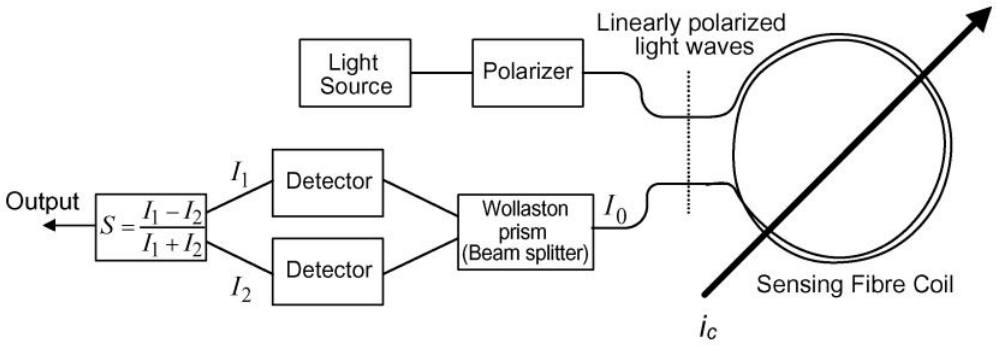

Figure 3.4: Dual polarimetric optical fiber current sensor [68]. © 2009 IEEE

In this configuration the linearly polarized light passes through a polarizing beam splitter after propagating through the sensing fiber coil. The beam splitter splits the linearly polarized light into two orthogonal linearly polarized light beams polarized at -45° and +45° with respect to the polarization of the light from the first polarizer, respectively [79], [76], [68]. The intensity of the two light beams is detected by two separate photodetectors. A signal processor calculates an output signal which is given by Equation (3.5),

$$S = \frac{I_1 - I_2}{I_1 + I_2} = \sin 2\theta \approx 2\ VNI \tag{3.5}$$

where I_1 and I_2 are the output signals from the two photodetectors [76], [68]. Equation (3.5) is only valid as long as the Faraday rotation angle is sufficiently small, that is when $\sin 2\theta \approx 2\theta$. The linearity of this type of sensor is therefore limited [68].

Sagnac Loop Interferometer Optical Fiber Current Sensor

Figure 3.5 displays the schematic of a Sagnac loop interferometer optical fiber current sensor, which measures the Faraday rotation interferometrically. A light beam is emitted from the light source and converted into linearly polarized light by the polarizer. The second coupler splits the light into two linearly polarized light beams, which subsequently propagate from the sensor electronics to the sensor head through separate polarization-maintaining fiber optic cables. Each light beam is transformed into circularly polarized light by a quarter-wave retarder before entering the sensing fiber coil [82], [76]. Quarter-wave retarders are made by the use of birefringent materials and have the following working principle. By orienting the polarization plane of the incident linearly polarized light at 45° with respect to the fast and slow axes of the retarder, the light beam is split into two orthogonal linearly polarized components with an accumulating differential phase shift. The length of the retarder is chosen in such a way that the phase shift between the two linearly polarized components equals 90° at the end of the retarder. The incident linearly polarized light is thus transformed into circularly polarized light [82].

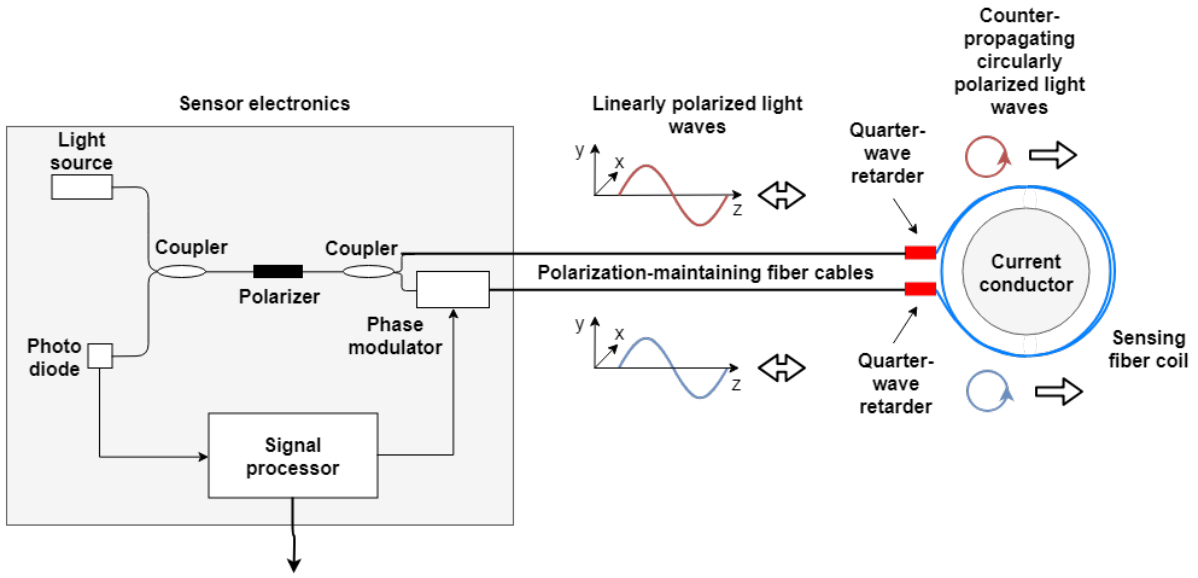

Figure 3.5: Sagnac loop interferometer optical fiber current censor. The figure is adapted from [82] © 2007 IEEE and [83] © 2002 IEEE.

As shown in Figure 3.5, the two circularly polarized light waves have the same sense of rotation, but propagate in opposite directions through the sensing fiber coil and thus with or against the direction of the magnetic field which surrounds the primary conductor [83]. Due to the Faraday effect, the speed of one of the light waves will increase, and the speed of the other decrease. When exiting the sensing fiber coil, the circularly polarized light waves are transformed back to linearly polarized light by the quarter-wave retarders. Due to the speed difference between the two light waves in the sensing fiber coil, a differential phase shift has accumulated, which is given by Equation (3.6) [68].

$$\Delta\phi_S = 2\ VNI \tag{3.6}$$

The returning linearly polarized light waves interfere at the polarizer, and the intensity of the output light, which is given by Equation (3.7), is detected by a photo diode [68].

$$I_d = \frac{I_0}{2}(1 + \cos\Delta\phi_S) \tag{3.7}$$

As can be seen from Equation (3.7), the sensitivity of the sensor is severely limited when the differential phase shift is close to zero. However, an output signal which is linearly related to the differential phase shift for $\Delta\phi_S \ll 90°$ can be obtained by the use of a phase modulator. The linearity of the sensor can be significantly improved by employing a closed-loop control scheme, as shown in Figure 3.5. In the closed-loop control scheme, the

phase modulator is used to compensate the phase shift which has accumulated between the two returning linearly polarized light waves. The differential phase shift is compensated in such a way that the two light waves are in phase when they are brought to interference at the polarizer. The size of the differential phase shift and thus the value of the primary current to be measured can be deduced from the control signal which is fed back to the phase modulator. With this control scheme the linearity of the measurement is maintained over a much wider range than for an open-loop sensor [68], [83], [84].

Reflective Interferometer Optical Fiber Current Sensor

The reflective interferometer optical fiber current sensor is another type of interferometric current sensor. The schematic of this sensor is displayed in Figure 3.6, As in the Sagnac loop configuration, the light source emits a light beam, which is subsequently transformed into linearly polarized light by the polarizer. However, in the reflective interferometer configuration, the linearly polarized light beam is split into two orthogonal linearly polarized light beams by the use of a 45° splice, and the two light beams travel towards the sensor head in the same polarization-maintaining fiber optic cable [76].

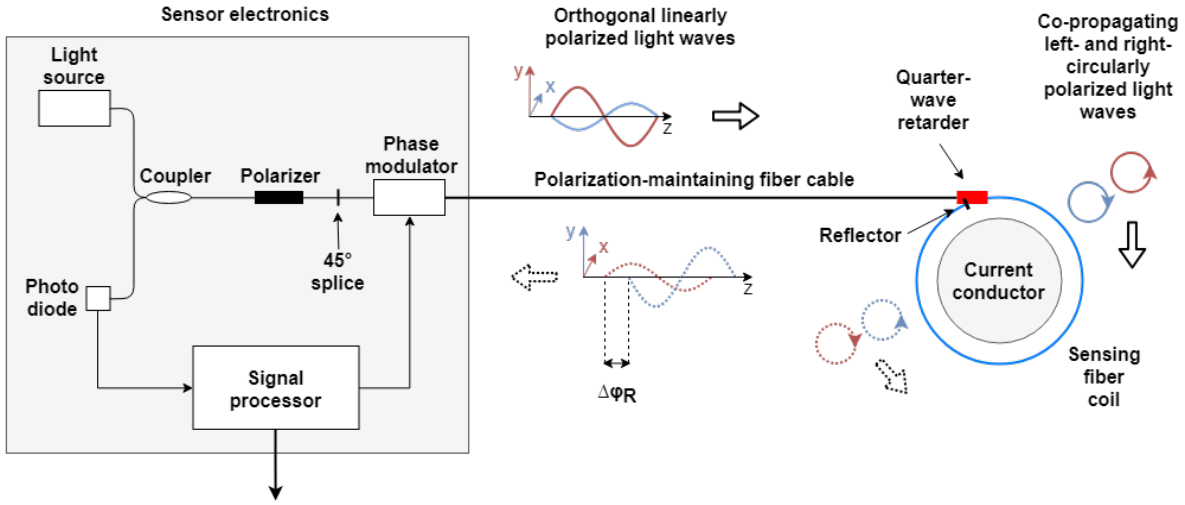

Figure 3.6: Reflective interferometer optical fiber current sensor. The figure is adapted from [85] © 2018 IEEE and [83] © 2002 IEEE.

Before entering the sensing fiber coil, the two linearly polarized light waves are converted into a right-hand circularly polarized light wave and a left-hand circularly polarized light wave by a quarter-wave retarder. At the end of the sensing fiber coil, the light waves are reflected in a mirror, and the polarization states of the waves are swapped. Thus, the forward-propagating right-hand circularly polarized light wave propagates back to the

quarter-wave retarder as a left-hand circularly polarized light wave and vice versa. Due to the Faraday effect, a phase shift accumulates between the two light waves as they propagate through the sensing fiber coil. When the light waves exit the sensing fiber coil, the differential phase shift is given by Equation (3.8). As can be seen, the differential phase shift is twice as big as for the Sagnac loop interferometer configuration due to the polarization swapping. Thus, the sensitivity of the sensor is also twice as high [68], [76], [83].

$$\Delta\phi_R = 4\,VNI \tag{3.8}$$

The circularly polarized light waves are converted back to two orthogonal linearly polarized light waves by the quarter-wave retarder and are brought to interference at the polarizer. In order to obtain the differential phase shift which is caused by the Faraday effect and thereby the value of the primary current, similar open-loop and closed-loop schemes to those described for the Sagnac loop interferometer configuration can be applied [68], [76].

3.3.2 Bulk Glass Optical Current Sensors

The other type of OCTs is the bulk glass optical current sensors. Instead of using optical fiber as the sensing element, these current sensors make use of magneto-optical glass or crystal. The sensing element can be shaped as a rectangular block, as shown in Figure 3.7, a triangular block or a glass ring enclosing the primary conductor. The sensor head can also be constructed as an open core which do not enclose the primary conductor entirely or simply a rod which is placed near the primary conductor [86], [87].

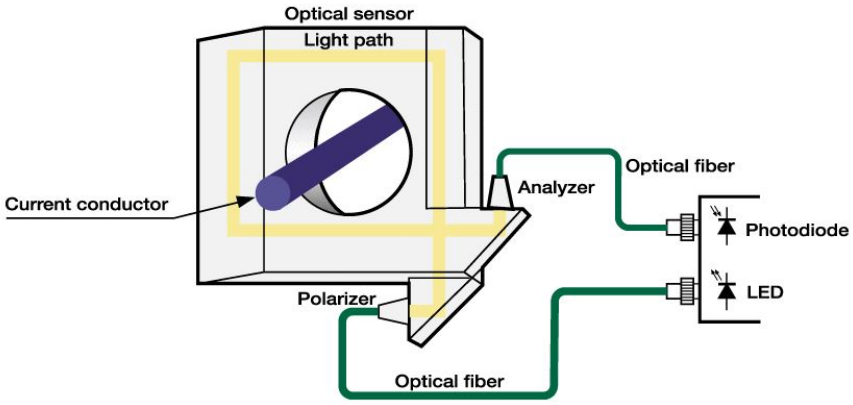

Figure 3.7: Bulk glass optical current sensor [74]. © 2015 IEEE

Bulk glass optical current sensors make use of polarimetric detection schemes in order to measure the Faraday rotation of the polarized light. The basic principle is the same as explained for the polarimetric optical fiber current sensor [74] in Subsection 3.3.1 and will thus not be repeated here.

3.4 Merging Unit

The associated MUs of OCTs is typically integrated with the sensor electronics. The signal processor, as shown in Figure 3.5 and Figure 3.6, outputs a digital signal, which is re-sampled and time stamped by the MU [35]. Standard sample rates are defined in IEC 61850-9-2 LE [54] and IEC 61869-9 [33], as mentioned in Subsection 2.4.2 and Subsection 2.4.3. The MU formats the digital samples as SV according to IEC 61850-9-2 LE and subsequently publishes the SV messages to the process bus [36]. The MU may be equipped with analog inputs, which can be used to interface Conventional Voltage Transformers (CVTs) and CCTs. These current and voltage signals are synchronized and merged with the currents which are measured by the OCT [48].

3.5 Sources of Error

Errors in OCT measurements are mainly caused by the effects of birefringence, temperature, vibration and non-ideal optical parts [74]. These effects will be described in more detail in the following subsections. For the same reasons stated in Subsection 3.3, the focus will be put on sources of error in optical fiber current sensors.

3.5.1 Linear Birefringence

Linear birefringence in the sensing fiber is the main source of error in optical fiber current sensors [74]. The linear birefringence may be intrinsic or induced by external effects. The intrinsic birefringence is caused by the fact that the shape of the sensing fiber core is not completely perfect. When it comes to induced birefringence, on the other hand, external effects, such as temperature variations and vibration, can change the linear birefringence of the sensing fiber. Linear birefringence can also be induced when the sensing fiber is bent around the primary conductor [88], [89].

Linear birefringence in the sensing fiber adversely affects the performance of optical fiber current sensors in several ways. First of all, linear birefringence may reduce the sensitivity of polarimetric sensors. As explained in Section 3.1.2, a linearly birefringent medium can

transform linearly polarized light into elliptically or circularly polarized light. If the output light from the sensing fiber coil turns into elliptically polarized light due to the linear birefringence in the sensing fiber, the sensor will be less sensitive to measuring the Faraday rotation which is induced by the magnetic field surrounding the primary conductor. If the output light is transformed into circularly polarized light, the Faraday rotation can no longer be measured [76].

The accuracy and stability of optical fiber current sensors are also disturbed by linear birefringence in the sensing fiber [76]. As already mentioned, environmental disturbances, such as vibration and temperature changes, can cause linear birefringence in the sensing fiber. As long as these disturbances are felt by the whole sensing fiber and do not vary in time, the phase shifts of the polarized light waves due to linear birefringence will generally be cancelled out in both the Sagnac loop and the reflective interferometer configurations. In the Sagnac interferometer configuration, the two counter-propagating light waves will gain phase shifts due to linear birefringence in the sensing fiber, which are equal. These phase shifts will thus be cancelled out when the two waves interfere at the polarizer. In the reflective interferometer configuration, the phase shifts due to linear birefringence are cancelled out as a consequence of the polarization swapping [90], [83].

Vibration and variations in temperature can also induce time-varying linear birefringence in the sensing fiber [88]. The effects of time-varying linear birefringence will not be cancelled out. In the Sagnac loop and the reflective interferometer configurations, the two polarized light waves are not at exactly the same point in the sensing fiber at the same time. Thus, the phase shifts which the light waves gain due to time-varying linear birefringence in the sensing fiber, will be different [78], [83]. However, the reflective interferometer configuration is about 1000 times less sensitive to vibration and temperature variations which cause time-varying linear birefringence in the sensing fiber, than the Sagnac configuration. This is due to the fact that the relative delay in time between the two co-propagating light waves in a reflective interferometer configuration is much smaller than the relative delay in time between the two counter-propagating waves in a Sagnac loop configuration [83].

There are several solutions which can be employed in order to reduce the effects of linear birefringence in optical fiber current sensors. First of all, the choice of optical fiber material has a great impact on the amount of linear birefringence in the sensing fiber. The proper choice of sensing material can reduce the amount of intrinsic linear birefringence in the sensing fiber as well as the linear birefringence caused by bending. Further reduction of the intrinsic linear birefringence of the sensing fiber can be achieved by annealing. The effects of linear birefringence can also be suppressed by inducing circular birefringence in the fiber. This can be done by twisting the sensing fiber [74], [88]. Descriptions of additional

solutions where the configuration of the sensing fiber is optimized, the configuration of the optical fiber current sensor is altered or additional optical devices are added to the sensor, can be found in [74].

3.5.2 Temperature

The accuracy of OCTs should be maintained over the whole operating temperature range [38]. In IEC 60044-8 three temperature categories are defined for NCCTs under normal service conditions. The widest ambient air temperature range is -40 °C to +40 °C [61]. All of the commercial OCTs which are considered in this thesis have specified outdoor operating temperature ranges which are equal to or wider than the one defined in IEC 60044-8 [49], [48], [46], [47].

The accuracy of OCTs may be affected by variations in the ambient temperature. This applies to both the sensor heads and the sensor electronics [74]. Variations in the temperature of the sensor heads change the Verdet constant of the optical sensing fiber. Since the amount of Faraday rotation depends upon the value of the Verdet constant, as shown in Equation (3.2), the Faraday rotation angle will change if the sensor head is subjected to temperature variations. The temperature dependency of the Verdet constant for fused silica fiber is given by Equation (3.9) [83].

$$\frac{1}{V}\frac{dV}{dT} = 0.7 \times 10^{-4}\ {}^{\circ}C^{-1} \tag{3.9}$$

As a result of the temperature dependency, the measured signal will have an error of up 0.56 % over the operating temperature range from -40 °C to +40 °C. This is not sufficient to satisfy the requirements of measuring class 0,2 S over the entire current range which is specified in IEC 60044-8. In order to meet the accuracy requirements, the temperature drift of the Verdet constant must be compensated for [74]. One solution is to equip the sensing fiber with a temperature sensor and implement temperature compensation as a part of the signal processing. IEEE recommends periodical verification of the accuracy of the temperature sensor if such a solution is employed [38]. Another solution is to make use of a quarter-wave retarder with a temperature dependency which counteracts the temperature dependency of the Verdet constant [68]. Bohnert, Gabus, Nehring and Brändle [83] demonstrated that an OCT with such a quarter-wave retarder maintained an accuracy of 0.2 % over an operating temperature range from -35 °C to + 85 °C [83].

A part of the sensor electronics which is especially sensitive to temperature variations is the light source. Superluminescent Diodes (SLEDs) are commonly used as the light

sources in OCTs [91]. The central wavelength of the light which is emitted from such a broadband semiconductor light source varies with the temperature. Since the value of the Verdet constant is dependent upon the wavelength of the light, variations in the temperature of the light source will cause variations in the Verdet constant and thus variations in the amount of Faraday rotation. In order to keep the wavelength of the light source stable, the temperature of the light source has to be controlled or compensated for [74].

3.5.3 Vibration and Stray Magnetic Fields

In a substation environment, OCTs can be subjected to vibrations, for instance due to operation of circuit breakers. Such vibrations should not affect the accuracy of OCTs [38]. However, the accuracy of Sagnac loop optical fiber current sensors may be affected by angular vibrations due to the Sagnac effect. In this configuration, two counter-propagating light waves travel around a closed circuit, as explained in Subsection 3.3.1. If the sensor experiences angular vibrations, the Sagnac effect will cause a phase shift between the two light waves, which creates an error in the measured current. However, if the OCT is constructed with a reflective interferometer configuration, the optical path does not form a closed circuit. Hence, there will be no Sagnac effect, eliminating the errors which are caused by it [76], [86], [78].

Bohnert, Gabus, Nehring and Brändle [83] experimentally compared the sensitivity of a reflective interferometer and a Sagnac loop interferometer fiber optic current sensor to linear vibrations. The sensing fiber coils of both sensors were subjected to vibrations at a frequency of 50 Hz. The acceleration of the vibrations was increased from 0 g to 10 g. Figure 3.8 shows the results of the tests. As seen in the figure, the vibrations did not affect the performance of the current sensor with the reflective interferometer configuration, in contrast to the one with the Sagnac loop interferometer configuration [83]. The results are in compliance with what was explained in Subsection 3.5.1 regarding the sensitivity of the two sensor configurations to vibrations which lead to time-varying linear birefringence in the sensing fiber.

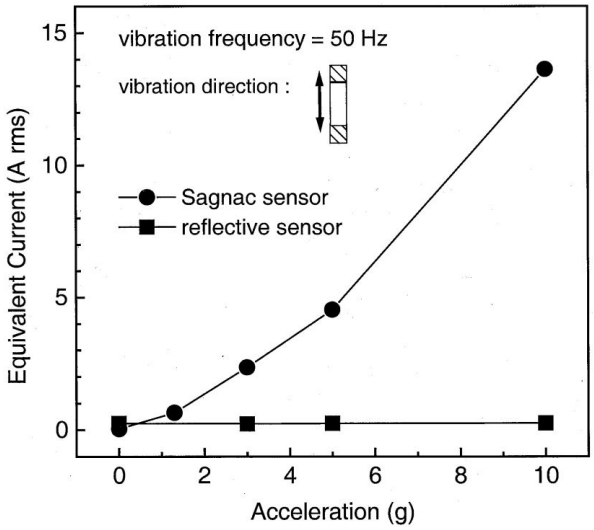

Figure 3.8: Sensitivity of a Sagnac loop and a reflective interferometer optical fiber current sensor to vibrations. The signals which were induced by the vibrations are expressed as equivalent RMS current [83]. © 2002 IEEE

The accuracy of optical fiber current sensors is not affected by external stray magnetic fields as long as the sensing fiber encloses the primary conductor entirely. If this is the case, the only current contributing to the Faraday rotation, will be the primary current which is enclosed by the sensing fiber coil. Optical fiber current sensors are therefore not affected by the magnetic fields from for instance other phases in a substation. In addition, the Faraday rotation is independent of the shape and diameter of the sensing fiber loop and of the position of the primary conductor. Thus, if the position of the primary conductor changes due to vibrations, this will not affect the accuracy of the fiber optic current sensor [82], [74], [68].

3.5.4 Non-Ideal and Aging Optical Parts

Another source of error in OCTs is optical parts which are not ideal. For instance, measurement errors may arise if the output light from the polarizers is not entirely linear or if the transmission axes of the two polarizers in a polarimetric detection scheme are not oriented at a relative angle of exactly 45°. In interferometric detection schemes, the retarders can cause errors in the measurement. The polarization plane of the input light has to be oriented at an angle of exactly 45° with respect to the fast and slow axes of the retarder. In addition, the relative angle which accumulates between the two linearly polarized components has to be exactly 90° when the light exits the retarder. If not, measurement errors will be introduced [74].

Aging of optical parts may also affect the accuracy of OCTs. For instance, as the light

source ages, the wavelength of the light changes, which will change the amount of Faraday rotation, as explained in Subsection 3.5.2. Unless the sensor electronics compensate for the changing wavelength, the accuracy of the OCT will change over time, which is undesirable since the stability of OCTs should be at least as good as that of CCTs [38].

3.6 Performance Characteristics

This section presents some of the most important performance characteristics of OCTs. In order to substantiate the descriptions, some experimental results obtained by other researchers will also be presented.

3.6.1 Linearity and Saturation

As explained in Subsection 3.3.1, OCTs have a transfer function which is linear over a limited dynamic range. However, by the use of digital signal processing, a measurement which is linear over a wide dynamic range is achieved [68]. Since OCTs do not have an iron core and employ a saturation-free measurement principle, OCTs cannot saturate [31]. Nevertheless, the measured current may be distorted in such a way that the peaks are clipped if the primary current exceeds the maximum detectable setting current of the OCT. Proper dimensioning of OCTs is sufficient to prevent distortion of the measured current. The maximum detectable setting current must simply exceed the highest short-circuit current which can possibly occur at the measurement point. This is done by designing the optical fiber current sensors with the proper number of sensing fiber coil turns. There is an inversely proportional relation between the number of sensing fiber coil turns and the maximum detectable current [50].

In 2010, Kucuksari and Karady [35] reported on an experimental comparison of a CCT and an optical fiber current sensor. Among other things, a comparison of the linearity of the two CTs was performed. The results are shown in Figure 3.9. Primary currents were applied to the optical fiber current sensor in the range from 5 to 20 times its rated current, and to the CCT in the range of 0.25 to 1.25 times its rated current. As shown in the figure, the linearity of the measurements from the optical fiber current sensor is maintained over the whole current range. The measurements from the CCT, on the other hand, become nonlinear already at an applied current of 0.8 times the rated current [35].

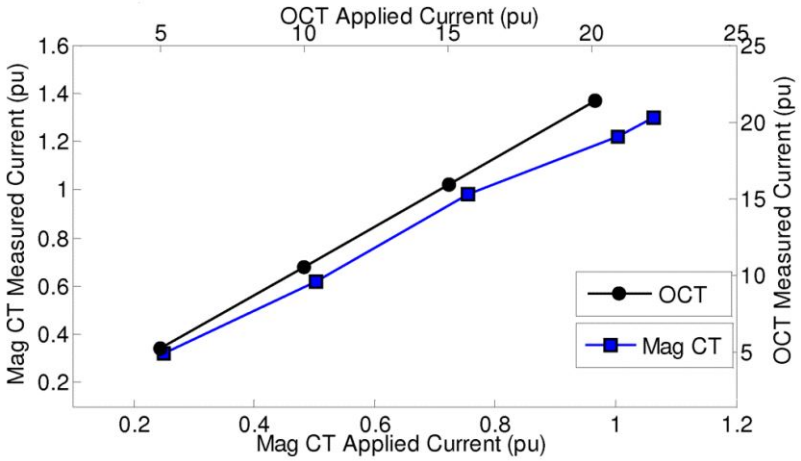

Figure 3.9: Linearity of an optical fiber current sensor compared to the linearity of a CCT. 1 pu equals 200 A and 400 A for the optical fiber current sensor and the CCT respectively [35]. © 2010 IEEE

3.6.2 Bandwidth

The bandwidth of the sensing element of OCTs is only limited by the propagation time of light between the light source and the detector. Hence, signals in a very wide frequency range (DC to GHz AC) can be measured. However, the bandwidth of the final output signal of OCTs is significantly lower. The output bandwidth is limited by the signal processing electronics, by the sample rate and by the digital communication [92], [38].

As mentioned in Section 2.4.2, the SV sample rates which are specified in IEC 61850-9-2 LE are 80 samples per cycle for measuring and protective applications and 256 samples per cycle for quality metering applications. According to the Nyquist sampling theorem, the sampling frequency should be twice as high as the highest frequency in the signal in order avoid aliasing of the input signal [7]. If the digital output of the OCT complies with the specifications in IEC 61850-9-2 LE, the output bandwidth will thus be limited to 2 kHz for measuring and protective applications and to 6 400 Hz for quality metering applications in a 50 Hz system [Appendix A].

Kucuksari and Karady [35] experimentally tested the bandwidth of the digital output of an optical fiber current sensor. A primary current with a constant amplitude and a frequency which varied from 60 Hz to 4.8 kHZ was applied to the optical fiber current sensor. The results of the test are shown in Figure 3.10. As shown in the figure, the optical fiber current sensor proved to have a bandwidth of about 2.4 kHz, which is half of the sample rate of 80 samples per cycle in a 60 Hz system [35].

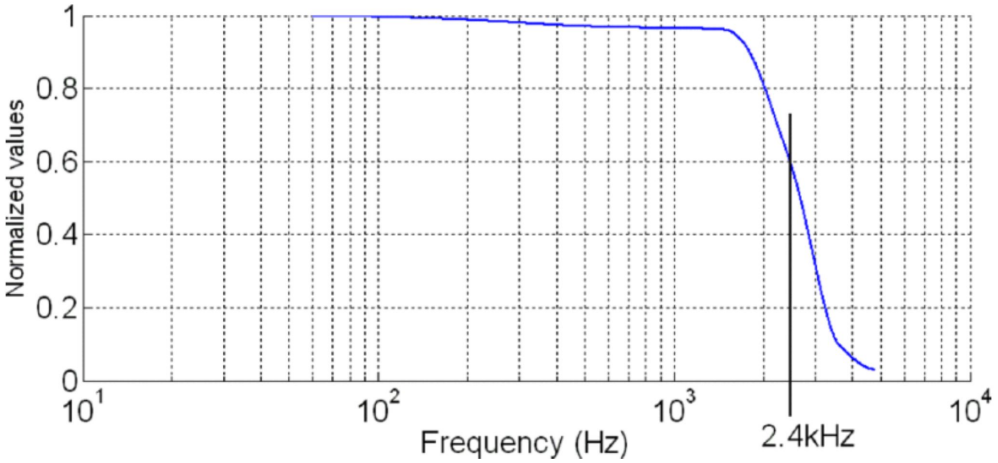

Figure 3.10: Frequency response of an optical fiber current sensor [35]. © 2010 IEEE

3.6.3 Steady State Performance

OCTs can provide a high accuracy [8] and are typically specified to conform to measuring accuracy class 0,2 S, as defined in IEC 60044-8 [38]. In 2016, Thomas et al. [93] reported on measuring the accuracy of a reflective interferometer optical fiber current sensor with a rated current of 2 kA. The results are shown in Figure 3.11. Figure 3.11a and Figure 3.11b display the magnitude and phase error of the OCT, respectively, at different current levels. The black lines indicate the requirements of measuring accuracy class 0,2 S, as defined in IEC 60044-8, and the blue dots represent the measured accuracy. The standard deviation of the measurements are represented by the red bars and the expected current error is indicated by the green lines. As shown in the figure, the magnitude and phase errors are within the standardized limits over the entire current range. However, a greater deviation in the measurements can be observed at lower current levels [93].

The limiting factor of the accuracy of OCTs is electronic noise, especially at low current levels [Appendix A]. At current levels which are significantly below the rated current of an OCT, the level of noise in the measured current may be significant [38]. In order to increase the Signal-to-Noise Ratio (SNR) of an optical fiber current sensor, the sensor can be designed with an increased number of fiber coil turns [31].

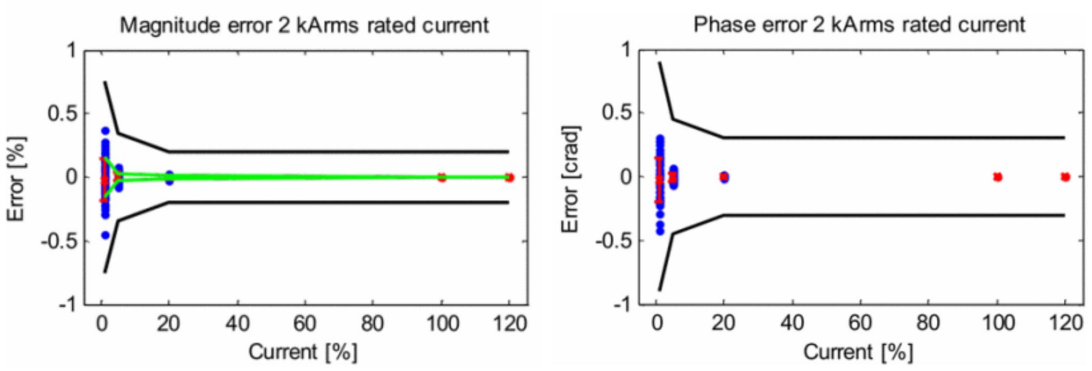

(a) Magnitude error. **(b)** Phase error.

Figure 3.11: Measured accuracy of a reflective interferometer optical fiber current sensor. The black lines indicate the requirements of measuring accuracy class 0,2 S [93]. © 2016 IEEE

Rahmamatian and Blake [8] demonstrated the ability of a reflective interferometer optical fiber current sensor to maintain a high accuracy over a wide dynamic range. The optical fiber current sensor had a rated current of 2 kA and maintained a measuring accuracy of 0.1 % over a range from 0.1 % to 180 % of the rated current (2 kA - 180 kA) [8].

3.6.4 Transient Performance

As mentioned in Subsection 2.4.4, the protective accuracy classes for OCTs are 5 P, 10 P and 5TPE, as defined in IEC 60044-8. The transient performance of OCTs is dependent on the associated sensor electronics [29]. OCTs are linear over a wide dynamic range and cannot saturate, as already stated. The primary current will thus be transformed without any distortion as long as the maximum detectable setting current of the OCT exceeds the highest short-circuit current which can possibly occur at the measurement point.

The excellent transient performance of OCTs has been confirmed by a number of researchers. Kucuksari and Karady [35] reported on performing an experimental test of the transient performance of an optical fiber current sensor. The current which was applied to the primary conductor had a maximum peak value of 20.65 times the rated primary current of the optical fiber current sensor and a DC offset which decayed within three power cycles. The resulting transient response of the OCT is shown in Figure 3.12. As seen in the figure, no signs of saturation or distortion can be observed [35].

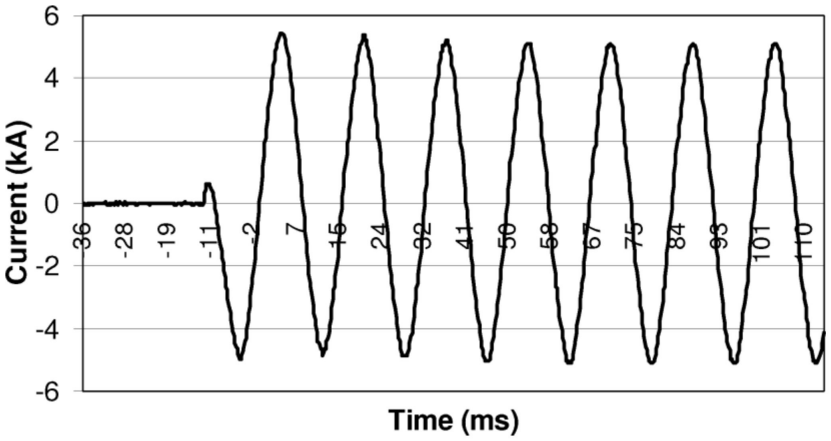

Figure 3.12: Transient response of an optical fiber current sensor [35]. © 2010 IEEE

Another transient performance test of OCTs was performed by Normandeau and Mahseredjian [94] who tested the transient performance of three OCTs. Both symmetrical and asymmetrical primary currents with a peak value in the range from 7 kA to 57 kA were applied to the OCTs. The composite and instantaneous errors of two of the OCTs were well within the limits of 5% and 10 % which are specified for protection class 5TPE in IEC 60044-8. The highest composite and instantaneous errors calculated were 1.39 % and 4.15 %, respectively. The composite and instantaneous errors of the third OCT exceeded the specified limits at an applied primary current of 57 kA_{peak}. However, it was discovered that the OCT was not correctly calibrated. The incorrect calibration was regarded as the cause of the composite and instantaneous errors exceeding the specified limits [94].

3.7 Attributes

OCT technology has been known for several decades. However, OCTs have not been widely adopted in substations yet [80], [38]. The different parts of an OCT have different expected lifetimes. The expected lifetime of the sensor heads is 30+ years, while the sensor electronics have an expected lifetime of around 15 years. The sensor electronics should thus be replaced once during the life of the sensor heads [Appendix A].

The insulation of OCTs can be made simpler than for CCTs and without use of SF_6 gas or oil. This is due to the fact that fiber optic cables are non-conductive and provide galvanic isolation [38]. OCTs have a small size and low weight, which facilitate integration into other primary equipment. This could for instance be a circuit breaker or a bushing [95]. For specific weights of commercially available OCTs, the reader is referred to Chapter 4.

Chapter 4

Commercial Products

In this chapter the attributes of some of the OCTs which are commercially available at the present time are presented and compared. Section 4.8 presents an overview of the specifications of these OCTs. OCTs from four different vendors have been considered. These will be referred to as OCT 1, 2, 3 and 4, respectively. The whole sensor electronics unit will hereafter be referred to as the MU. The information in this chapter is based on the available technical documentation of the different OCTs in addition to information obtained from contact with the vendors. In Appendix A the relevant e-mails are given.

4.1 Types of Optical Current Transformers

All of the considered OCTs except one are interferometric optical fiber current sensors with different sensor configurations [49], [48], [46], [Appendix A]. OCT 2 has a Sagnac loop interferometer configuration, while OCT 1 and OCT 3 have reflective interferometer configurations [84], [Appendix A]. The last vendor uses glass rings instead of optical fiber as the sensing element [47].

4.2 Design

All four vendors offer free-standing OCTs were each sensor head is mounted on top of an insulator. An example is shown in Figure 4.1. The insulators are dry-type insulators, either solid insulators or insulators filled with nitrogen or air, and are thus free of SF_6 gas and oil [49], [48], [46], [47]. There are also possibilities for integration of the sensor heads into other primary equipment, such as disconnecting switches and circuit breakers, or installation of the sensor heads in conjunction with other primary components, such as cable terminals and bushings [48], [47]. Other products, such as a disconnecting circuit breaker with an integrated optical current sensor and a combined optical current and voltage sensor are also on the market. The disconnecting circuit breaker combines the functionality of a disconnector, a circuit breaker and an optical current sensor into one

device [93] [Appendix A].

All of the OCTs are said to be equally suited for both measuring and protective applications [Appendix A]. The specified accuracy classes are given in Table 4.1. OCT 1 is designed with two sensing fiber coils in each sensor head and can be equipped with two MUs for redundancy. The sensor heads of OCT 2 can also be made with two sensing fiber coils in each. The only vendor which has intended to place the MU outdoor in the substation yard is the vendor of OCT 1. This MU shall be installed in a heated outdoor cubicle, which is mounted to one of the insulator support frames. The fiber optic cables connecting the MU to the sensor heads can be up to 300 m long [49], [84]. The other three vendors offer solutions where the MU is installed indoor in a protection and control panel [48], [46], [47]. The maximum length of the fiber optic cables connecting the MU to the sensor heads is typically 1000 m [47], [Appendix A].

Figure 4.1: A commercially available OCT. Courtesy of ARTECHE [48].

4.3 Interfaces and Time Synchronization

The digital output of all MUs conform to the IEC 61850-9-2 LE implementation guideline. OCT 2 is also specified to comply with the newer IEC 61869-9 standard [49], [48], [46], [47]. For time synchronization different solutions are used. At the present time only the MU of OCT 2 supports both Precision Time Protocol (PTP) and 1 Pulse Per Second (PPS) time synchronization [48]. Other vendors make use of 1PPS and possibly IRIG-B.

Only one of the vendors answered to questions regarding support of network redundancy protocols. This OCT supports both Parallel Redundancy Protocol (PRP) and High-Availability Seamless Redundancy (HSR) [Appendix A]. The MUs of OCT 2 and OCT 3 are equipped with three-phase analog voltage inputs to interface with conventional voltage transformers [48], [Appendix A]. The MU of OCT 2 also has analog current inputs, which could for instance be used to acquire the neutral current [48].

4.4 Sensitivity to Environmental Disturbances

Only one of the vendors answered to questions regarding the sensitivity of the OCT to temperature, vibration and stray magnetic fields. This vendor guarantees that the accuracy of the OCT is maintained over the whole operating temperature range. Temperature compensation is employed by the use a temperature sensor which senses the temperature of the sensing fiber [Appendix A]. Two other vendors also specify using temperature sensors [96], [46]. The operating temperature range of the different OCTs are given in Table 4.1. The contacted vendor also stated that the OCT is not sensitive to vibration or stray magnetic fields [Appendix A].

4.5 Expected Lifetime and Maintenance

The expected lifetime of the OCTs is considered to be approximately 15 years for the sensor electronics and 30 years or more for the sensor heads [Appendix A]. The vendors specify that their OCTs require no maintenance or a low level of maintenance [46], [47], [Appendix A]. According to the vendor of OCT 2, the entire OCT does not have to be replaced if a single sensor head or the MU fails. Any sensor head or MU can be replaced [Appendix A].

4.6 Weight

The total weight of one of the OCTs is estimated to be approximately 160 kg for a maximum system voltage rating of 420 kV. The weight of the sensor head is 15 kg. Another vendor specifies a total weight of 65 kg for an OCT with a maximum system voltage rating of 245 kV [Appendix A]. Information on the approximate weights of the other OCTs could not be obtained.

4.7 Price

One of the vendors estimates the price of a three-phase OCT with a maximum system voltage rating of 420 kV to be approximately 45 000 €. This includes a set of three sensor heads and one MU. Once industrialized, this OCT is expected to be more cost-effective than CCTs for voltage levels higher than 245 kV [Appendix A]. Information on the prices of the other OCTs could not be obtained.

4.8 Overview

An overview of the specifications of the different OCTs which were considered in this chapter is given in Table 4.1.

Table 4.1: Overview of the specifications of some commercially available OCTs [49], [48], [46], [47], [Appendix A].

	OCT 1	**OCT 2**	**OCT 3**	**OCT 4**
Maximum System Voltage	245 kV-800 kV	145 kV-550 kV	72.5 kV-800 kV	123 kV-800 kV
Rated Primary Current	2 kA-4 kA	Up to 2.5 kA	Up to 4 kA	Up to 5 kA
Rated Dynamic Current	164 kA	187.5 kA	210 kA	200 kA
Measuring Accuracy Class	0,2 S	0,2 S	0,2 S	Up to 0,2
Protective Accuracy Class	5 P, 5TPE	5 P	5 P	Up to 5P
Time Synchronization	1PPS	1PPS, PTP	1PPS, IRIG-B	1PPS
Network Redundancy	Not given	PRP, HSR	Not given	Not given
Temperature Range of Sensor Head	-40°C-+45°C	-40°C-+85°C	-40°C-+55°C	-40°C-+40°C
Temperature Range of Sensor Electronics	Not given	-5°C-+55°C	-5°C-+40°C	Not given

Chapter 5

Stand-Alone Merging Units

This chapter treats SAMUs. Section 5.1 describes the purpose of applying SAMUs in digital substations. In Section 5.2, the working principle of SAMUs is described and in Section 5.3 the steady state and transient performance of SAMUs are treated.

5.1 Purpose

The application of SAMUs allows CITs to be integrated into digital substations, as shown to the right in Figure 5.1. The figure compares the hardwired connections of CITs in conventional substations to the connection of CITs to the process bus by means of SAMUs in digital substations [36]. SAMUs convert the analog signals from CCTs and CVTs to digital form and publish the measurements as SV on the process bus in accordance with IEC 61850-9-2 LE [6]. This makes the measurements from CITs accessible to all of the secondary devices which are connected to the process bus. SAMUs are equipped with analog inputs where the secondary circuits of CITs can be connected [36]. Different vendors offer slightly different solutions in terms of, among other things, the number of analog inputs, support of time synchronization and the placement of the SAMU indoor in the control room or in an outdoor cubicle [48], [97], [98].

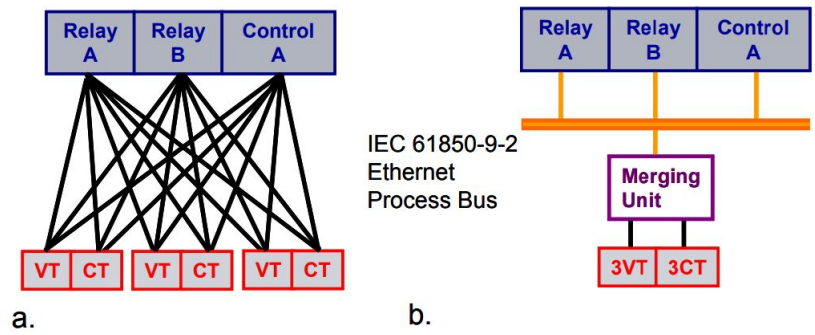

Figure 5.1: Connection of CITs to secondary IEDs [36]. © 2011 IEEE
a. Hardwired connections in a conventional substation.
b. Connection to the process bus via a SAMU in a digital substation.

5.2 Working Principle

The working principle of a SAMU is as follows. First, the analog input signals have to be scaled down to levels which are appropriate for the electronics [44]. Different manufacturers may employ different types of analog input elements for this purpose. For the current input elements, shunts, Hall elements, Rogowski coils or various types of CCTs may be used [27]. The analog signals are then filtered by an anti-aliasing filter in order to avoid aliasing of the input signal. Following the filtering, the analog signals are periodically sampled and converted from analog to digital form. The above-mentioned steps may introduce nonlinearities in the magnitude and phase angles of the signals as well as time delays. In order to remove these, digital filtering and calibration is performed. The digital data may subsequently be re-sampled in order to provide an output with the correct sample rate [44]. Typically the sample rate of the output is 80 or 256 samples per cycle, as defined in IEC 61850-9-2 LE [56].

In order to synchronize the sampling, SAMUs are equipped with an internal clock, which shall be synchronized to an external time source [33]. For this purpose, SAMUs typically receive 1PPS signals via dedicated wiring or is synchronized from the process bus by the use of PTP [7]. SV messages have a sample counter attribute called SmpCnt with a value which is set by the merging unit and used to time stamp SV. Take a sample rate of 80 samples per cycle, that is 4000 Hz, as an example. The SmpCnt of the first SV in each second will be given a value of 0000. For each successive SV within the same second, the value of the SmpCnt attribute will be increased by one until a value of 3999 is reached. The SmpCnt of the next SV is set to 0000 and the counting continues [44]. The SAMU encodes the digital data as SV and publish the messages to the process bus in accordance with IEC 61850-9-2 LE [6]. The subscribing IEDs make use of the SmpCnt attribute in combination with their own time synchronization to align the received SV in time [99].

5.3 Steady State and Transient Performance

Dutra et al. [100] compared the performance of a SAMU to the performance of a conventional analog acquisition system by the use of a digital fault recorder. The analog outputs of a relay test set were connected directly to the analog inputs of the disturbance recorder and via the SAMU. There were only small differences in the amplitude and phase angles of the recorded currents and voltages from the analog acquisition system and the SAMU when nominal currents and voltages were applied. The response of the SAMU and the analog acquisition system to transitory signals were also indistinguishable. It was further found that the SAMU had a linear output [100].

The transient performance of SAMUs will among other things depend on the chosen technology for the analog input elements. The current input elements could be shunts, Hall elements, Rogowski coils or various types of CCTs, as already mentioned. In present day protection IEDs, the current input elements are typically CCTs. These input current transformers could for instance be of the LR or NR types, which are designed with small and large air gaps in the CT cores, respectively. As mentioned in Section 2.2, air gaps in the CT core reduce the chance of saturation, but also result in a CT which cannot properly reproduce the DC component in transient primary currents. How quickly the DC component is damped out depends on the size of the air gaps [27]. As mentioned in Subsection 2.4.3, Part 13 of IEC 61869, which will apply to SAMUs once it is released, will recommend using non-saturable input elements in future SAMUs, that is other types of input elements than CCTs [60].

The typical waveform of a saturated secondary current from a CCT was shown in Figure 2.4 in Section 2.2. In the figure it can be seen that the saturated current has a very distinct waveform, which is easy to recognize. Recognizing the saturated current of input current transformers, on the other hand, may not be as simple. When a CCT saturates, most of the secondary current will flow through the magnetizing impedance for a period of time each cycle, as explained in Section 2.2. This is due to the fact that the magnetizing impedance will have a value which is considerably lower that the value of the secondary circuit impedance.

However, when it comes to the input current transformers in SAMUs or protection IEDs, the secondary circuit impedance is typically very small. Thus, a much larger current may flow through the secondary winding during saturation, and the measured current will not have the typical saturated waveform. It can be difficult to see the difference between the waveform of a saturated current from an input current transformer and the waveform of a secondary current from a CT which cannot reproduce the DC component in transient currents properly [27]. Holst and Zakonjšek [27] have presented examples of secondary current waveforms from HR, LR and NR types of CTs and a comparison of a saturated current waveform from an input current transformer and a current waveform from a CT which cannot reproduce DC components properly.

Chapter 6

Considerations in Digital Substations

In this chapter some considerations regarding the use of OCTs and other NCITs as well as SAMUs in digital substations are treated. Section 6.1 points out the differences between the measurement chains in conventional and digital substations, and Section 6.2 describes some of the requirements which will apply in digital substations. In Section 6.3, Section 6.4, Section 6.5 and Section 6.6 some considerations regarding the use of differential protection, protection IEDs, energy meters and fiber optic cables in digital substations are described, respectively.

6.1 Measurement Chain

There are some important differences between the measurement chains in digital and conventional substations. In conventional substations, the hardwired cables from the high voltage bays, which are used for measurement and control circuits, are directly connected to the analog and binary inputs of the protection, control and monitoring devices in the control building. In other words, the secondary devices are hardwired to specific pieces of primary equipment [100]. The conversion from analog to digital form of the current and voltage measurements takes place in the respective protection, control and monitoring devices.

In digital substations, on the other hand, the analog to digital conversion of current and voltage measurements has been moved from the protection, control and monitoring devices to MUs associated with NCITs and SAMUs. The current and voltage measurements from instrument transformers are converted to digital form by MUs or SAMUs in the case of NCITs and CITs, respectively. The measurements are subsequently published as SV streams to the process bus, which the secondary devices can subscribe to [100].

6.2 Requirements in Digital Substations

6.2.1 Requirements of the Protection Systems

In conventional substations, the protection systems have some requirements for the analog measuring chain in order to ensure satisfactory performance of the protection functions. Examples are requirements for the protective CT cores and the power which is provided by the CCTs in the secondary circuits. This subsection aims to point out some of the requirements which protection systems will have for the digital measuring chains in digital substations.

Transient Performance of NCITs and SAMUs

The transient performance of SAMUs and NCITs with associated MUs may affect the performance of the protection functions in digital substations. The transient performance of NCITs is specified in IEC 60044 and IEC 61869. Together with IEC 61850-9-2 and IEC 61850-9-2 LE, theses standards define the digital measuring chain of NCITs, which is of great importance in order to facilitate the realization of multivendor digital substations [18].

At the present time, manufacturers of protection IEDs specify requirements for the dimensioning of CCTs in accordance with the guidelines given in IEC 60255, "Measuring relays and protection equipment". For protection IEDs subscribing to SV over the process bus, on the other hand, guidelines on how to specify requirements for NCITs have not been defined. A possible way for the manufacturers of protection IEDs to define requirements for NCITs is to specify requirements for the frequency response of the associated MUs, similar to those which are defined in IEC 61869-6 [101]. IEC 61869-6 uses a frequency mask concept where prohibited regions of MUs' frequency response have been specified. MUs are required to operate within the defined frequency mask limits. However, these limits are are not particularly strict. For instance, IEC 61869-6 permits a low cut-off frequency of up to 1 Hz. This may cause some challenges for the manufacturers of protection IEDs [60].

In 2016 IEC Technical Committee 95, "Measuring Relays and Protection Equipment", (IEC TC 95) decided to create a new Ad hoc group (AHG 3) called "Use case of digital sampled values instead of analog input" [101]. This group is evaluating the requirements for measuring relays and protection equipment in relation to the requirements for instrument transformers [Appendix A]. One of the issues which is under consideration is if and how manufacturers of protection IEDs should define requirements for NCITs in order to

ensure satisfactory performance of the protection functions [101].

Part 13 of IEC 61869, which will apply to SAMUs, is a work in progress and has not yet been released, as mentioned in Subsection 2.4.3. At the present time, the transient performance of SAMUs is thus not standardized. It is therefore important to verify that SAMUs and protection IEDs from different vendors are interoperable in terms of transient performance [18]. As mentioned in Section 5.3, different manufacturers may employ different types of analog input elements in SAMUs, such as shunts, Hall elements, Rogowski coils or various types of input current transformers with different transient performances. Combining SAMUs which have input elements with different capabilities of reproducing DC components and low frequency components in the primary current could potentially lead to incorrect operation of protection functions, especially differential protection functions [27].

Time Delays

In digital substations, the total fault detection time is directly affected by the processing delay time of merging units, the transfer time of SV over the process bus and the communication stack processing time in the subscribing protection IEDs. These times must be added to the fault detection time of the protection IEDs in order to estimate the total fault detection time, which in turn will affect the total fault clearance time [44], [52], [18]. The different components of the total fault clearance time in a digital substation are illustrated in Figure 6.1.

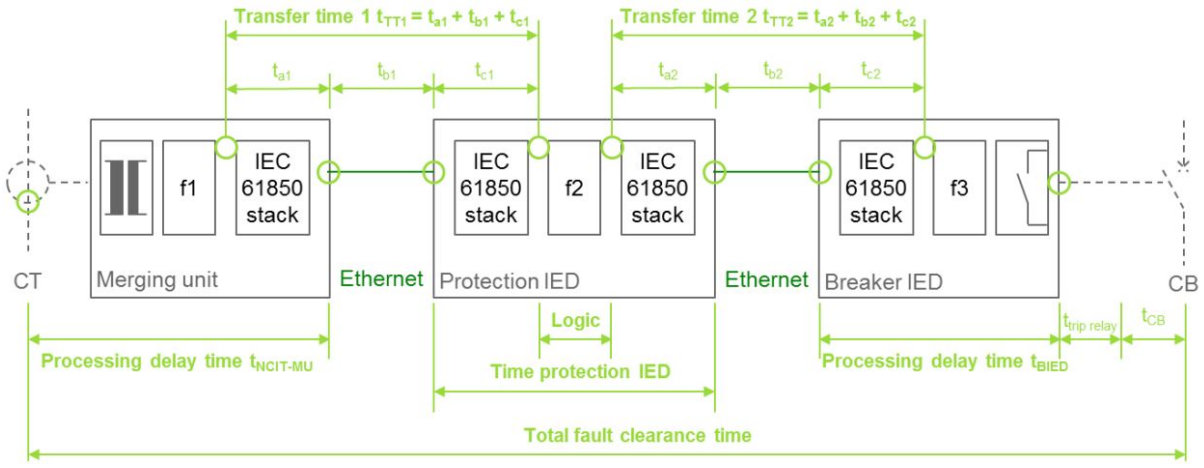

Figure 6.1: Total fault clearance time in a digital substation [18]. © 2016 IEEE

Since protection functions are time-critical functions, requirements are put on the maximum processing delay time of merging units and the maximum transfer time of SV. Application specific requirements for the maximum processing delay time of merging units

are defined in IEC 61869-9. For protective and measuring applications the maximum processing delay time is 2 ms [33].

Requirements for the transfer time of SV have also been specified. These are found in IEC 61850-5, where different transfer time classes and different message types with associated performance classes are defined. For SV (message type 4), two performance classes are defined, P7 and P8. SV which are intended for protection applications belong to performance class P7 and must satisfy transfer time class TT6 with a maximum transfer time of 3 ms [102].

As shown in Figure 6.1, the transfer time of a SV message ((t_{TT1}) comprises of the communication stack processing time of the merging unit (t_{a1}), the network transfer time over the process bus (t_{b1}) and the communication stack processing time of the receiving protection IED (t_{c1}) [52], [18], [102]. The communication stack processing times of the merging unit and the protection IED shall amount to a maximum of 40 % of the total transfer time each. Hence, 20 % or more of the total transfer time is left for the network transfer time. For protection applications this results in a maximum communication stack processing time in merging units of 1.2 ms and a network transfer time of 0.6 ms [52], [18], [103].

Time Synchronization

In digital substations, application functions which are dependent on current and/or voltage measurements from several sources require highly accurate time synchronization. Examples of such applications are differential protection and distance protection [102]. SV from different merging units cannot be aligned unless they are synchronized in time [45]. In addition, the accuracy of the sampling synchronization directly affects the accuracy of the signal processing in protection IEDs and thus the performance of the protection functions [104], [52]. Inaccuracies in the sampling synchronization give phase errors in the measured data, which could for instance result in incorrect operation of differential protection functions [45], [105].

IEC 61850-5 defines time synchronization classes for the synchronization of IEDs. The time synchronization classes T4 and T5 have the highest accuracy requirements, 4 µs and 1 µs, respectively. In a 50 Hz system, a time synchronization inaccuracy of 4 µs will result in a phase angle error of 0.1°. The resulting phase angle error of a time synchronization inaccuracy of 4 µs is 0.02° [102].

According to IEC 61850-9-2 LE, the sampling synchronization accuracy in a merging unit should satisfy the requirements of time synchronization class T4 [56]. Sampling

synchronization with an accuracy of ±4 µs will be sufficient for most protection and control applications [52]. The accuracy requirement also applies for a specified amount of time in a potential situation where the merging unit looses the external time synchronization [52]. This time is specified to be minimum 5 s in IEC 61869-9 [33], [52]. SV messages have a SmpSynch attribute which contains information regarding the quality of the sampling synchronization [33]. How measuring relays and protection equipment should behave in case they receive SV which are not time synchronized, is one of the issues IEC TC 95 AHG 3 is presently working on [101].

In order to achieve highly accurate time synchronization in a digital substations, different methods can be applied. In IEC 61869-9-2 LE it is stated that merging units shall be synchronized with a 1PPS input [56]. IEC 61869-9, on the other hand, recommends using PTP for time synchronization [33]. The distribution of 1 PPS signals requires dedicated wiring, while PTP is a network-based protocol, which allows time synchronization signals to be distributed over the process bus [106], [107]. In any case, the time synchronization source shall provide a time signal with an accuracy which is better than ±1 µs, as defined in both IEC 61850-9-2 LE [56] and IEC 61869-9 [33].

Sampled Values Message Integrity

SV messages that are malformed, missing or arrive at the protection IEDs out of sequence may affect the performance of the protection functions in digital substations [44]. Up to a certain limit, protection IEDs are typically still able to operate correctly if a some of the SV are lost [108]. Chen, Guo and Crossley [109] experimentally tested the impact of SV loss on the performance of two protection IEDs from different vendors. Six tests were carried out in total where the protection IEDs subscribed to SV generated by merging units from three different vendors, respectively. The results showed that the protection IEDs were affected differently by the loss of SV and that the type of merging unit generating the SV also had an impact. For one of the protection IEDs, the loss of SV resulted in unstable readings of the voltage. At certain loss rates, the protection IED stopped issuing trip signals. For the other protection IED, the loss of SV had different impacts on the protection IEDs within specific loss rate intervals. Based on these results it can be expected that different protection IEDs will have different limits for the acceptable loss rate of SV. [109]. How measuring relays and protection equipment should behave if SV are lost is another issue IEC TC 95 AHG 3 is presently working on [101].

Process Bus Network

A well functioning process bus network is critical for the performance of the protection functions in digital substations since the process bus enables the time-critical transmission of the required SV and protection trip GOOSE messages. The process bus network should therefore be designed in such a way that it does not limit the performance of the protection functions in digital substations. This puts requirements on, among other things, the network bandwidth, speed of transmission and availability of the network [110], [45]. The availability of the protection functions in a digital substation is directly affected by the availability of the process bus network. Thus, the process bus network has to satisfy requirements of high availability [104], [111]. In order to satisfy these requirements, the process bus network should provide bumpless redundancy. This means that there has to be an alternative path for the data traffic in the network and that the switchover from one path to the other has to take place without any time passing. Zero switchover time is achieved by having both paths in operation during normal operating conditions. IEC 61850 recommends the use of either PRP or HSR protocols to achieve bumpless redundancy [104], [7].

A poorly designed process bus network can for instance result in unacceptably long transfer times of SV or loss of SV [108], [44]. Multiple SV streams generate quite a lot of continuous data traffic in the process bus. In addition, there is other data traffic, such as GOOSE messages and time synchronization data. Designing the process bus with a sufficient bandwidth and employing network traffic management are some of the keys to achieve a well functioning process bus network [112], [104]. Statnett has designed the process bus network in their pilot digital substation with a bandwidth of 1 Gbps, which is also the bandwidth planned for future digital substations. A bandwidth of 5 Gbps would also be possible. The connection of the protection IEDs to the network is typically limited to 100 Mbps [Appendix A].

Interoperability

An important requirement in digital substations is interoperability between secondary IEDs, SAMUs and NCITs with associated MUs. Interoperability between devices from the same vendor is typically tested by the manufacturer in order to make sure that the different devices will be interoperable in a system. Interoperability testing between devices from different vendors, on the other hand, is typically more limited. Conformity with the IEC 61850 standard shall ensure interoperability between devices from different vendors. However, standards may be interpreted differently [108].

An example of standards being interpreted differently is the handling of the SV quality

attribute in merging units. The quality attribute contains information regarding the quality of the SV. Aune [113] performed research on how the quality attribute of SV are handled in digital substations [113]. IEC 61850-7-3 leaves some degrees of freedom in terms of setting the validity of the SV to questionable or invalid based on how some detail qualities, such as outOfRange and inaccurate, are set. Additional specifications for how this should be handled are given in IEC 61869-9. However, Aune's work, which was based on participation in a factory acceptance test and contact with another vendor, showed that different vendors have interpreted the handling of quality attributes differently. In addition, it has not yet been defined in any of the standards how the subscribing IEDs should respond to the quality declaration of the received SV [113], [33], [114]. This is another issue IEC TC 95 AHG 3 is presently working on [101].

6.2.2 Requirements of the Optical Current Transformers

According to one of the vendors which was contacted during the product survey on OCTs, their OCT does not pose any specific requirements for the surrounding systems in order to perform satisfactory, except for the following. There are certain requirements for the connection of the MU to the process bus in terms of physical interface, type of optical connectors and type of fiber optic cables [Appendix A]. IEC 61869-9 recommends using duplex LC type of optical connectors [33]. However, different IEDs, MUs and SAMUs may be equipped with different types of optical contacts. This was experienced during the laboratory tests which were performed as a part of this thesis. Chen, Guo and Crossley [108] also reported that the IEDs used in an interoperability performance assessment of a multivendor process bus had optical contacts which were not compatible with those of other vendors [108]. Hence, different types of fiber optic patch cords may have to be used in order to connect the devices in a digital substation. Another requirement is that the protection, control and monitoring devices have to comply with IEC 61850-9-2 LE or possibly IEC 61869-9 in order to receive the SV streams from the MUs [49], [Appendix A].

6.2.3 EMP and EMI Requirements

As mentioned in Section 4.2, different suppliers of OCTs have different solutions for the location of the associated MUs, either indoor installation in a protection and control panel or in an outdoor cubicle. Statnett is planning to employ a flexible solution with regards to the placement of the MU indoor or outdoor [Appendix A]. As mentioned in Section 2.5, there are regulatory requirements for the protection against Electromagnetic Pulse (EMP) and Electromagnetic Interference (EMI) in transmission substations. Electronic

components which are to be placed outdoor in the substation yard, have to be installed in cabinets which are secured againts EMP and EMI [4]. This applies to both the cabinet itself and the cable feedthroughs.

6.3 Application of Differential Protection

When applying differential protection in digital substations, there are some new factors which have to be considered compared to conventional solutions with analog inputs to the protection IEDs. First of all, as already mentioned, inaccuracies in the sampling synchronization of merging units could potentially cause incorrect operation of differential protection functions. It is thus important that the sampling synchronization is sufficiently accurate. Ingram, Schaub, Taylor and Campbell investigated how errors in the sampling synchronization of merging units influence the performance of transformer differential protection. Errors from 4 µs to 1000 µs were introduced in the time synchronization signal to the merging units under test. The test results showed that the transformer differential protection operated at lower differential currents than specified by the operate-restrain characteristic when synchronizing errors of 500 µs and 1000 µs were introduced. A synchronizing error of 100 µs did not affect the performance of the transformer differential protection [112].

An example of an operate-restrain characteristic of a conventional transformer differential protection is shown in Figure 6.2. If the differential current, which is the sum of the current phasors from the CTs on each side of the transformer, is above the operate-restrain characteristic and the operation of the differential protection function has not been blocked, the differential protection will trip [115]. The operate-restrain characteristic comprises of three sections with different purposes. The purpose of section 2 and 3 in the figure is mainly to prevent the differential protection from operating due to inaccuracies caused by CCTs. The performance of the CCTs on each side of the transformer may not be exactly the same, especially when the current level is high. The third section has a steeper slope in order to prevent the differential protection from operating due to CT saturation during external faults. Since OCTs are linear over a wide dynamic range and cannot saturate, the slopes of the operate-restrain characteristic can be significantly reduced in digital substation. The result is a differential protection with a higher sensitivity [18].

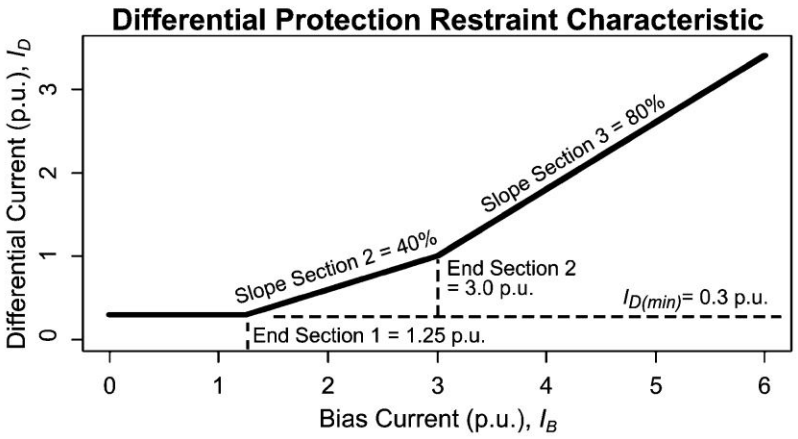

Figure 6.2: Operate-restrain characteristic of a transformer differential protection [112]. © 2013 IEEE

However, the maximum detectable setting current of OCTs has to be taken into consideration. When applying OCTs for line differential protection, it is important to ensure that the maximum detectable currents of the OCTs are equal. Unwanted operations of the differential protection may occur if the short-circuit current exceeds the maximum detectable current of one or both of the OCTs since this will cause unequal distortion of the currents which are measured. For line differential protection, the maximum detectable currents of the OCTs do not have to exceed the maximum possible short-circuit current as long as the maximum detectable currents of the OCTs are equal. If the measured currents are distorted, they will be equally distorted. When applying OCTs for busbar and transformer differential protection, on the other hand, the maximum detectable currents of the OCTs should exceed the maximum possible short-circuit current since different CT ratios are involved [50].

In future substations, differential protection may be employed in schemes which involves combinations of NCITs and SAMUs. As mentioned in Subsection 2.3.2, the migration from the present day conventional substations to digital substations will be a gradual process, and CITs are likely to be replaced on a step-wise basis. In addition, a continuous use of CITs may be desirable in some parts of substations due to lack of commercially available OCTs specified for the lowest voltage levels. An example of such a hybrid solution could be a transformer differential protection with an OCT on the High Voltage (HV) side of the power transformer and a SAMU on the LV side. In such a scheme, it is of great importance to make sure that any differences in the transient response of the different NCITs and SAMUs will not affect the performance of the differential protection functions [50], [99]. Preferably the transient responses should be similar and the currents from different MUs and SAMUs have to be accurately synchronized [50].

6.4 Application of Protection IEDs

At the present time, there are many vendors which supply protection IEDs supporting IEC 61850-9-2 LE process bus [Appendix A]. Statnett uses frame agreements with suppliers of protection IEDs and requires two separate protection IEDs supplied by different vendors for distance protection as a redundancy measure [116]. Currently, Statnett has a frame agreement with two suppliers of protection IEDs. Both of these offer protection IEDs which support IEC 61850-9-2 LE process bus. However, these protection IEDs are newer versions of protection IEDs which have been approved by Statnett. These versions will thus have to be approved before they can be applied in digital substations. In addition, it is uncertain whether good solutions for busbar protection in bigger substations are presently available [Appendix A].

6.5 Application of Energy Meters

There are regulatory requirements which apply to the electrical energy metering in transmission substations. An accredited meter inspection has to be performed by an approved accreditation company after the electrical energy meter has been put into operation in order to control the accuracy. There is currently an electrical energy meter available which can subscribe to SV measurements from an IEC 61850-9-2 LE process bus. However, so far a solution to how accredited meter inspections can be performed in digital substations has not been worked out. The issue is being discussed both internationally and within Statnett [4], [Appendix A].

6.6 Application of Fiber Optic Cables

The application of fiber optic cables reduces the need for large cable trenches. In digital substations, the large number of copper cables for measurement and control circuits, which run from the control building to the high voltage bays will be replaced by a process bus, which can be realized by a smaller amount of fiber optic cables [4]. Fiber optic cables can be laid in pipes or smaller cable trenches. The installation can be performed by blowing or pulling the cables into the pipes. It is expected that the cost of cabling and cable trenches in addition to the cost of installing the cables will be reduced in digital substations. However, special competence will be needed in order to connect the fiber optic cables [Appendix A]. Fiber optic cables are not conducting and will thus provide galvanic isolation between the connected devices [19]. In addition, fiber optic cables are not sensitive to EMI, in contrast to copper cables [117].

Chapter 7

Laboratory Test Setup and Method

In this chapter the test setup and method of the laboratory tests which were conducted in the ProSmart lab at NTNU during the spring semester of 2018 is presented. In Section 7.1 the equipment and test setup is described. Section 7.2 presents the simulations which were performed in ATPDraw and Section 7.3 describes the test method.

7.1 Test Setup

A SAM600 SAMU was tested in a laboratory test setup emulating the hybrid mode configuration of a transformer differential protection which is shown in Figure 7.1. The reason behind the choice of this particular configuration is that it allows the steady state and transient performance of the SAM600 SAMU to be investigated and compared to those of a conventional analog acquisition system. In addition, the test setup allows the performance of a transformer differential protection (RET670) in hybrid mode configuration to be investigated.

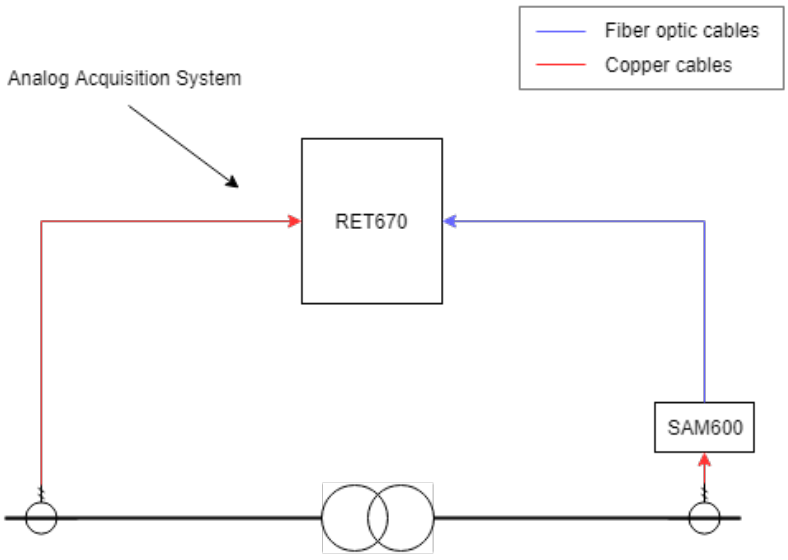

Figure 7.1: Transformer differential protection in hybrid mode configuration.

The laboratory test setup is illustrated in Figure 7.2.

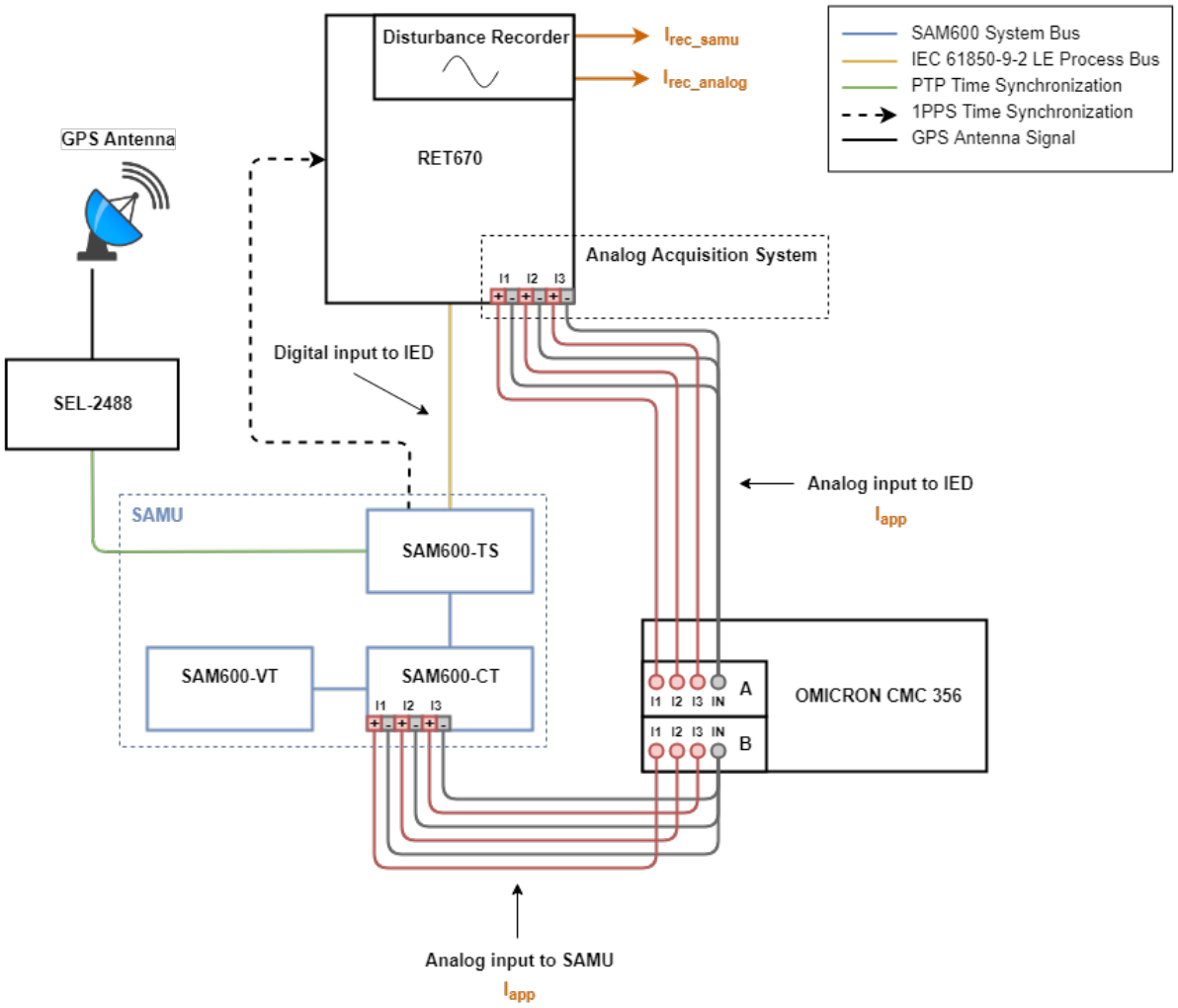

Figure 7.2: Laboratory test setup.

The test setup comprises of a OMICRON CMC 356 test set, three SAM600 SAMU modules, a SEL-2488 network clock and a RET670 transformer protection IED. In the following subsections the equipment and connections will be described in further detail.

7.1.1 OMICRON CMC 356 Test Set

The OMICRON CMC 356 test set has has six current sources, each with a maximum output of 32 A_{RMS} (45 A_{peak}). For connected loads with a resistance $R_{load} \leq 0.5\ \Omega$, the accuracy of the current outputs is given by Equation (7.1) [118].

$$Error < 0.05\ \%\ of\ reading\ value + 0.02\ \%\ of\ upper\ range\ value \tag{7.1}$$

In this test setup the six current sources were configured as two three-phase current sources. The test set has an associated software, OMICRON Test Universe, which comprises of various test modules. By the use of the Quick CMC test module, the test set can generate symmetric steady state AC currents. The Advanced TransPlay test module can be used to reproduce current waveforms from an actual fault recording or a simulation [119].

7.1.2 SAM600 Stand-Alone Merging Unit

SAM600 is a modular SAMU, which encompasses three types of modules, SAM600-TS, SAM600-CT and SAM600-VT, each with its own functionality [97]. This test setup included one of each of the three types of SAM600 modules. The modules can be connected in a chain or a ring to form a SAM600 system. Such a system may comprise of up to 10 modules, depending on the requirements for analog interfaces, communication ports and time synchronization [97].

The SAM600-CT and SAM600-VT modules are analog input modules used to interface CCTs and CVTs, respectively. Each analog input module has four analog input channels and four Ethernet communication ports, two of which are optical, the other two electrical. The SAM600-CT module can be ordered with an input current rating of 1 A_{RMS} or 5 A_{RMS} [97]. The SAM600-CT module which was used in this test setup has an input current rating of 5 A_{RMS}. The analog input elements of the SAM600-CT module are shunt resistors, and the measurement range is up to 80 times the rated current. The rated input of the SAM600-VT module can be set in the range from 100 V to 125 V. Neutral current and voltage can be configured to be measured or calculated by the analog input modules [97]. In this test setup the neutral values were set to be calculated by the analog input modules. The SAM600 system was configured by the use of ABB's Protection and Control IED manager software, PCM600.

The SAM600-TS module does not have any analog input channels and is an optional part of a SAM600 system. The purpose of the SAM600-TS module is to provide 1PPS time synchronization functionality and additional access points for connecting the SAM600 system to the process bus. The modules in a SAM600 system are time synchronized internally by the use of PTP. Any of the modules may be connected to a PTP synchronized network and used to synchronize the SAM600 system to an external time source. However, if 1PPS time synchronization is desired, a SAM600-TS module is required. The SAM600-TS module has one 1PPS input and five 1PPS outputs. The 1PPS input can be used to synchronize the SAM600-TS module and thereby the rest of the SAM600 modules in a SAM600 system to an external time source. The 1PPS outputs can be used to synchronize

other devices, such as secondary IEDs, to the SAM600 system [97].

7.1.3 SEL-2488 Satellite-Synchronized Network Clock

The SEL-2488 satellite-synchronized network clock has an associated antenna, which receives Global Navigation Satellite System (GNSS) time signals. Based on these time signals, the network clock can supply precise time, which can be used to synchronize different devices. The SEL-2488 network clock provides several options for the distribution of time. SEL-2488 is equipped with eight configurable BNC ports, which can provide IRIG-B, PPS or kPPS time signals. The network clock also supports network-based time distribution. The clock has four Ethernet ports supporting Network Time Protocol (NTP) and PTP. In this test setup, the network clock was configured to use PTP for time synchronization, providing a time stamp accuracy of ±100 ns [120].

7.1.4 RET670 Transformer Protection IED

The RET670 transformer protection IED which was used in this test setup has 6 input current transformers with a rated current of 1 A_{RMS}. The nominal range of the input current transformers is 0.2 to 40 times the rated current [121]. The RET670 protection IED was configured as a transformer differential protection for a two winding transformer by the use of PCM600. The transformer differential protection obtains the fundamental frequency differential currents in a phase-wise manner. For each phase the fundamental frequency differential current is calculated as the sum of the fundamental frequency current phasors from the LV and the HV side of the protected power transformer. The highest fundamental frequency current after taking the phase shift and ratio of the power transformer into account, is chosen as the restrain current. All fundamental frequency phase currents are referred to one side of the protected power transformer, typically the HV side [115].

The operate-restrain characteristic of the transformer differential protection is given in Figure 7.3 and the associated settings in Table 7.1. These settings are the default settings. Id_{min} is the sensitivity of Section 1, $Id_{Unrestrained}$ is the unrestrained protection limit and I2/I1 is the maximum ratio of the second harmonic component to the fundamental frequency differential current [115]. The base current, I_{Base}, was set equal to 412 A, which is the rated HV side current of a 420 kV/132 kV power transformer with 300 MVA rating. The RET670 protection IED has a disturbance recorder function, which was used to record the currents from the SAMU and the analog acquisition system. The associated software, Wavewin, was used to analyze the recorded currents.

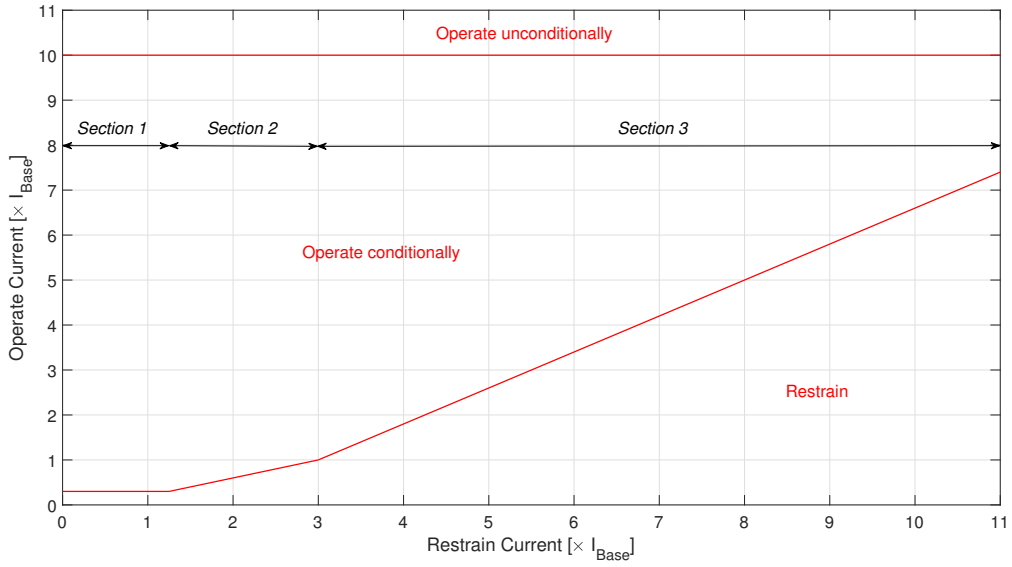

Figure 7.3: Operate-restrain characteristic of RET670 transformer differential protection. The figure is adapted from [115].

Table 7.1: Settings of RET670 transformer differential protection.

Data	Value
End of Section 1 [×I Base]	1.25
End of Section 2 [×I Base]	3
Id_{Min} [×I Base]	0.30
Slope of Section 2 [%]	40
Slope of Section 3 [%]	80
$Id_{Unrestrained}$ [×I Base]	10
I2/I1 [%]	15

7.1.5 Connections

As shown in Figure 7.2, the three SAM600 modules (SAM600-CT, SAM600-VT and SAM600-CT) were connected by Ethernet cables in a chain to form a SAM600 system. Each of the two sets of three-phase current outputs of the OMICRON CMC 356 test set were connected in a star configuration to the current inputs of the SAM600-CT module and the RET670 protection IED, respectively. The process bus represented an ideal process bus and was realized as a direct fiber optic link between the SAM600-TS module and the RET670 protection IED. For this particular test setup, several time synchronization methods and configurations were possible. The following solutions for time synchronization were considered. These are also illustrated in Figure 7.4.

1. Network-based time synchronization by the use of PTP.
2. Time synchronization by the use of 1PPS signals from SEL-2488.
3. Network-based time synchronization of SAM600-TS by the use of PTP. 1PPS signals from SAM600-TS is used to synchronize RET670.
4. Time synchronization of RET670 by the use of a GPS antenna. 1PPS signals from RET670 is used to synchronize SAM600-TS.

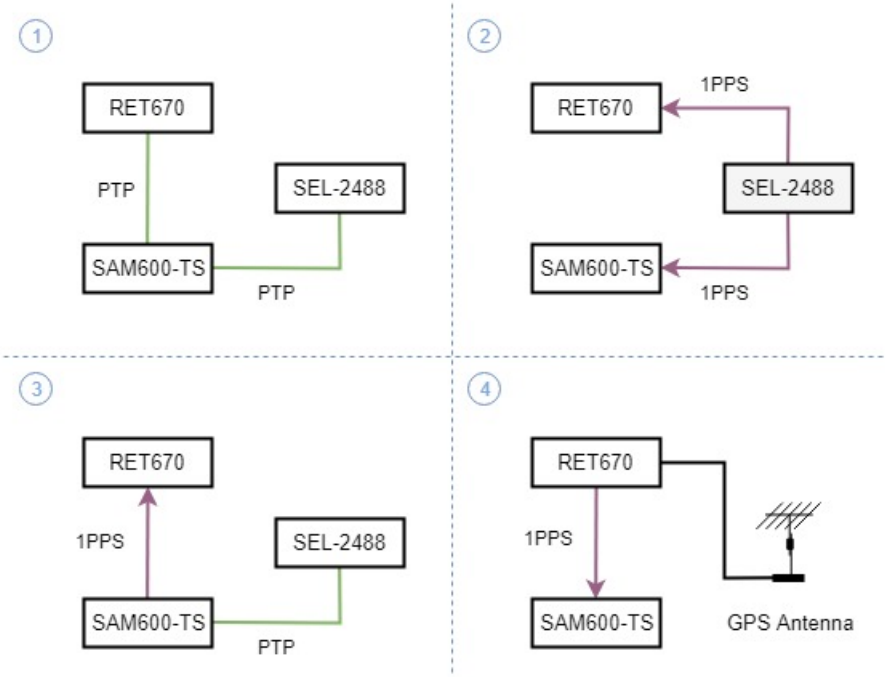

Figure 7.4: Possible time synchronization solutions.

The simplest and preferred choice for time synchronization of the devices in the test setup is the first solution. However, when using PTP for process bus time synchronization, every device which is connected to the network must support PTP [104]. Since the RET670 protection IED which was used in this test setup does not support PTP, PTP could only be used to synchronize the SAM600-TS module to the SEL-2488 network clock and to synchronize the three SAM600 modules to each other.

The second option required additional time synchronization modules to be installed in the RET670 protection IED since these were not initially present. In addition, it turned out that the 1PPS output contacts of the SEL-2488 network clock were not directly compatible with the 1PPS input contacts of the RET670 protection IED and the SAM600-TS module. The SEL-2488 network clock is equipped with electrical output contacts for for 1PPS time synchronization signals, whereas the RET670 protection IED and the SAM600-TS module

both have optical input contacts. Hence, an electrical to optical converter would have been needed, possibly introducing additional errors.

By the use of the third option, the issues of non-compatible 1PPS contacts were solved. The SAM600-TS module was connected to the SEL-2488 network clock by an Ethernet cable and synchronized by the use of PTP. The RET670 protection IED was connected to the SAM600-TS module with an additional fiber optic cable for time synchronization and synchronized by the use of 1PPS signals.

Another time synchronization method which was tested out initially is the fourth solution. This solution is not preferred since it differs significantly from the typical configuration in a digital substation. However, this solution was the only feasible solution before the time synchronization modules were installed in the RET670 protection IED. The method was tested out successfully, but was later replaced in favor of the third method following the installation of the tims synchronization modules.

7.2 ATPDraw Simulations

In order to test the SAMU in the transformer differential protection configuration shown in Figure 7.1 under different operating conditions, models for five simulation cases were created in ATPDraw. The simulation cases are listed below.

Simulation Case 1: Normal Load Conditions
Simulation Case 2: Internal High Voltage Side Fault
Simulation Case 3: Internal Low Voltage Side Fault
Simulation Case 4: External Fault
Simulation Case 5: Current Transformer Saturation
Simulation Case 6: Transformer Inrush

The basic simulation model and the different simulation cases will be described in the following subsections.

7.2.1 Basic Simulation Model

Figure 7.5 shows the basic simulation model, which represents normal load conditions. This model provides the basis for the development of the models used in the other simulation cases. The basic simulation model comprises of a supply grid, a power transformer, CTs located on each side of the power transformer and a load.

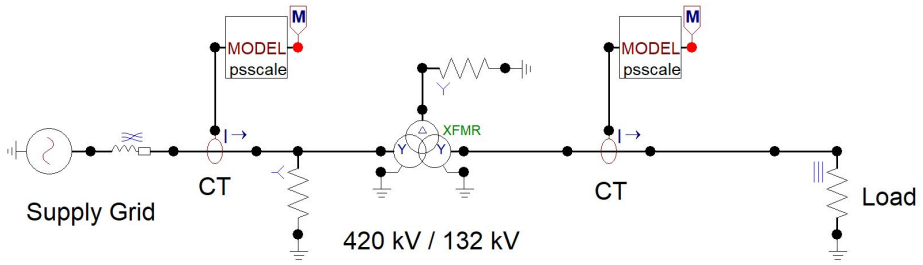

Figure 7.5: ATPDraw basic simulation model and simulation model of simulation case 1: normal load conditions.

Supply Grid

The supply grid is modelled as a three-phase AC voltage source in series with a symmetric three-phase RL coupled line. The rated line-to-line voltage of the source is 420 kV_{RMS} and the rated frequency 50 Hz. The short-circuit capacity of the supply grid was initially set to 10 000 MVA. However, in some of the simulation cases, the short-circuit capacity had to be reduced due to the limited maximum current output of the OMICRON CMC 356 test set. The positive and zero sequence impedances of the RL coupled line were calculated based on the short-circuit capacity of the supply grid in each simulation case. The reactance of the line was assumed to be ten times the resistance of the line and the zero sequence impedance three times the positive sequence impedance. The formulas used in these calculations and the resulting impedances are given in Appendix B.1.

Power Transformer

The power transformer is modelled as a three-phase three-winding hybrid transformer with a three-leg stacked core. The ratings and connections of the power transformer are given in Table 7.2. The transformer is modelled based on data of a real transformer.

Table 7.2: Ratings and connections of the power transformer.

Data	Primary (P)	Secondary (S)	Tertiary (T)
Line-to-Line Voltage [kV]	420	132	12
Apparent Power [MVA]	300	300	100
Connection	Y	Y	D
Phase shift [Degrees]	0	0	330

The leakage inductance and winding resistance of the power transformer is determined based on the short-circuit test results given in Table 7.3.

Table 7.3: Short-circuit test results for the power transformer.

Data	**P-S**	**P-T**	**S-T**
Impedance [%]	15	8	16
Apparent Power [MVA]	300	100	100
Loss [kW]	1000	200	250

The magnetization and losses of the legs and yokes are determined based on the results from a no-load test performed at the secondary side of the power transformer. The no-load test results are given in Table 7.4.

Table 7.4: No-load test results for the power transformer.

Voltage [%]	**Loss [kW]**	**Current [%]**
90	75	0.03
100	100	0.04
110	125	0.1

Current Transformers

Each CT is modelled as an ideal CT by the use of a current probe whose output is divided by the rated CT ratio. For the hybrid mode configuration of the transformer differential protection shown in Figure 7.1, the current probe on the HV side of the power transformer represents the CT which is hardwired to the RET670 protection IED, while the current probe on the LV side of the power transformer represents the CT which is connected to the SAM600 SAMU. The rated secondary currents of the two CTs are set equal to the rated input currents of the RET600 protection IED and the SAM600 SAMU, respectively. The rated primary currents of the CTs are determined based on the rated power and voltages of the power transformer, which are given in Table 7.2. The formulas used in these calculations are given in Appendix B.2. The current transformer on the HV side of the power transformer has a ratio of 500 A/1 A and the current transformer on the LV side has a ratio of 1500 A/5 A.

Load

The load is modelled as a three-phase pure resistive linear branch element. The load is kept constant in all simulation cases and equal to the rated power of the power transformer (300 MW). An initial value for the resistance of the load was calculated based on the rated power and LV side voltage of the power transformer. The formulas used in these calculations and the resulting impedances are given in Appendix B.3.

7.2.2 Simulation Cases

In simulation cases 2, 3, 4 and 5, a three-phase-to-ground fault is introduced at different locations in the basic simulation model. The fault resistance is set to zero and the resistance to ground to 1 Ω.

Simulation Case 1: Normal Load Conditions

The model for the first simulation case is the basic simulation model displayed in Figure 7.5. This simulation case represents normal load conditions. The short-circuit capacity of the grid is set to 10 000 MVA.

Simulation Case 2: Internal High Voltage Side Fault

The model for the second simulation case is displayed in Figure 7.6. This simulation case represents a three-phase-to ground fault occurring after 380.7 ms on the HV side of the power transformer within the protected zone. The short-circuit capacity of the grid is set to 6 800 MVA.

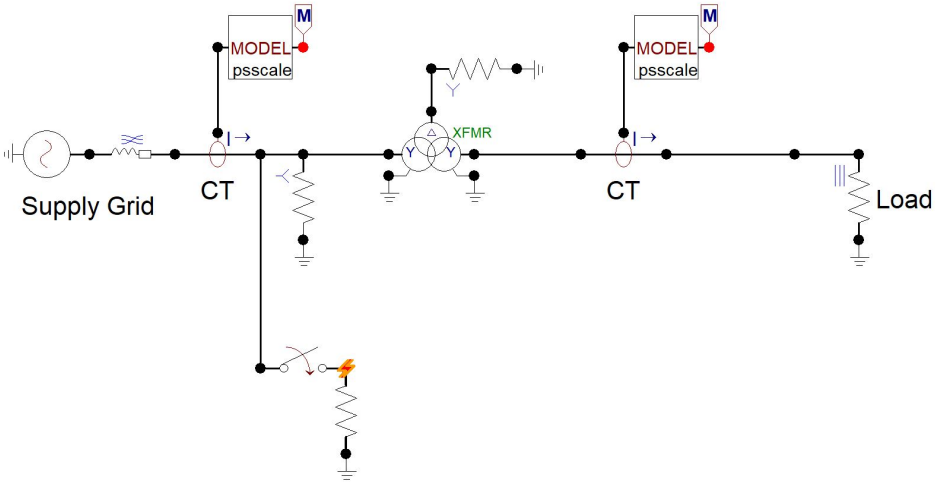

Figure 7.6: ATPDraw simulation model of simulation case 2: internal high voltage side fault.

Simulation Case 3: Internal Low Voltage Side Fault

The model for the third simulation case is displayed in Figure 7.7. This simulation case represents a three-phase-to ground fault occurring after 380.6 ms on the LV side of the power transformer within the protected zone. The short-circuit capacity of the grid is set to 10 000 MVA.

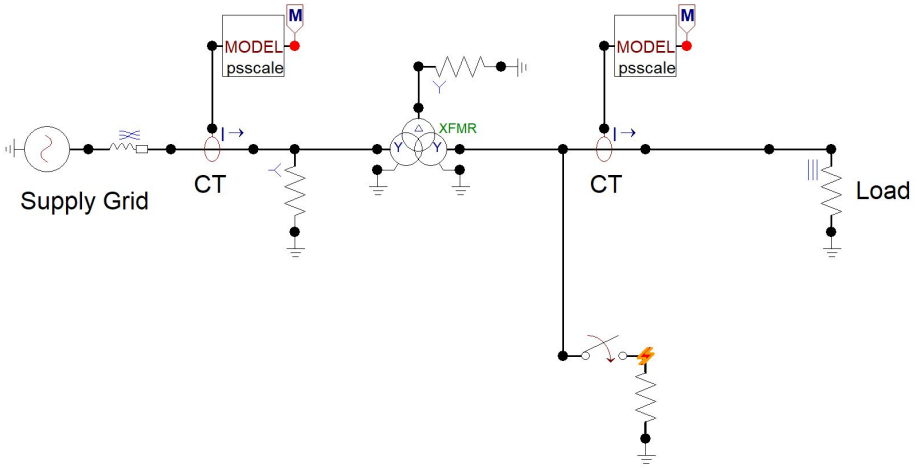

Figure 7.7: ATPDraw simulation model of simulation case 3: internal low voltage side fault.

Simulation Case 4: External Fault

The model for the forth simulation case is displayed in Figure 7.8. This simulation case represents a three-phase-to ground fault occurring after 380.9 ms on the low voltage side of the power transformer outside of the protected zone. The short-circuit capacity of the grid is set to 3 300 MVA.

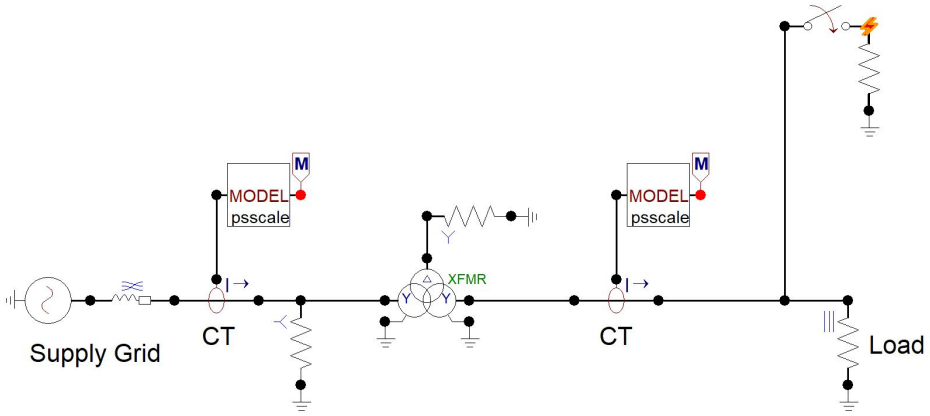

Figure 7.8: ATPDraw simulation model of simulation case 4: external fault.

Simulation Case 5: Current Transformer Saturation

In the fifth simulation case, the ideal CTs in the previous fault simulation cases are replaced by saturable CTs. The CTs are modelled as shown in Figure 7.9.

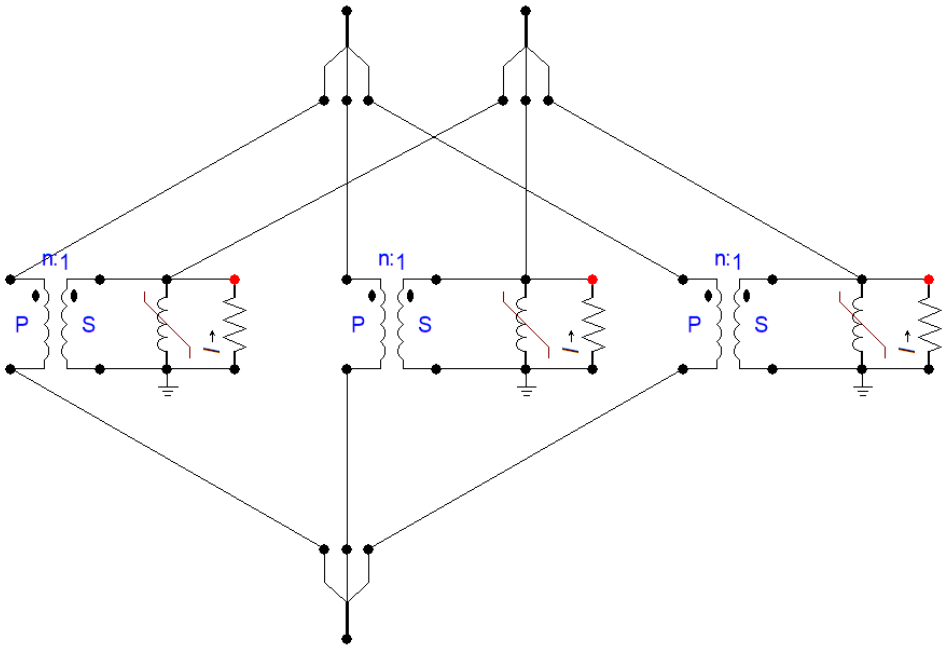

Figure 7.9: ATPDraw model of three saturable CTs.

The magnetization curves of the two CTs are shown in Figure 7.10.

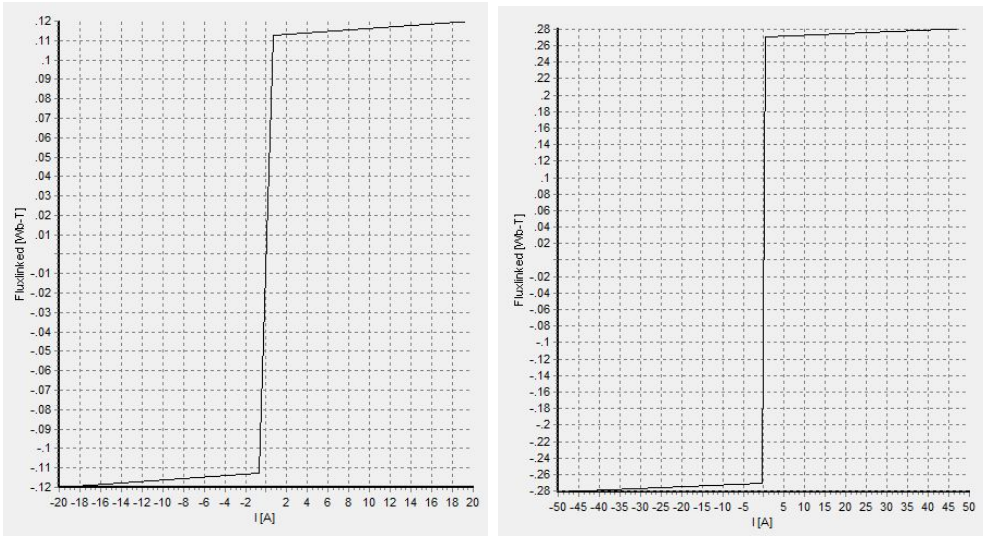

(a) HV side current transformer. **(b)** LV side current transformer.

Figure 7.10: Magnetization curves of the modelled CTs.

Simulation Case 6: Transformer Inrush

The model for the sixth simulation case is shown in Figure 7.11. This simulation case represents a transformer inrush. The load is replaced by a resistive three-phase branch with a per-phase resistance of 10 000 000 Ω in order to simulate no-load conditions. The power transformer is energized after 5 ms. The simulated current is multiplied by a factor of 10 in order to generate high enough currents for the SAMU and the protection IED to detect in the laboratory tests.

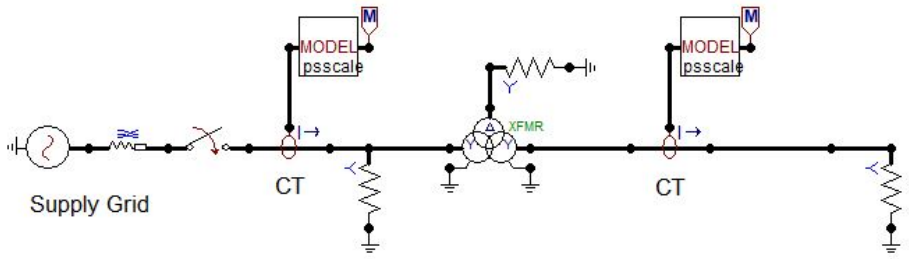

Figure 7.11: ATPDraw simulation model of simulation case 6: transformer inrush.

7.3 Method

The laboratory test setup presented in Section 7.1 and shown Figure 7.2 was used throughout all of the tests. Two sets of three-phase currents were generated by the OMICRON CMC 356 test set and applied to the current inputs of the RET670 IED and the SAM600-CT module, respectively. The applied currents will be referred to as I_{app}, as indicated in Figure 7.2. The disturbance recorder of the RET670 protection IED was used to record the currents from the SAMU and the analog acquisition system. The recorded currents will be referred to as I_{rec_samu} and I_{rec_analog}, respectively. The recordings were exported from the RET670 protection IED, loaded into Wavewin for analysis and exported as CSV-files in order to further processes the results.

7.3.1 Steady State Performance

For the steady state tests, the current transformer ratio settings for the SAMU and the protection IED were set to 2500 A/5 A and 500 A/1 A, respectively, in order to simplify the comparison of I_{rec_samu} and I_{rec_analog}. The power transformer ratio was set to 1:1. The steady state tests were performed using the QuickCMC test module of the OMICRON Test Universe software. Two equal sets of 50 Hz three-phase currents were generated by the test set and applied to the current inputs of the SAMU and the protection IED, respectively. Eight tests were performed in total at increasing current levels. The RMS values of I_{app} were: 1 A_{RMS}, 5 A_{RMS}, 10 A_{RMS}, 15 A_{RMS}, 20 A_{RMS}, 25 A_{RMS}, 30 A_{RMS}, 32 A_{RMS}.

The amplitudes of I_{rec_samu} and I_{rec_analog} were compared with the amplitude of I_{app}. The amplitude errors were calculated separately for the negative peaks and the positive peaks according to Equation (7.2) and Equation (7.3) and averaged over a time period of 100 cycles.

$$Amplitude\ Error\ SAMU\ [\%] = \frac{\left|\hat{I}_{rec\_samu}\right| - \left|\hat{I}_{app}\right|}{\left|\hat{I}_{app}\right|} \times 100\% \tag{7.2}$$

$$Amplitude\ Error\ Analog\ [\%] = \frac{\left|\hat{I}_{rec\_analog}\right| - \left|\hat{I}_{app}\right|}{\left|\hat{I}_{app}\right|} \times 100\% \tag{7.3}$$

where $\hat{I}_{rec\_samu}$ and $\hat{I}_{rec\_analog}$ are the peak values of the recorded currents from the SAMU and the analog acquisition system, respectively, and $\hat{I}_{app}$ is the peak value of the applied

currents from the test set. The Root-Mean-Square (RMS) values of I_{rec_samu} and I_{rec_analog} were also calculated and compared with the RMS value of I_{app}. The RMS values were calculated over a time period of one cycle (80 samples) according to Equation (7.4).

$$i_{RMS} = \sqrt{\frac{1}{n}(i_1^2 + i_2^2 + ... + i_n^2)} \quad and \quad n = 80 \tag{7.4}$$

where n is the number of samples and i_n is the instantaneous value of current sample n. The phase difference between the phase angles of I_{rec_samu} and I_{rec_analog} was calculated according to Equation (7.5) for each current sample and averaged over a time period of 100 cycles.

$$Phase\ Difference\ [^\circ] = \phi_{samu} - \phi_{analog} \tag{7.5}$$

where ϕ_{samu} and ϕ_{analog} is the phase angles of I_{rec_samu} and I_{rec_analog}, respectively. Due to lack of time synchronization between I_{app} and I_{rec_samu}/I_{rec_analog}, the phase angles of I_{rec_samu} and I_{rec_analog} could only be compared to each other, not to the phase angle of I_{app}.

7.3.2 Transient Performance

The transient performance tests were performed using the Advanced TransPlay test module of the OMICRON Test Universe software. These tests were based on the ATPDraw simulations which were described in Section 7.2. The currents from the two CTs in the different simulation case models were exported in PL4-files, imported to Advanced TransPlay and applied from the test set to the current inputs of the SAMU and the protection IED, respectively. The transient performance tests were performed in two parts.

First part: Performance of the SAMU

In order to assess the transient performance of the SAMU and to compare it to the transient performance of the analog acquisition system, the same three-phase currents were applied to the current inputs of the SAMU and the protection IED. That is to say, the currents from either the LV side or the HV side of the power transformer in the simulations were applied to both current inputs. Similarly to the steady state tests, the current transformer ratio settings for the SAMU and the protection IED were set to 2500 A/5 A and 500 A/1 A, respectively. The power transformer ratio was set to 1:1.

A Discrete Fourier Transform (DFT) was performed in MATLAB in order to filter out the fundamental frequency and second harmonic components from I_{rec_samu} and I_{rec_analog} when fault currents and transformer inrush currents were applied, respectively.

Second part: Performance of the Transformer Differential Protection

In order to investigate the response of the transformer differential protection, the actual three-phase currents from the simulations cases were applied to the inputs of the SAMU and the protection IED. That is to say, the currents from the HV side of the power transformer were applied to the protection IED and the currents from the LV side of the power transformer were applied to the SAMU. The current transformer ratio settings for the SAMU and the protection IED were set to 1500 A/5 A and 500 A/1 A, respectively, in accordance with the CT ratios in the simulation model. The power transformer ratio was also set in accordance with the power transformer ratio in the simulation models. A DFT was performed in MATLAB in order to filter out the fundamental frequency components from I_{rec_samu} and I_{rec_analog} when fault currents were applied. The fundamental frequency differential currents were subsequently calculated. The response times of the transformer differential protection to the fault currents from the different simulation cases were recorded by the disturbance recorder in the protection IED.

Chapter 8

Laboratory Results

In this chapter the most important results from the laboratory tests which were described in Chapter 7 are presented. The findings will be discussed in Chapter 9. The results of the steady state and transient performance tests are given in Section 8.1 and Section 8.2, respectively. A summary of the response of the transformer differential protection to the currents from the different simulation cases is presented in Section 8.3.

8.1 Steady State Performance

Figure 8.1 shows the steady state response of the SAMU and the analog acquisition system at applied currents (I_{app}) of 1 A_{RMS} and 32 A_{RMS}, respectively. These two current levels represent the lowest and the highest currents which were applied to the current inputs of the SAMU and the analog acquisition system during the steady state tests. $I_{rec\_samu\_x}$ and $I_{rec\_analog\_x}$ are the recorded currents from the SAMU and protection IED, respectively, where x = A, B, C indicates the three phases A, B and C.

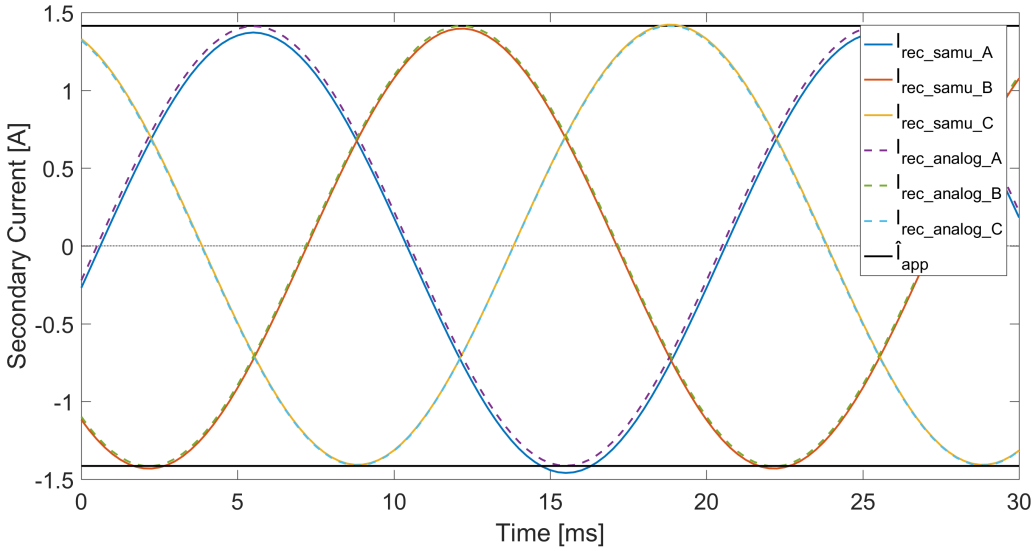

(a) Steady state response at $I_{app} = 1\ A_{RMS}$.

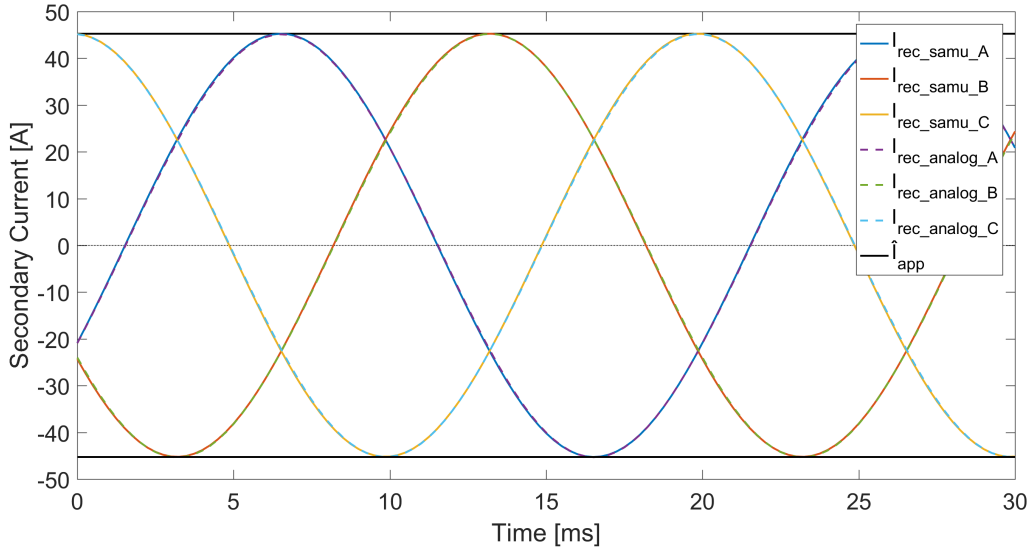

(b) Steady state response at $I_{app} = 32\ A_{RMS}$.

Figure 8.1: Steady state response of the SAMU and the analog acquisition system.

8.1.1 Amplitude

Figure 8.2, Figure 8.3 and Figure 8.4 display the average amplitude errors of phase A, B and C, respectively, of I_{rec_samu} and I_{rec_analog} at increasing levels of I_{app}. The amplitude errors were calculated by the use of Equation (7.2) and Equation (7.3) given in Section 7.3.1.

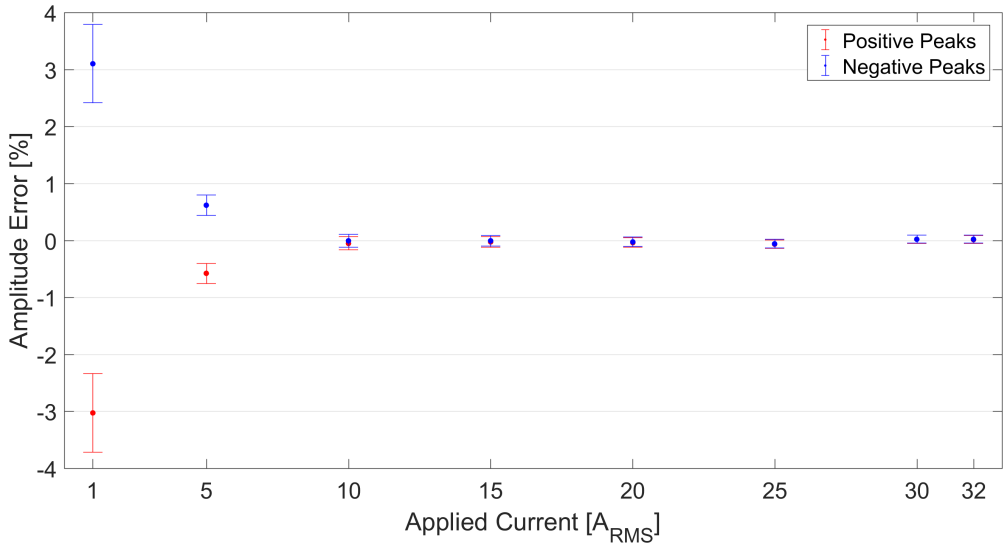

(a) Average amplitude error of I_{rec_samu}.

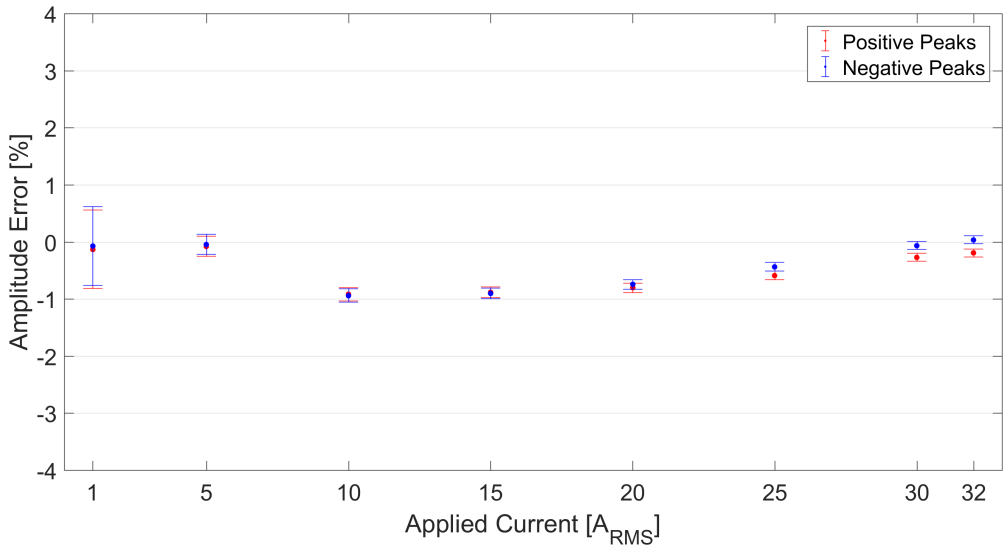

(b) Average amplitude error of I_{rec_analog}.

Figure 8.2: Average amplitude error of phase A. The dots represent the average amplitude errors and the error bars the errors in the current output from the test set.

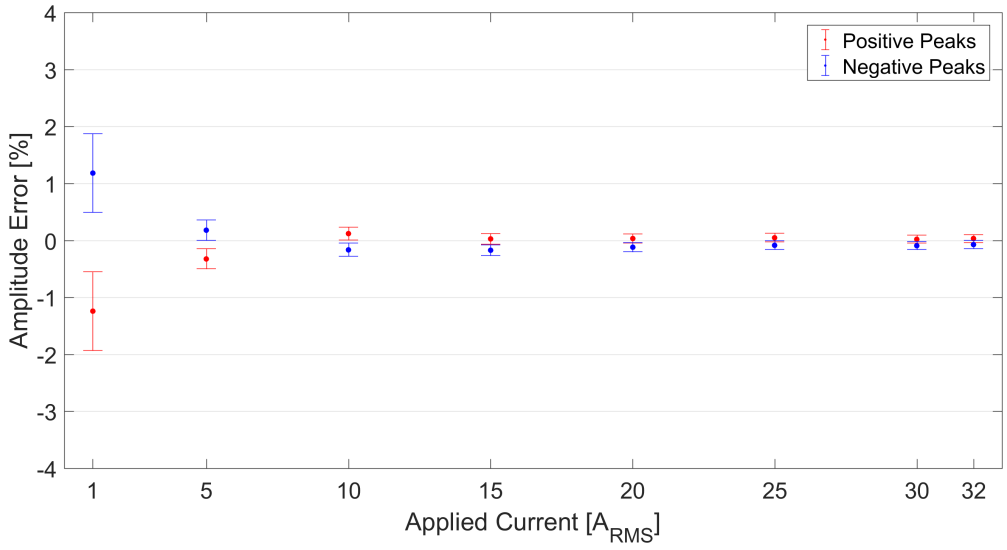

(a) Average amplitude error of I_{rec_samu}.

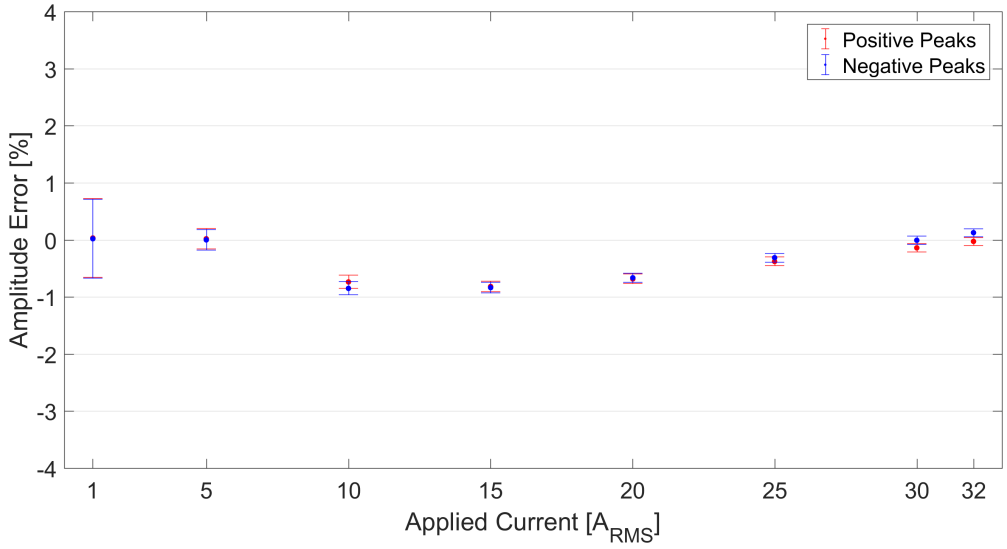

(b) Average amplitude error of I_{rec_analog}.

Figure 8.3: Average amplitude error of phase B. The dots represent the average amplitude errors and the error bars the errors in the current output from the test set.

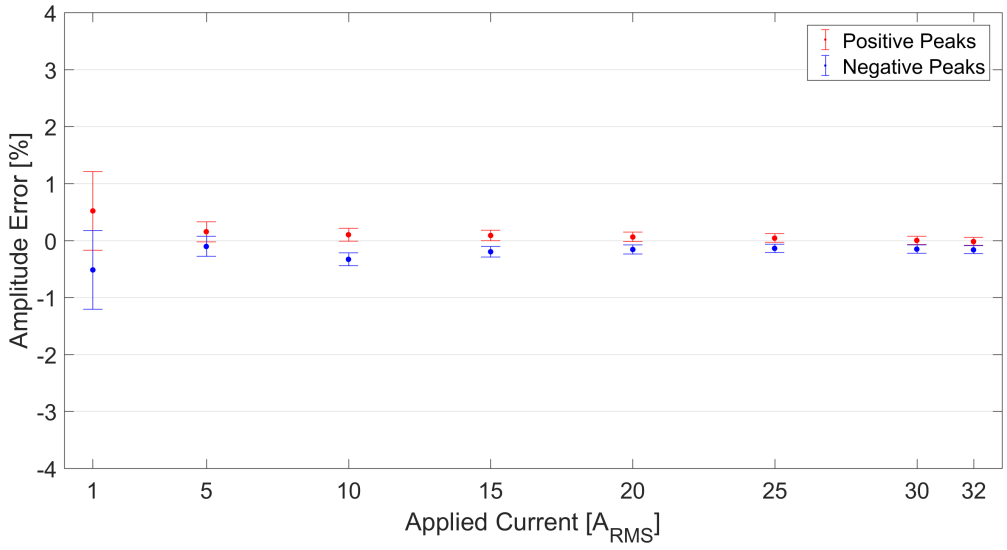

(a) Average amplitude error of I_{rec_samu}.

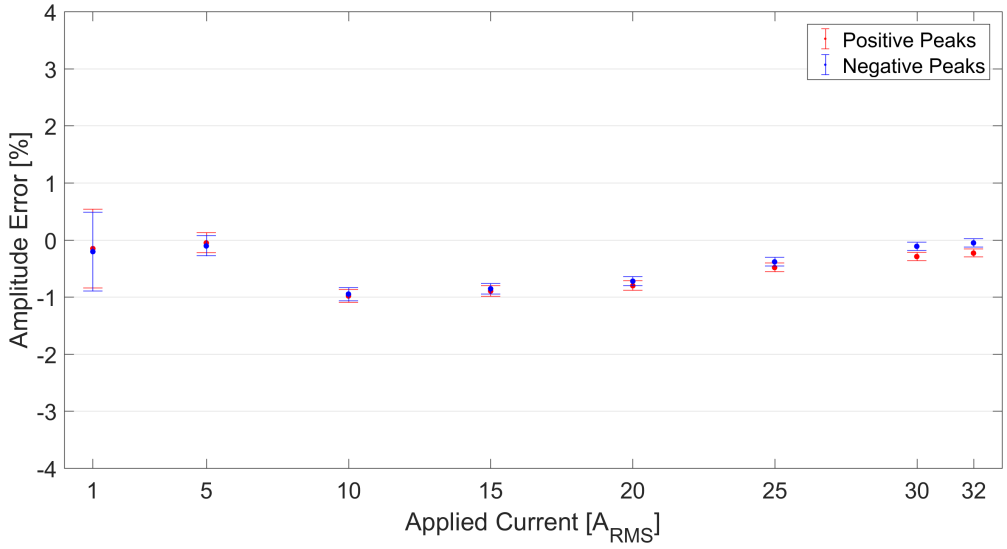

(b) Average amplitude error of I_{rec_analog}.

Figure 8.4: Average amplitude error of phase C. The dots represent the average amplitude errors and the error bars the errors in the current output from the test set.

In Figure 8.5 the average peak values of I_{rec_samu} at increasing levels of I_{app} are plotted. The plot of the peak values of I_{rec_analog} was practically identical and is therefore not shown.

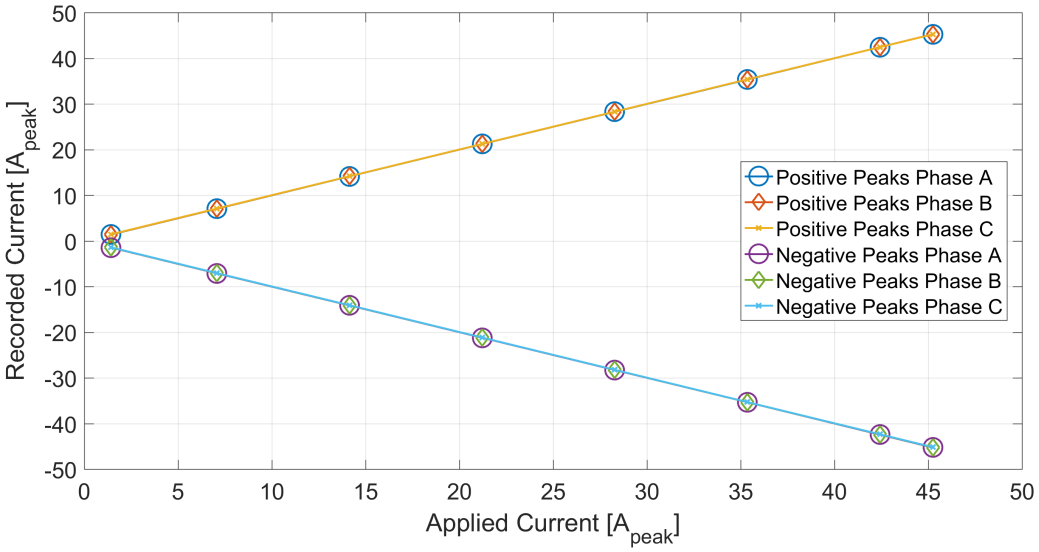

Figure 8.5: Average peak values of I_{rec_samu}.

The RMS values of phase A of I_{rec_samu} and I_{rec_analog} are given in Table 8.1. The RMS values of the other two phases were almost identical and are therefore not given. The RMS values were calculated by the use of Equation (7.4) given in Section 7.3.1.

Table 8.1: RMS values of phase A of I_{rec_samu} and I_{rec_analog}.

$\mathbf{I_{app}}$ $[\mathbf{A_{RMS}}]$	$\mathbf{I_{rec\_samu}}$ $[\mathbf{A_{RMS}}]$	$\mathbf{I_{rec\_analog}}$ $[\mathbf{A_{RMS}}]$
1 A	1.00	1.00
5 A	5.00	5.00
10 A	10.0	9.94
15 A	15.00	14.88
20 A	20.00	19.84
25 A	25.00	24.85
30 A	30.01	29.89
32 A	32.01	31.91

8.1.2 Phase Angle

Figure 8.6 displays the average phase difference between the phase angles of I_{rec_samu} and I_{rec_analog} at increasing levels of I_{app}. The phase differences were calculated by the use of Equation (7.5) given in Section 7.3.1.

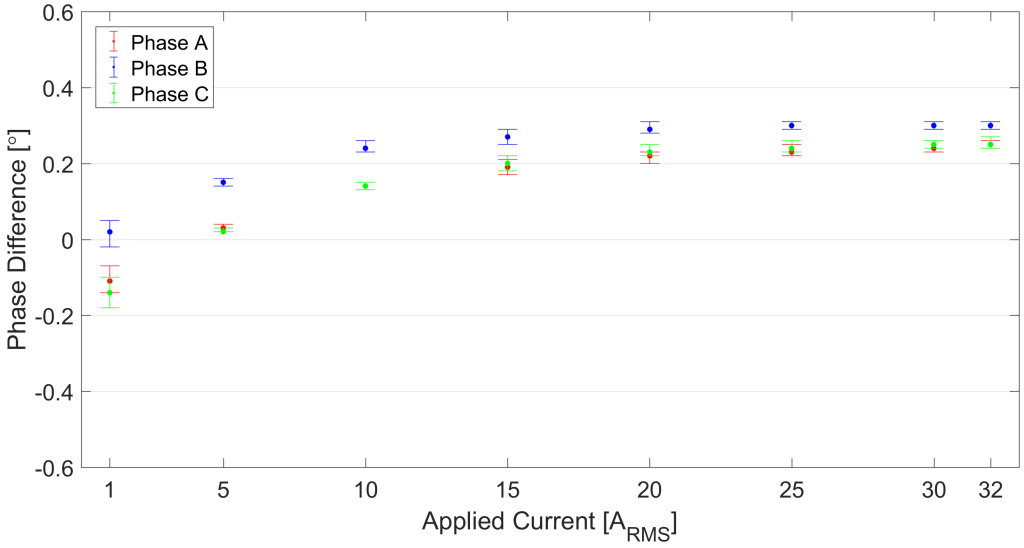

Figure 8.6: Average phase difference between the phase angles of I_{rec_samu} and I_{rec_analog}. The dots represent the average phase difference and the error bars the minimum and maximum phase differences.

8.2 Transient Performance

8.2.1 Faults

The transient response of the SAMU and the analog acquisition system to fault currents of different magnitudes are shown in Figure 8.7 and Figure 8.8. I_{app} represents the currents on the HV side and the LV side of the power transformer during an external fault, respectively. The transient responses to the internal faults on the HV side and the LV of the power transformer were very similar to the ones shown in Figure 8.7 and Figure 8.8 and are therefore not given.

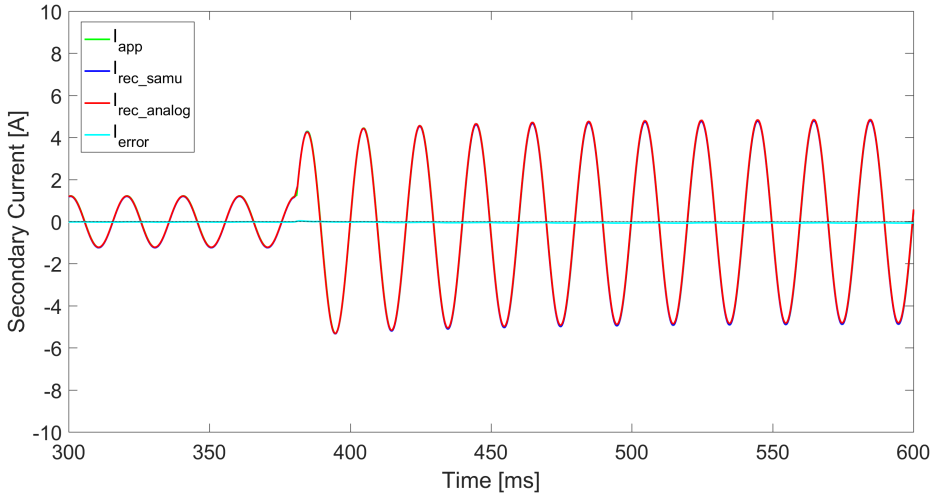

(a) Transient response of phase A.

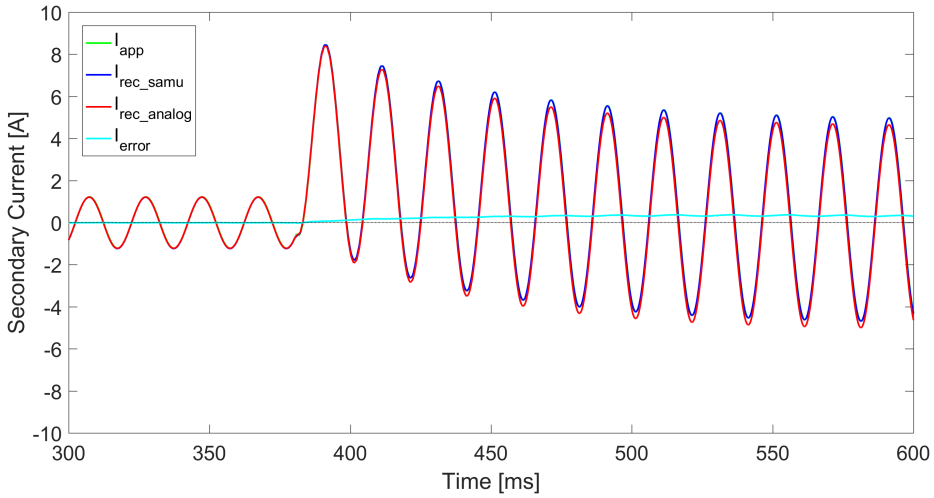

(b) Transient response of phase B.

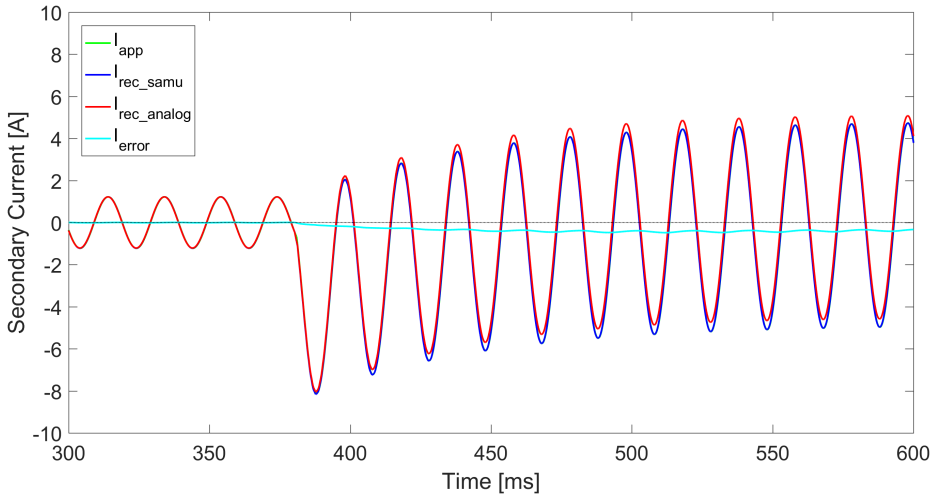

(c) Transient response of phase C.

Figure 8.7: Transient response of the SAMU and the analog acquisition system to fault currents. I_{app} represents the fault currents on the HV side of the power transformer during an external fault. I_{app} cannot be seen in the plots since it is hidden by I_{rec_samu}. I_{error} is the difference between I_{rec_samu} and I_{rec_analog}.

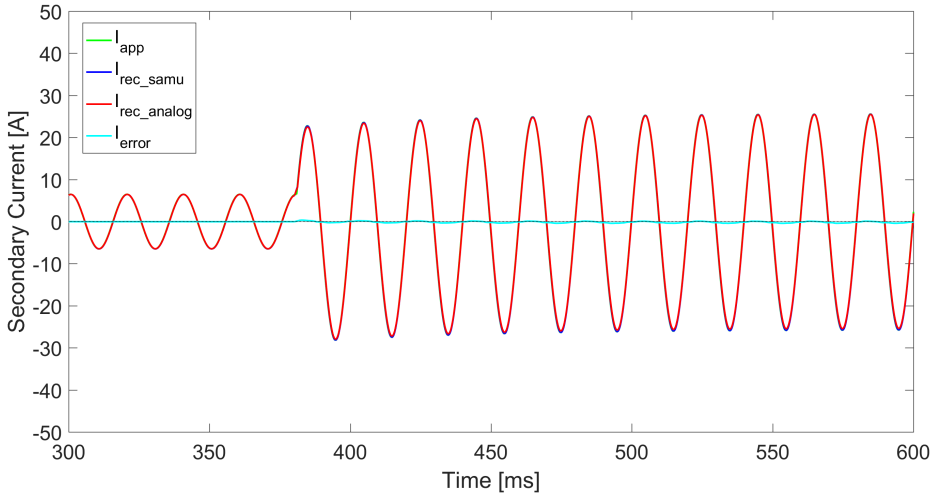

(a) Transient response of phase A.

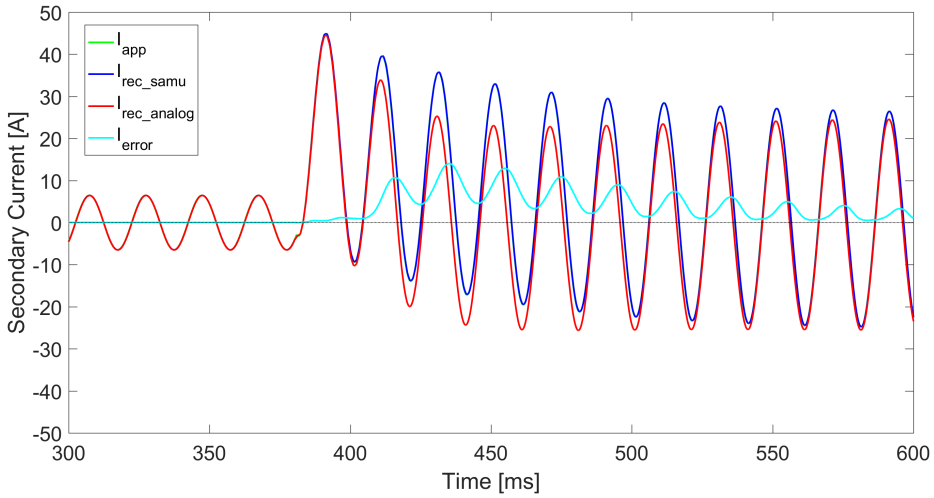

(b) Transient response of phase B.

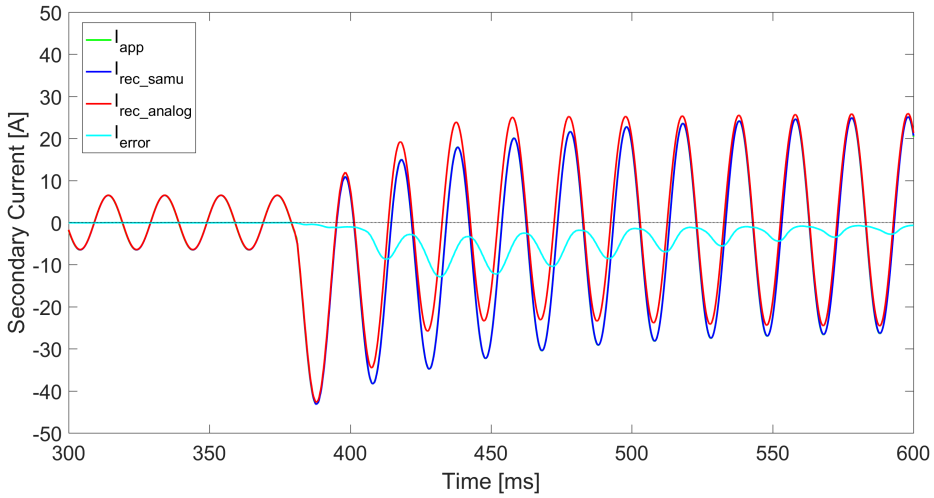

(c) Transient response of phase C.

Figure 8.8: Transient response of the SAMU and the analog acquisition system to fault currents. I_{app} represents the fault currents on the LV voltage side of the power transformer during an external fault. I_{app} cannot be seen in the plots since it is hidden by I_{rec_samu}. I_{error} is the difference between I_{rec_samu} and I_{rec_analog}.

8.2.2 Current Transformer Saturation

Figure 8.9 shows the transient response of the SAMU and the analog acquisition system to saturated fault currents. No saturation occurred in phase A, and the transient response of this phase is therefore not given. I_{app} represents the saturated fault currents on the LV side of the power transformer during an external fault. The transient responses to the saturated currents from the internal faults on the HV side and the LV of the power transformer were very similar to the ones shown in Figure 8.9 and are therefore not given.

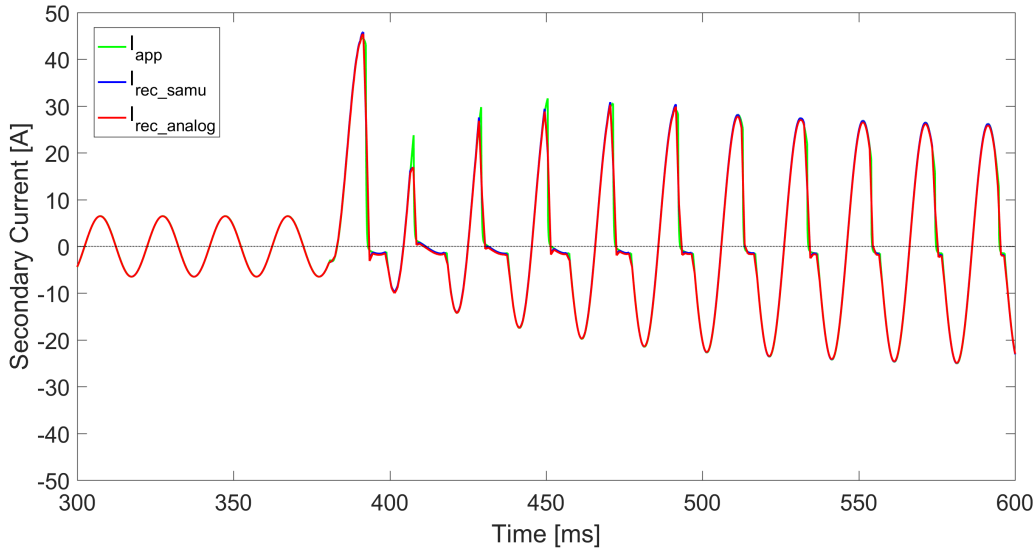

(a) Transient response of phase B.

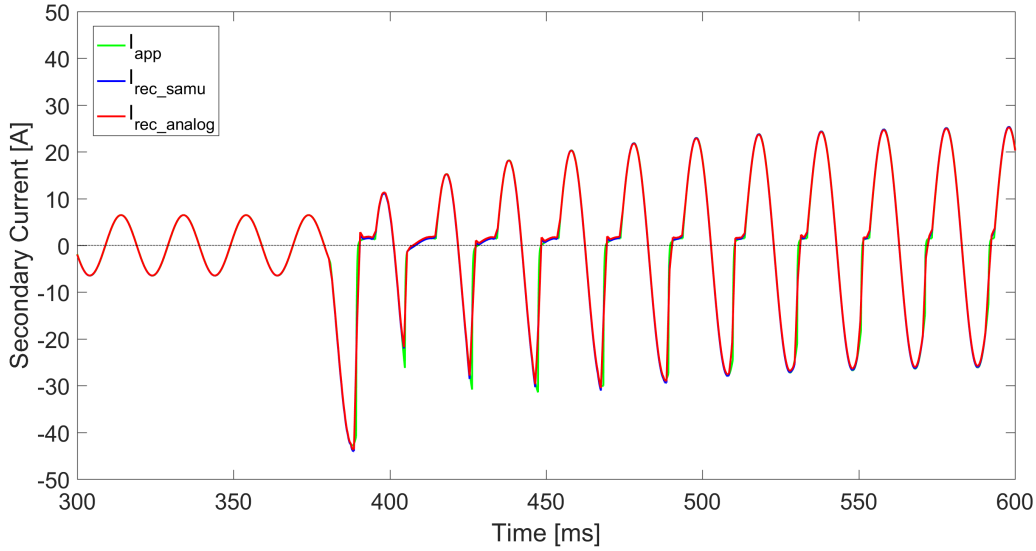

(b) Transient response of phase C.

Figure 8.9: Transient response of the SAMU and the analog acquisition system to saturated fault currents. I_{app} represents the saturated fault currents on the LV voltage side of the power transformer during an external fault.

8.2.3 Transformer Inrush

The transient response of the SAMU and the analog acquisition system to transformer inrush currents is shown in Figure 8.10 and zoomed in in Figure 8.11.

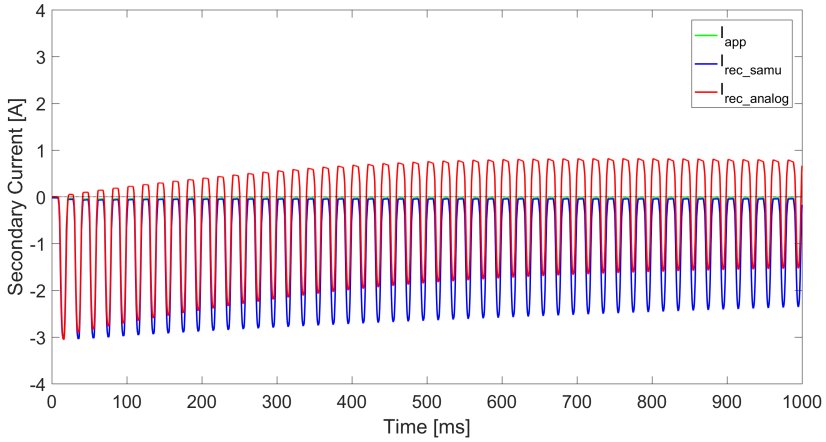

(a) Transient response of phase A.

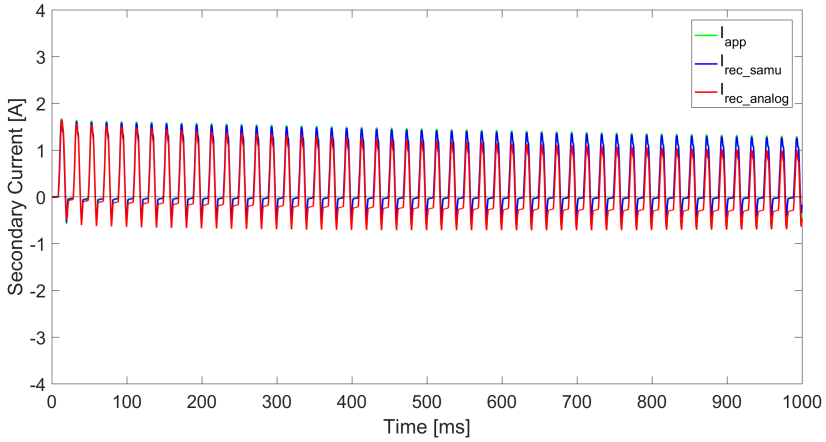

(b) Transient response of phase B.

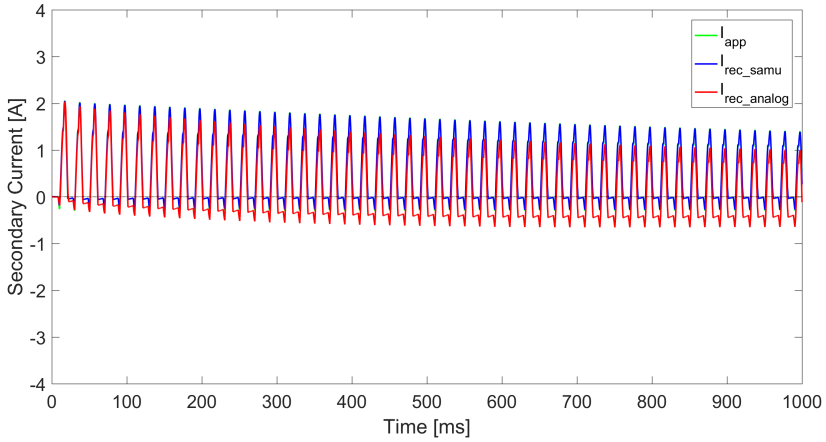

(c) Transient response of phase C.

Figure 8.10: Transient response of the SAMU and the analog acquisition system to transformer inrush currents. I_{app} cannot be seen in the plots since it is hidden by I_{rec_samu}.

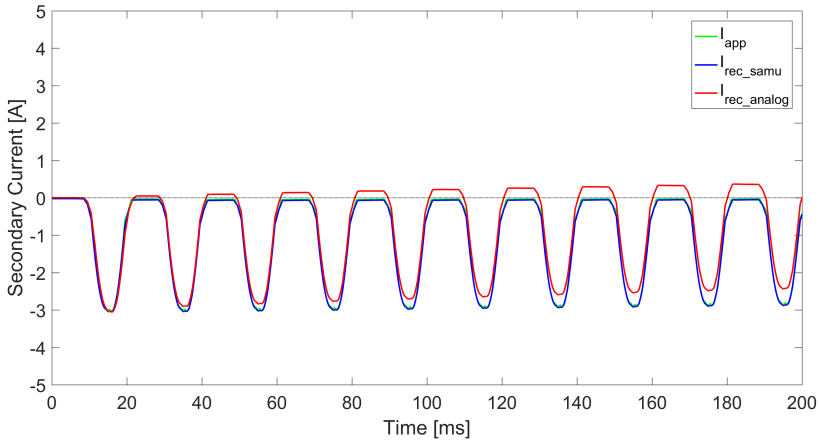

(a) Transient response of phase A.

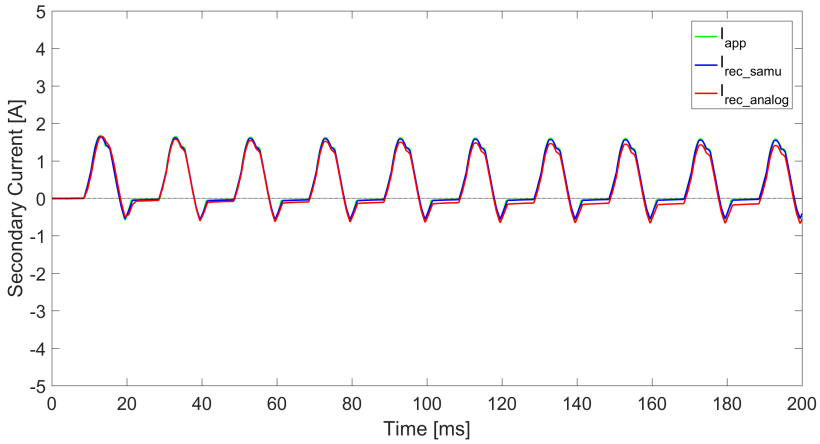

(b) Transient response of phase B.

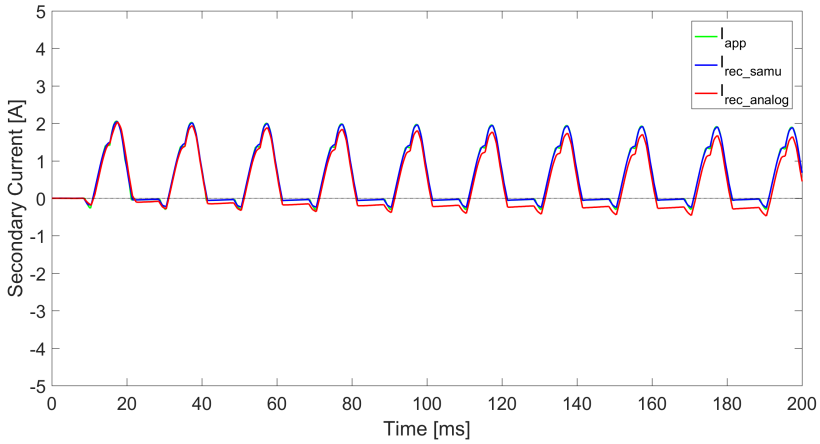

(c) Transient response of phase C

.

Figure 8.11: Transient response of the SAMU and the analog acquisition system to transformer inrush currents. I_{app} cannot be seen in the plots since it is hidden by I_{rec_samu}.

8.3 Response of Transformer Differential Protection

Table 8.2 summarizes the response of the transformer differential protection to the currents from the simulation cases presented in Subsection 7.2.2. The response time of the differential protection was recorded by the disturbance recorder.

Table 8.2: Response of the transformer differential protection.

Simulation Case	**Response**	**Response Time**
1) Normal load conditions	No trip	-
2) Internal HV side fault	Trip	11 ms
3) Internal LV side fault	Trip	11 ms
4) External fault	No trip	-
5a) CT saturation during an internal HV side fault	Trip	11 ms
5b) CT saturation during an internal LV side fault	Trip	10 ms
5c) CT saturation during an external fault	No trip	-

Chapter 9

Discussion of Laboratory Tests

In this chapter the laboratory results which were presented in Chapter 8 are discussed. The objective of the laboratory tests was threefold: to investigate the steady state and transient performance of a SAMU, to compare the steady state and transient performance of a SAMU to those of a conventional analog acquisition system and to investigate whether a hybrid mode configuration could have an impact on the performance of transformer differential protection. The results of the laboratory tests are discussed in light of these objectives.

9.1 Steady State Performance

In Figure 8.2a, Figure 8.3a and Figure 8.4a, it can be observed that there are some small differences between the amplitude accuracies of the recorded currents of phase A, B and C from the SAMU, particularly at the lowest levels of applied current. In all three phases the average amplitude error in percent of the applied current is highest at an applied current of 1 A_{RMS}, which is 20 % of the nominal input current of the SAMU. The highest average amplitude error occurs in phase A and is approximately 3 %, which is equivalent to 0.04 A. At the lowest levels of applied current, there seems to be a small DC offset in the recorded currents from the SAMU since the average amplitude errors of the negative peaks are approximately equal to the average amplitude errors of the positive peaks and of opposite sign. This DC offset is also observable in the steady state response of the SAMU which is shown in Figure 8.1a. However, the DC offset is not consistent and does not occur in the recorded currents from the SAMU at all levels of applied current, as shown in Figure 8.1b. Either the DC offset only occurs at low levels of applied current or there are other sources of error. Anyhow, the average amplitude errors are so small that they do not affect the linearity of the SAMU, as can be seen in Figure 8.5. Dutra et al. [100], whose work was mentioned in Section 5.3, also found that the SAMU which they tested had a linear output.

There are some small differences between the amplitude accuracy of the recorded currents from the SAMU and the analog acquisition system, as shown in Figure 8.2, Figure 8.3 and Figure 8.4. Judging from the results, the analog acquisition system seems to have a slightly better amplitude accuracy at 1 A_{RMS} and 5 A_{RMS} and the SAMU in the range from 10 A_{RMS} to 25 A_{RMS}. The results in Table 8.1 show that the RMS values of the recorded currents from the SAMU and the analog acquisition system are almost equal and coincide well with the RMS values of the applied current. The observed amplitude errors are so small that they should not affect the performance of the transformer differential protection in hybrid mode configuration.

There is a small phase difference between the phase angles of the recorded currents from the SAMU and the analog acquisition system, as can be seen in Figure 8.6. At all levels of applied current above 1 A_{RMS}, the recorded currents from the SAMU leads the recorded currents from the analog acquisition system. In all three phases the phase difference increases with the applied current. The phase difference could partially be caused by inaccuracies in the time synchronization of the SAMU and the protection IED. However, since the phase difference increases with the applied current, it cannot be caused solely by inaccuracies in the time synchronization. A possible explanation could be that the phase difference is caused by the different types of input elements which are used in the SAMU and in the protection IED, that is shunt elements in the SAMU and input current transformers in the protection IED. The phase difference could possibly be a result of the inductance of the input current transformers in the protection IED. The highest phase difference observed was 0.31°, which corresponds to a magnitude error of only 0.54 %.

The insignificance of the observed phase difference can also be proved by considering the operate-restrain characteristic of the transformer differential protection which is shown in Figure 7.3 in Subsection 7.1.4. The most critical point on the characteristic is at the end of Section 1. The applied current level closest to this point is 1 A_{RMS}, corresponding to a primary current of 500 A_{RMS} or 1.21 times the base current of 412 A_{RMS}. Under these conditions, the phase difference between the phase angles of the recorded currents from the SAMU and the analog acquisition system would have had to be 14.3° in order to cause an incorrect operation of the differential protection. By comparing the value of the highest phase difference which was observed during the laboratory tests to this number, it can be seen that the observed phase difference is insignificant.

Figure 8.6 shows that the phase difference is not equal in all three phases. The phase differences of phase A and C are almost identical at all levels of applied current. The phase difference of phase C, on the other hand, differs from the others. However, the change of the phase differences with increasing levels of applied current is similar in all three phases. Dutra et al. [100] also investigated the phase difference between the recorded

currents from a SAMU and an analog acquisition system, but only at an applied current of 5A. Similar results were obtained at this current level, though with smaller differences between two of the phases and the third than what was observed during these laboratory tests.

9.2 Transient Performance

9.2.1 Faults

The transient response of the SAMU to various faults is almost identical to the applied fault currents. Two examples are shown in Figure 8.7 and Figure 8.8. The recorded currents from the SAMU are not distorted, and the DC component in the fault currents is reproduced well. When comparing the transient response of the SAMU to that of the analog acquisition system, on the other hand, differences can be observed. As mentioned in Section 5.3, some types of input current transformers cannot reproduce the DC component in transient primary currents properly. Judging from the transient response shown in Figure 8.7, this seems to be the case for the input current transformers of the protection IED.

It was also mentioned in Section 5.3 that the waveform of saturated currents from input current transformers may not have the typical appearance of saturated CT currents due to the very low impedance of the secondary circuit. The transient response which is shown in Figure 8.8 is the result of applying fault currents with a maximum value of approximately 32 times the rated input current the protection IED. Comparing with previous work of Holst and Zakonjšek [27], which was mentioned in Section 5.3, it may look like the input current transformers of the protection IED are saturating after approximately 410 ms. The error between the recorded currents from the SAMU and the analog acquisition system is much larger in Figure 8.8 than in Figure 8.7, where fault currents with a maximum value of only 6 times the rated input current of the protection IED were applied. The error currents in Figure 8.8 also vary much more over time than the error currents in Figure 8.7. Based on a comparison with the waveforms of currents from different types of CTs which was presented in the work of Holst and Zakonjšek [27], it may look like the input current transformers of the protection IED are of the LR CT type, that is the type with small air gaps in the CT core.

The maximum value of the fault currents in Figure 8.8 is within the measurement range of both the protection IED and the SAMU. However, this current is only about 6 times higher than the rated input current of the SAMU, compared to 32 times the rated input current of the protection IED. In order to properly compare the transient response of the

SAMU and the analog acquisition system, the SAMU and the protection IED should have had the same rated input current. On the other hand, it is not expected that the transient response of the SAMU will show any signs of saturation even at an applied current of 32 times its rated input current since the SAMU has shunts as input elements instead of input current transformers.

In order to evaluate whether the observed differences in the transient response of the SAMU and the analog acquisition systems may affect the performance of the differential protection in a hybrid mode configuration, a digital filter was implemented in MATLAB by the use of DFT. The MATLAB script is given in Appendix C.1. The filter was used to extract the fundamental frequency phase currents from the recorded phase currents of the SAMU and the analog acquisition system. The fundamental frequency phase currents of the recorded currents in Figure 8.7 and Figure 8.8 are shown in Figure 9.1 and Figure 9.2, respectively.

In Figure 9.1 it can be observed that there is a small difference between the amplitudes of the fundamental frequency phase currents from the SAMU and the analog acquisition system in phases B and C. The difference is likely to be caused by the differing abilities of the SAMU and the analog acquisition system to reproduce the DC component in the fault current. A larger difference between the fundamental frequency phase currents from the SAMU and the analog acquisition system can be observed in Figure 9.2. In phases B and C, the fundamental frequency phase currents from the analog acquisition system have a higher amplitude than the fundamental frequency phase currents from the SAMU and oscillates around a lower value after fault occurrence.

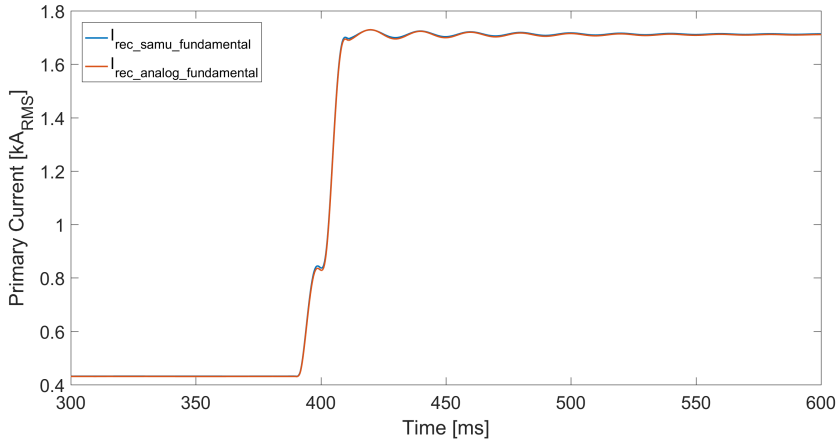

(a) Fundamental frequency currents of phase A.

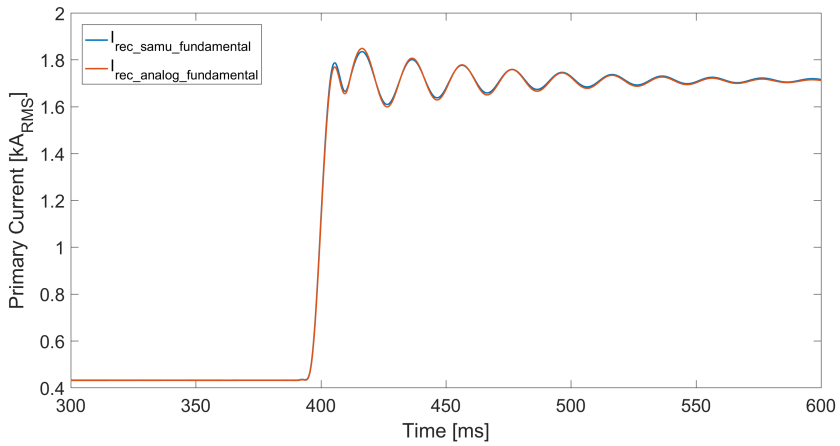

(b) Fundamental frequency currents of phase B.

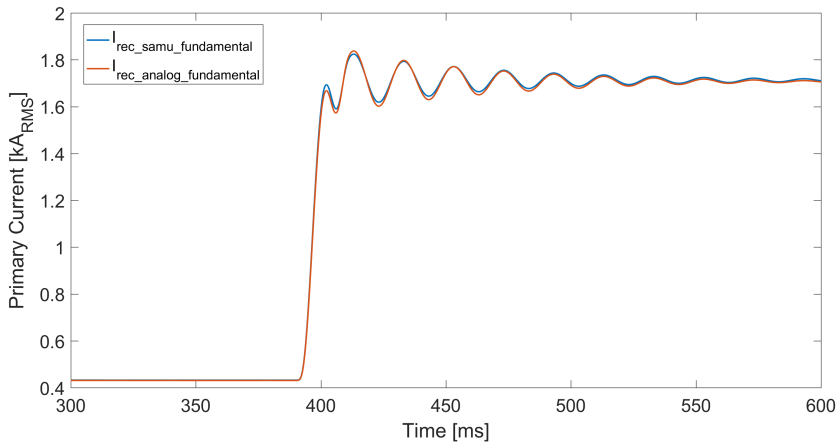

(c) Fundamental frequency currents of phase C.

Figure 9.1: Fundamental frequency phase currents of the recorded currents from the SAMU and the analog acquisition system in Figure 8.7. Figure 8.7 shows the transient response of the SAMU and the analog acquisition system to fault currents on the HV side of the power transformer during an external fault.

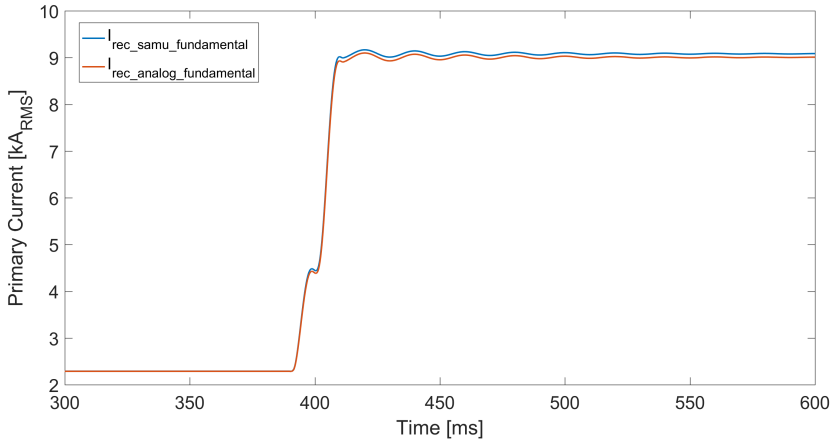

(a) Fundamental frequency currents of phase A.

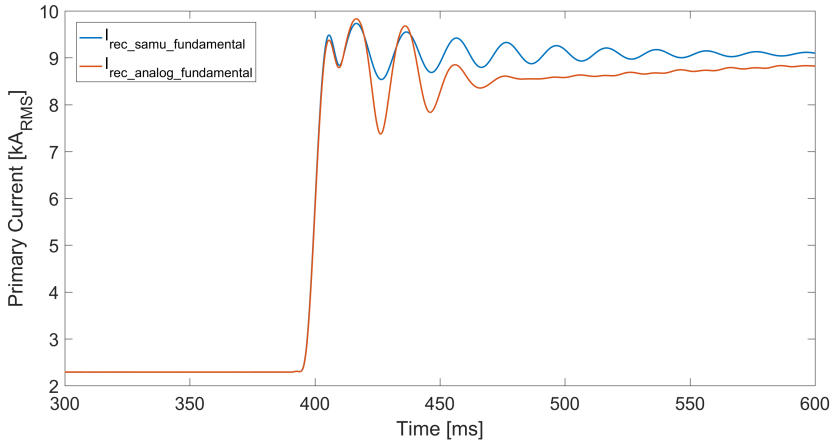

(b) Fundamental frequency currents of phase B.

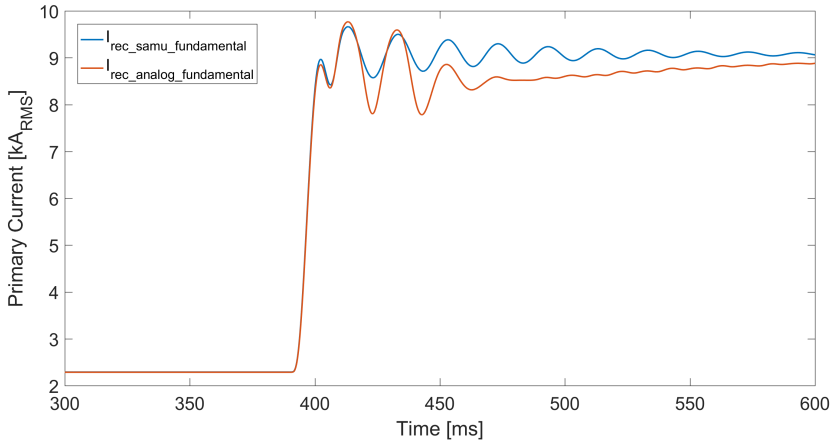

(c) Fundamental frequency currents of phase C.

Figure 9.2: Fundamental frequency phase currents of the recorded currents from the SAMU and the analog acquisition system in Figure 8.8. Figure 8.8 shows the transient response of the SAMU and the analog acquisition system to fault currents on the LV side of the power transformer during an external fault.

It should be noted that these two cases do not represent true fault scenarios since the same phase currents were applied to both the SAMU and the analog acquisition system. The observed differences between the fundamental frequency phase currents from the SAMU and the analog acquisition system were further analyzed by considering the external fault simulation case. In this test currents from the HV side of the power transformer were fed to the analog acquisition system and currents from the LV side of the power transformer to the SAMU. A DFT was performed in MATLAB and the fundamental frequency differential current of each phase calculated. The MATLAB script is given in Appendix C.2 and the results in Figure 9.3.

Fundamental frequency differential currents can be observed around t = 0 ms in Figure 9.3. These are most likely caused by some irregularities in the recorded currents from the SAMU and the analog acquisition system at the instant when the currents from the test set were applied. These may be ignored. In phases B and C, where the recorded currents from the analog acquisition system were affected by the limited ability of the input current transformers to reproduce the DC component in the fault currents, increased fundamental frequency differential currents can be observed around t = 400 ms. The maximum values are 20.0 A_{RMS} and 23.5 A_{RMS} in phase B and C, respectively, compared to 8.8 A_{RMS} in phase A where the recorded currents from the analog acquisition system were almost equal to the recorded currents from the SAMU.

As described in Subsection 7.1.4, the base current in the transformer protection IED was set to 412 A_{RMS} and the minimum differential current (Id_{Min}) to 30 % of the base current. The differential current would thus have to be at least 123.6 A in order for the transformer differential protection to trip. In addition, this is the limit of Section 1 in the operate-restrain characteristic of the transformer differential protection. Based on the fundamental frequency phase currents shown in Figure 8.7, it can be estimated that the highest fundamental frequency current and thus the restrain current was at least three times the base current. This number marks the end of Section 2 in the operate-restrain characteristic. Thus, the fundamental frequency differential current would have to be even greater than 123.6 A in order for the transformer differential protection to trip.

Exactly how this particular transformer differential protection filters out the fundamental frequency phase currents and calculates the fundamental frequency differential currents is not known. The fundamental frequency phase currents shown in Figure 9.1 and Figure 9.2 and the fundamental frequency differential currents displayed in Figure 9.3 may not exactly represent the currents calculated by the protection IED. However, the approach applied here should represent a fairly good approximation.

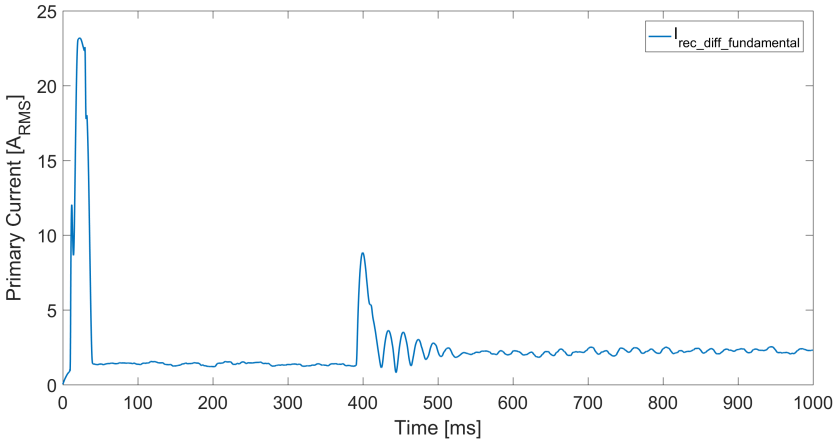

(a) Fundamental frequency differential current of phase A.

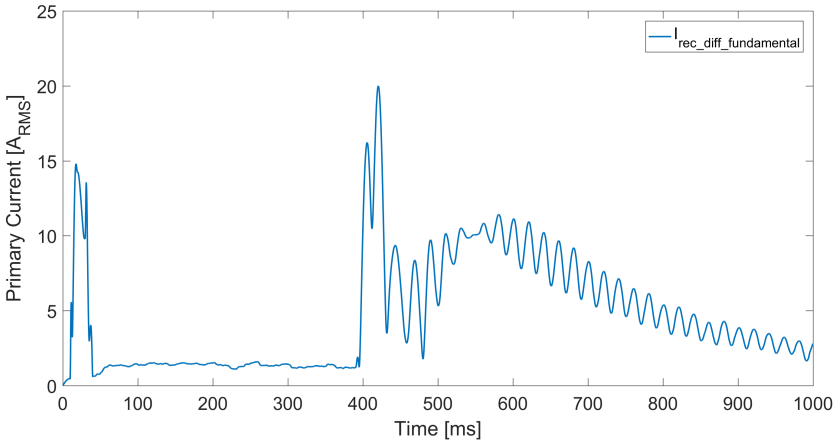

(b) Fundamental frequency differential current of phase B.

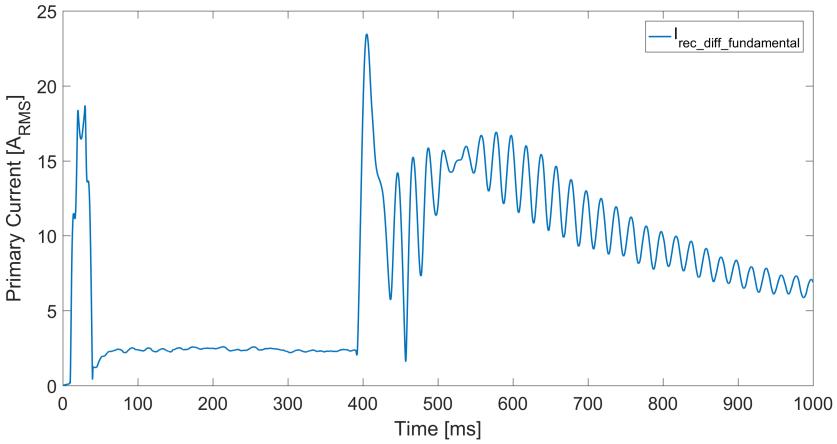

(c) Fundamental frequency differential current of phase C.

Figure 9.3: Fundamental frequency differential phase currents from the external fault simulation case.

9.2.2 Current Transformer Saturation

The transient response of the SAMU to saturated fault currents is almost identical with that of the analog acquisition system, as shown in Figure 8.9. Neither the SAMU nor the analog acquisition system manage to reproduce the steepest peaks of the simulation. Apart from that, both the SAMU and the analog acquisition system reproduce the waveforms of the saturated fault currents well.

9.2.3 Transformer Inrush

There are distinct differences between the transient response of the SAMU and the analog acquisition system to transformer inrush currents, as shown in Figure 8.10 and Figure 8.11. In all three phase currents, there is a DC component. As with the fault cases, the analog acquisition system cannot reproduce the DC component in the primary currents properly. The SAMU on the other hand, reproduces the waveforms of the applied inrush currents well.

Since transformer inrush currents are characterized by the presence of second harmonics, a DFT was performed in MATLAB in order to compare the content of second harmonics in the recorded currents from the SAMU and the analog acquisition system. The MATLAB script is given in Appendix C.3. The resulting second harmonic phase currents are given in Figure 9.4. In the figure it can be observed that the content of second harmonics in the recorded currents from the SAMU and the analog acquisition system is similar. The biggest difference occurs around 40 ms in all phases. Judging from the results, it does not seem like the differing transient responses of the SAMU and the analog acquisition system have a significant impact of the content of second harmonics.

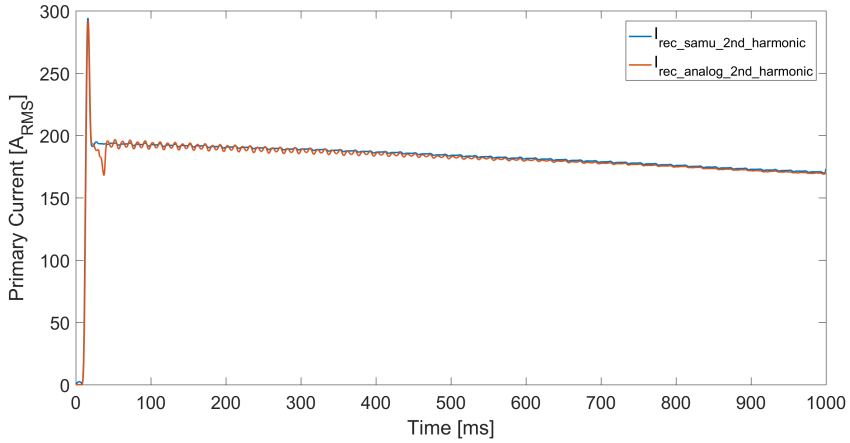

(a) Second harmonic currents of phase A.

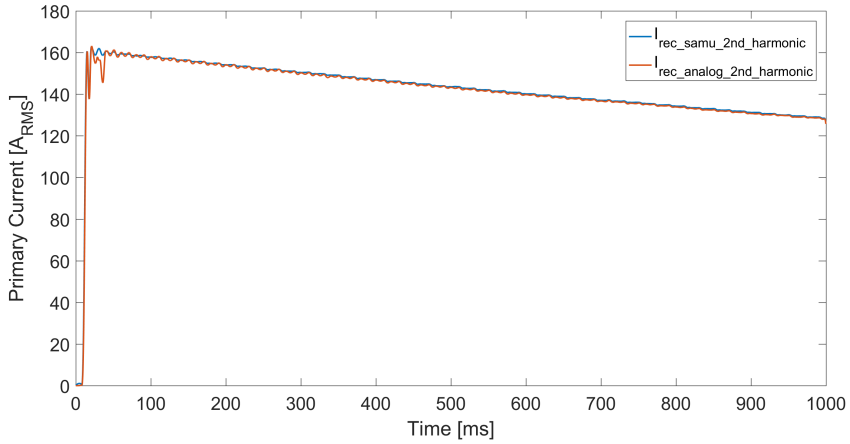

(b) Second harmonic currents of phase B.

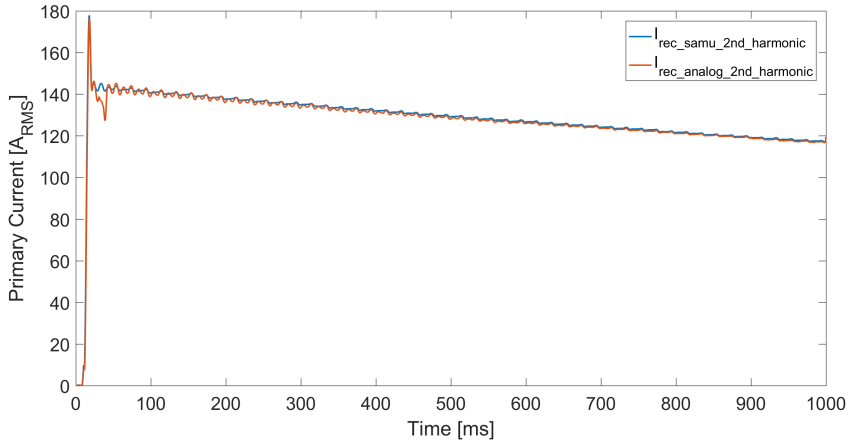

(c) Second harmonic currents of phase C.

Figure 9.4: Second harmonic phase currents of the recorded currents from the SAMU and the analog acquisition system in Figure 8.10. Figure 8.10 shows the transient response of the SAMU and the analog acquisition system to transformer inrush currents.

9.3 Performance of Transformer Differential Protection

The transformer differential protection operated correctly for all simulation cases, as shown in Table 8.2. The response time of the differential protection was approximately the same in all cases. Judging from these results, the hybrid mode configuration does not seem to affect the performance of the transformer differential protection. However, these simulation cases only represent a sparse selection of possible operating scenarios. In addition, the response time of the transformer differential protection was only roughly estimated. In order to properly assess the influence of a hybrid mode configuration on the transformer differential protection, the response time should have been accurately measured. Another aspect to consider is that the process bus in an actual digital substation will not be ideal as it was in the tests performed here. Among other things, possible loss of SV and network delays may affect the stream of SV from the SAMU to the subscribing protection IED.

Chapter 10

Conclusion of Laboratory Tests and Future Work

In this chapter some preliminary conclusions are drawn from the discussion of the laboratory tests in Chapter 9. Suggestions for future laboratory work are also described. The final conclusion to this thesis will be given in Chapter 12.

10.1 Conclusion

The laboratory tests showed that the SAMU under test has a steady state and transient performance which makes it adequate for use in digital substations. The SAMU provided SV with a small, but acceptable amplitude error. The amplitude error was highest at applied currents below the rated current of the SAMU. In order to achieve the best performance possible, the rated secondary current of the associated CIT and thus the rated current of the SAMU should be chosen in such a way that the secondary current is higher than the rated current under most operating conditions.

The tested SAMU has a steady state performance which is comparable to the steady state performance of a conventional analog acquisition system. There is a small phase difference, which increases with the applied current, between the phase angles of the recorded currents from the SAMU and the analog acquisition system. However, the phase difference is too small to affect the performance of the transformer differential protection in hybrid mode configuration.

The SAMU under test has a better transient performance than the conventional analog acquisition system. The laboratory tests showed that the SAMU can close to perfectly reproduce the DC component in transient currents without any distortion. The ability of the analog acquisition system to reproduce DC components, on the other hand, was a bit more limited, and the recorded currents were distorted at current levels significantly above the rated current of the input current transformers of the protection IED.

The differing transient responses of the SAMU and the analog acquisition system resulted in fundamental frequency differential currents when employed in a hybrid mode transformer differential protection configuration. In the tested case the resulting fundamental frequency differential currents were not big enough to affect the performance of the transformer differential protection. However, one should be aware that different SAMUs, NCITs and conventional protection IEDs can have different transient performances. In a digital substation it should be made sure that differing transient responses will not affect the performance of the protection functions.

10.2 Future Work

Due to limitations in time and the laboratory test setup, some tests were left for future work. The SAMU could only be tested at a limited current level of 6.4 times its rated input current due to limitations in the maximum current output from the test set. In future tests a SAMU with a lower rated input current of 1 A should thus be tested. In addition, the phase accuracy of the SAMU could not be investigated due to lack of time synchronization between the output from the test set and the output from the SAMU. A solution to this issue should be found and further tests conducted. The performance of the voltage module of the SAMU should also be investigated. Only a rough estimate of the response time of the protection IED was found in the performed laboratory tests. In order to properly assess the performance of the transformer differential protection under different operating conditions, the trip signal should be properly measured in future tests.

As mentioned in Section 5.3, SAMUs from different suppliers may employ different input elements and thus have different transient responses. Interoperability between devices from different vendors may also be an issue in digital substations, as mentioned in Section 6.2. Future tests should thus include SAMUs from different vendors and combinations of SAMUs and protection IEDs from different vendors.

In the performed laboratory tests, the SAMU was connected with a direct fiber optic link to the protection IED, representing an ideal process bus network. In an actual digital substation, the process bus network is likely to include several switches and fiber optic cables. There will also be SV streams from other SAMUs and the associated MUs of NCITs in addition to other background traffic. The effects of a non-ideal process bus network on the performance of the SAMU and the protection IED should thus be investigated in future tests. A possible test is to introduce time delays of different length or possibly background traffic in the process bus network and investigate the response of the transformer differential protection. Another possible test is to investigate the response of the transformer differential protection when SV messages are discarded.

Chapter 11

Discussion

This chapter provides a discussion of the benefits and drawbacks of applying OCTs in digital substations compared to the use of CCTs in conventional substations. It is also discussed whether OCTs are suitable for application in digital substations in the transmission network.

11.1 Health, Safety and Environment

OCTs offer significant improvements in terms of health, safety and environment compared to CCTs. In conventional substations the secondary circuits of CCTs are connected to the back of the protection and control panels in the control room, as mentioned in Section 2.2. Personnel may therefore get electrocuted if the contacts are touched. There is also a risk that a secondary circuit of a loaded CCT can be open-circuited. As explained in Section 2.2, this will lead to a very high voltage across the secondary winding, which in turn can result in arcing and potentially the CCT exploding. This is an unwanted situation which presents a danger to both personnel and equipment in the substation.

The safety of personnel and equipment can be significantly improved by replacing the CCTs with OCTs and substituting the analog measuring circuits with a process bus realized by the use of fiber optic cables. As mentioned in Section 6.6, fiber optic cables are non-conductive and provides galvanic isolation. This means that personnel cannot get electrocuted from touching the contacts at the back of the protection and control panels. In addition, OCTs do not have any secondary circuits which can be open-circuited and do not contain any oil. There is thus no risk of an OCT exploding.

By replacing CCTs with OCTs, the environmental impact can also be reduced. Since OCTs do not contain any oil or SF_6 gas, as apposed to CCTs, the risk of oil or SF_6 gas leaking into the ambient environment is removed. OCTs also offer a significant weight reduction compared to CCTs. Based on information from the product survey which was conducted in this thesis, a weight reduction of approximately 80 % or more can be

expected when replacing CCTs with OCTs. As a consequence of the reduced weight, it can be expected that the CO_2 emissions associated with the transport of CTs to the substation will decrease. The 80 % weight reduction does not take into account the reduced weight of cables due to the replacement of a large number of copper cables with a smaller number of fiber optic cables. An even higher weight reduction can therefore be expected.

11.2 Performance

As mentioned in Section 2.2, the accuracy of CCTs is limited by the use of an iron core. The literature review shows that OCTs can offer significant improvements in terms of performance compared to CCTs. Thomas et al. [93] and Rahmamatian and Blake [8] demonstrated that the accuracy of OCTs can satisfy and may even outperform the measuring accuracy requirements of IEC instrument transformer standards, and that OCTs can maintain this accuracy over a wide dynamic range. However, one should bear in mind that these practical demonstrations are experimental tests of specific OCTs. As described in Section 3.3, OCTs can be designed in many ways, and it is therefore likely that the performance of OCTs from different vendors will differ to some degree.

The literature review also shows that OCTs have the advantage of an excellent transient performance without saturation effects. As mentioned in Section 2.2, saturation of CCTs may for instance result in incorrect operation of differential protection functions or differential protection functions not operating when required to. In Section 6.3 it was explained how the sensitivity of differential protection has to be reduced in order to prevent incorrect operation due to saturation of CCTs during external faults. Since OCTs are linear over a wide dynamic range and do not saturate, the sensitivity of differential protection can be increased. However, it is still important to design the OCTs with the proper number of sensing fiber coil turns since distortion of the measured current can occur if the short-circuit current exceeds the maximum detectable current of the OCTs.

11.3 Substation Layout and Footprint

The high weight of CCTs puts requirements on the supporting structures which are needed in the substation yard. As mentioned in Section 3.7, the low weight and compact size of OCTs open up the possibility for integration of the sensor heads into other primary equipment. If such installation solutions are chosen, separate supporting structures for the OCTs will not be needed. In turn, this reduces the required space in the substation yard, which allows the footprint of future digital substations to be reduced. As mentioned in Section 4.2, there are also products on the market which combine several primary

functions into a single device. Examples are the disconnecting circuit breaker and the combined optical current and voltage transformer. Adoption of such solutions will also reduce the required space in the substation yard.

All of the OCT which were considered in the product survey can be installed as free-standing devices with a configuration similar to that of CCTs, as described in Section 4.2. This means that one does not have to change the arrangement of the primary equipment in present day transmission substations in order to apply OCTs. However, such free-standing solutions does not offer the benefit of saving space in the substation yard. Nevertheless, it should be possible to make the supporting structures lighter than those required today since the weight of OCTs is much lower than the weight of CCTs.

The cores of CCTs and the dedicated wiring from each core to specific secondary devices make the design of conventional substations inflexible. The CT cores limit the number of associated applications, which means that a CCT might have to be replaced by one having more cores if new applications are required and there are no free CT cores. This situation changes in a digital substation with OCTs. Due to the ability of OCTs to maintain a high accuracy over a wide dynamic range, the same sensing element can be used for both measuring and protective applications, possibly two for redundancy. In addition, the process bus makes all current and voltage measurements available to all protection, control and monitoring devices. This makes the substation design more flexible. In addition, it facilitates the integration of several application functions into the same IED, resulting in fewer IEDs in the control room. In turn, this will reduce the required space in the control building and possibly the need for cooling and power supply.

The present day solution with CCTs and dedicated wiring from each CT core to specific secondary devices also makes it difficult to satisfy the regulatory requirements regarding duplicated and physically independent routing of cables, which was mentioned in Section 2.5. With the application of a redundant process bus, these requirements may become easier to satisfy. As mentioned in Section 6.6, there will also be a reduced need for large cable trenches in digital substations since fewer fiber optic cables are needed in order to realize the process bus than the number of copper cables which are required for the measurement and control circuits in conventional substations. Instead of using large cable trenches, the fiber optic cables can be laid in pipes or smaller cable trenches.

11.4 Installation and Replacement

Due to the large weight of CCTs, heavy cranes are typically required for the installation and replacement of such CTs. With a weight reduction of approximately 80 % when

replacing CCTs with OCTs, it can be expected that there will be a reduced need for heavy cranes during installation and replacement of OCTs in digital transmission substations. However, at least for the higher voltage levels, it is reasonable to assume that some type of lifting equipment will still be required based on the weight information provided by the vendors during the product survey.

The workers which install CCTs today are probably unfamiliar with OCT technology and how to install OCTs. It can therefore be assumed that some training will be required. In addition, as mentioned in Section 6.6, the connection of fiber optic cables requires special competence. In order to expand the competence of the workforce, resources have to be put down. On the other hand, there will be fewer cables to install, which should result in a reduction in the time spent on cable installations.

11.5 Maintenance and Expected Lifetime

It can be expected that OCTs require less maintenance than CCTs since the insulators do not contain any oil. This assumption was confirmed by the vendors which were contacted during the product survey. According to them, the OCTs require little or no maintenance. As mentioned in Section 2.2, it is estimated that the periodical maintenance of a single CCT takes approximately 30 minutes per month. As a result, around one an a half hour of maintenance could be saved per month for a set of three CCTs which is replaced by a three-phase OCT in a substation.

CCTs have proven to be reliable and show a good stability over a lifetime of approximately 25 to 40 years, as described in Section 2.2. Based on information from the product survey, it can be expected that the lifetime of the sensor heads of an OCT is comparable to the expected lifetime of a CCT. The sensor electronics, on the other hand, have an expected lifetime which is about half as long as that of the sensor heads. The sensor electronics will thus have to be replaced once during the lifetime of the OCT. Developments in the technology are probable to occur within that time span, and it should be considered whether compatibility issues between old and new parts could be a potential problem.

11.6 Interoperability and Compatibility

As mentioned in Section 2.2, CCTs have a standardized analog interface. This facilitates the use of CCTs and secondary devices from different vendors in conventional substations. Since the interface is simply an analog 1 A or 5 A connection, it may be assumed that there will not be significant developments in the interface over time and that is relatively

unproblematic to replace a CCT from one vendor with a CCT from another vendor, and to connect CCTs and secondary IEDs of different age or from different vendors.

When it comes to digital substations, on the other hand, it may be expected that there will be more challenges related to interoperability and compatibility between NCITs with associated MUs, SAMUs and secondary IEDs. Even though standards such as IEC 61850 shall ensure that devices from different vendors are interoperable, these standards often leave some room for interpretation. One example of standards being interpreted differently is the handling of the SV quality attribute, which was mentioned in Subsection 6.2.1. Such differences in the interpretation of standards can prevent interoperability between devices from different vendors and result in systems which are not working optimally or possibly not working at all. There is no guarantee that devices from different vendors will actually be interoperable in a digital substation, even though the specifications state that the devices conform to the standards. Real-life testing of interoperability between devices from different vendors is thus of great importance. In addition, it can be discussed whether there is a need to make the standards more specific. However, this would leave less freedom to the vendors in the design of their products.

One can also imagine that there will be greater changes in the digital interface between MUs or SAMUs and secondary IEDs over time than what has been the case for the analog interface of CITs. As a result, one may face greater difficulties in terms of compatibility when replacing devices in a digital substation. Experiences from the laboratory tests confirmed this assumption. The protection IED used in the laboratory tests was too old to support time synchronization via PTP. There were also issues with the compatibility of the contacts of different devices. Since the network clock was only equipped with electrical output contacts for distribution of 1PPS signals, while the protection IED had optical input contacts, an electrical to optical converter would have been needed in order to connect these devices. Such a solution would most likely not be desirable in a digital substation since it adds another possible point of failure and could introduce errors. In addition, the vendors might not be able to guarantee that their equipment will work as promised if such a solution is employed.

11.7 Maturity and Availability of Products

Since CCTs have been in wide use for a long time, utilities and manufacturers are well acquainted with the technology and have learned how to deal with its downsides, such as adapting the operate-restrain curve of differential protection in order to avoid incorrect operation due to CT saturation. In addition, there is a large selection of commercially available CCTs and compatible secondary devices from multiple vendors.

As mentioned in Section 3.7, OCT technology has also been known for quite some time now. However, the technology has not been widely adopted in substations yet. Naturally, the operational experience with such sensors is much more limited than for CCTs. As described in Subsection 6.2.1, there are still several unanswered questions regarding the application of OCTs, other NCITs and SAMUs in digital substations. Several examples were mentioned. One example is if and how manufacturers of protection IEDs should specify requirements for NCITs and SAMUs in order to ensure satisfactory performance of the protection functions. Other examples are how the protection IEDs should respond to missing SV, SV whose validity is set to questionable or invalid and SV which are not sufficiently time synchronized. In addition, some standards are still being developed and have not been released yet, such as IEC 61869-13, which will apply to SAMUs. All of this may be interpreted as signs of immaturity. However, there is clearly a lot of work going on and interest in this area at the present time, such as the work of IEC TC 95 AHG 3. It is therefore reasonable to assume that solutions to the above-mentioned questions can be found not too far ahead in the future.

The product survey in Chapter 4 showed that there are several vendors offering OCTs at the present time. However, it was discovered that only one of the considered OCTs supports network-based PTP time synchronization, as recommended by the new IEC 61869-9 standard. The other OCTs, which use 1PPS for time synchronization, will require dedicated wiring for the distribution of time synchronization signals. Another attribute which was investigated was the support of network redundancy protocols. Since it could only be confirmed that one of the OCTs supports PRP and HSR, further inquires should be made in order to establish whether the other OCTs support these network redundancy protocols. The present day regulatory requirement regarding duplicated and physically independent routing of cables, which was given in Section 2.5, will most likely apply in digital substations as well. The requirement could be interpreted in such a way that the process bus shall be redundant. Hence, OCTs should support PRP and/or HSR. Lack of such attributes may limit the selection of OCTs which could actually be applied in a digital transmission substation.

11.8 Vulnerability

There are several factors which may make digital substations with OCTs more vulnerable than the present day conventional substations. Some examples are the placement of MUs, SAMUs and other electronics in the substation yard and the need for highly accurate time synchronization [122]. In digital substations with OCTs, several electronic devices such as MUs and SAMUs will be placed outdoor in the substation yard. As described in

Section 6.2.3, the electronics have to be installed in suitable cabinets which are secured against EMP and EMI. In addition, as can be seen from Table 4.1 in Section 4.8, the sensor electronics of OCTs typically have a more limited operating temperature range than the sensor heads. Comparing with the large outdoor temperature variations in Norway, heating would be needed in order to keep the temperature inside the cabinet within the operating temperature range of the MUs. Cooling could also be required. The dependency on proper heating and cooling may make OCTs more vulnerable than CCTs, which do not have such requirements. In addition, the lifetime of the electronics may be affected by the outdoor conditions.

Highly accurate time synchronization is an important requirement of several protection applications in digital substations, as described in Subsection 6.2.1. Inaccuracies in the sampling synchronization will result in phase errors in the measured currents, and these errors may for instance lead to incorrect operation of differential protection functions. Digital substations can thus be expected to be more vulnerable than present day substations if inaccuracies in the time synchronization or a possible loss of time synchronization were to occur.

The literature review shows that OCTs are inherently sensitive to environmental disturbances such as temperature variations and vibrations. However, as described in Section 3.5, there are several methods which can be used to mitigate the effects of such disturbances. Based on information from one of the vendors stating that the accuracy of the OCT is maintained over the whole operating range and is not sensitive to vibrations, it can be assumed that the vendors have managed to adopt successful methods which mitigates the effects of environmental disturbances. The practical demonstrations described in Subsection 3.5.2 and Subsection 3.5.3 corroborates this assumption. An example is the use of temperate sensors on the sensing fiber in conjunction with temperature compensation. However, this implies that the accuracy of the sensor will be dependent on a well functioning temperature sensor. As it was mentioned in Subsection 3.5.2, IEEE recommends periodical verification of the accuracy of the temperature sensor if such a solution is employed.

11.9 Costs

Based on information from the product survey which was conducted in this thesis, it can be estimated that the price of a three-phase OCT with an associated MU is about twice as high as the price of a set of three CCTs rated for a maximum system voltage of 420 kV. However, the application of OCTs in digital transmission substations can lead to several other cost savings, which should be taken into account when comparing the two

solutions. Some examples are as follows. Since lighter or fewer supporting structures will be required for the OCTs, savings can be made in the amount of foundation work which is required when building new substations. In addition, due to the reduced cabling and the replacement of copper cables by fiber optic cables, savings are expected to be made on cabling, cable trenches and the installation of cables, as mentioned in Section 6.6. If decided to make use of solutions where the OCTs are integrated with other primary equipment, less space will be required in the substation yard, which may reduce the capital expenses of new substations.

11.10 Hybrid Mode Differential Protection

From the specifications of the commercially available OCTs given in Table 4.1 in Section 4.8, it can be seen that the maximum system voltages which the OCTs are specified for, do not cover the lowest voltage levels which are included in the transmission network, according to the definition given in Section 2.1. Hence, it may for instance be desirable to continue using CCTs at the low voltage side of some power transformers in transmission substations. In order to integrate these CCTs into the digital substation, SAMUs can be applied. This is one of the reasons why differential protection is likely to be applied in configurations which involve combinations of NCITs and SAMUs in future digital substations.

As mentioned in Section 5.3, different manufacturers may employ different types of current input elements for SAMUs, which can have different transient performances. Some types of input current transformers cannot reproduce the DC component in transient currents properly and may go into saturation at current levels significantly above the nominal value. This was demonstrated for the input current transformers of the protection IED in the laboratory tests and reported by Holst and Zakonjšek [27]. Differences in the transient response of different input elements could potentially cause unwanted operation of differential protection when employed a hybrid mode configuration. The laboratory tests showed that the combination of shunt input elements and input current transformers, most likely of the LR type, did not affect the performance of the differential protection in this case. However, the differing transient performances did result in a fundamental frequency differential current, which could potentially be higher in other cases and with other combinations of input elements.

11.11 Fulfillment of Application Requirements

CCTs cover the needs of the applications in present day transmission substations. This includes energy metering, protection, busbar protection, disturbance recording, monitoring, control, quality metering etc. However, as mentioned in Section 2.2, in order to satisfy the requirements of these applications in terms of accuracy, dynamic range and bandwidth, different types of CT cores are required. In addition, several cores are needed in order to segregate different protection applications.

When it comes to the application of OCTs in digital substations, on the other hand, the requirements of both protective and measuring applications can be covered with a single sensing element, possibly two for redundancy. However, as mentioned in Section 6.5, it has not yet been sorted how to perform accredited meter inspections in digital substations. Since this is a regulatory requirement, CITs may have to be used for electrical energy metering applications until the issue is worked out. In other words, OCTs are not able to fulfill the requirements of electrical energy metering applications at the present time.

11.12 Supported Functionality in Digital Substations

In order to apply OCTs in transmission substations while fully realizing the potential of digital substations, protection IEDs of all types needed in a transmission substation, which support IEC 61850-9-2 process bus, have to be commercially available. Preferably, there should be multiple vendors offering such protection IEDs. Since Statnett requires two separate protection IEDs supplied by different vendors for distance protection as a redundancy measure [116], there has to be at least two vendors offering distance protection for digital substations.

As mentioned in Section 6.4, there are presently several vendors offering protection IEDs with IEC 61850-9-2 LE process bus support, including the two suppliers Statnett has frame agreements with. However, it is not clear yet whether all types of protection which will be needed in digital substations are presently available. In particular, it is uncertain whether good busbar protection solutions for bigger substations exists. Hence, investigations and possibly testing will be required in order to find new solutions. Statnett will also have to approve new protection IEDs in order to realize a digital substation since the protection IEDs which support IEC 61850-9-2 LE process bus are newer versions of protection IEDs which have been approved by Statnett.

11.13 Fulfillment of the Digital Substation Concept

Only one out of the four vendors which were contacted during the product survey offers a solution where the MU is placed in an outdoor cabinet, as mentioned in Section 4.2. Placing MUs in the protection and control panel does reduce the number of cables used for measuring to some extent. However, the largest gain in terms of reduction of cables running from the high voltage bays to the control building is achieved if the MUs are placed in outdoor cubicles in the substation yard. It may be discussed whether the indoor placement of MUs actually fulfills the concept of digital substations where measurements are digitized close to the source, and if such a solution realizes the full potential of digital substations.

When it comes to the issue regarding how to perform accredited meter inspections in digital substations, the full potential of digital substations will not be realized if the solution is to apply CITs for electrical energy metering applications. A solution where one is forced to keep some parts of the substation analog and others digital will probably not be desirable.

Chapter 12

Conclusion and Future Work

12.1 Conclusion

In this thesis a literature review and a product survey on OCTs have been performed in order to evaluate whether OCTs are suitable for application in digital substations in the transmission network. The analysis includes a discussion of the benefits and drawbacks of applying OCTs in digital substations compared to the use of CCTs in conventional substations in addition to an evaluation of potential performance limitations, maturity of the products and solutions, and fulfillment of the substation application requirements and the digital substation concept.

Experimental testing of a SAMU has also been conducted in order to investigate its steady state and transient performance and compare with those of a conventional analog acquisition system. In addition, it has been investigated whether a hybrid mode configuration could have an impact on the performance of transformer differential protection. In the rest of this section, answers to the main research questions stated in Section 1.2, will be given and final conclusions drawn.

The literature review and product survey have shown that OCTs offer many benefits compared to CCTs. Some of these are the improved safety of personnel and equipment in the substation, the reduced environmental impact and the reduced need for maintenance. OCTs also have a lower weight, which reduces the need for heavy cranes during installation and replacement, and facilitates integration of the sensor heads into or in conjunction with other primary equipment. This allows space to be saved in the substation yard, which in turn can reduce the footprint of future digital substations. In addition, the application of OCTs in combination with the process bus makes the design of digital substations flexible and facilitates the integration of several application functions into the same secondary IED, which allows space to be saved in the control building. Even though the price of OCTs are presently about twice as high as that of a set of three CCTs, the application of OCTs and the process bus allows many other costs to be reduced in a substation.

On the other hand, it may be expected that there will be more challenges related to interoperability and compatibility between NCITs with associated MUs, SAMUs and secondary IEDs in digital substations. CCTs have the benefit of a standardized and fairly stable analog interface. The digital interface of NCITs and SAMUs is defined in the IEC 61850 standards. However, the standards leave some room for interpretation, which may lead to lack of interoperability between devices from different vendors. Compatibility issues when connecting different devices may also occur. Real-life testing of multivendor digital substations is thus of great importance in order to ensure that the whole system is working and that its performance is as desired. In addition, competence building will be required since it is likely that most workers do not have experience with OCTs and digital substations. Digital substations may also be expected to become more vulnerable than the present day conventional substations due to factors such as the outdoor placement of electronics and the increased need for highly accurate time synchronization.

The literature review has not uncovered any limitations in the performance of OCTs themselves which may prevent their application in digital transmission substations. OCTs can offer improvements in both steady state and transient performance compared to CCTs. OCTs have the ability to maintain a high accuracy over a wide dynamic range, can measure primary currents over a wide bandwidth and cannot saturate. However, the application of OCTs in digital substations introduces some new considerations to take into account. Inaccuracies in the sampling synchronization will result in phase errors in the measured current, which may cause incorrect operation of differential protection functions. The potential effects of the process bus network, such as time delays and SV that are malformed, lost or arrive at the secondary IEDs out of sequence, can also affect the performance of protection functions. It is important to ensure highly accurate and reliable time synchronization and to properly design the process bus in order to minimize the risk of the network affecting the performance of protection functions or other application functions in digital substations.

Based on information from the literature review, it may be expected that different NCITs and SAMUs will have different transient performances. Since combinations of NCITs and SAMUs, possibly from different vendors, are likely to be applied in future digital substations, it is important to ensure that any differences in the transient performances will not affect the performance of the protection functions. In particular, this applies to differential protection functions. The laboratory tests showed that differences in the ability of the input current elements of a SAMU and a conventional protection IED to reproduce the DC component in transient fault currents, resulted in fundamental frequency differential currents. Even though the resulting differential currents were too small to affect the performance of the transformer differential protection, one should be aware of the

issue when combining different technologies in digital substations. Other combinations of SAMUs and NCITs under different operating conditions could cause larger differential currents and possibly result in incorrect operation of protection functions.

CCTs have the benefit of having been in wide use for a long time. CCTs have proven to be reliable and stable over time, utilities and manufacturers are well acquainted with the technology and there is a large selection of commercially available products and compatible secondary equipment. When it comes to OCTs and SAMUs, on the other hand, there are several signs that the products and solutions are not completely mature yet. There are still several unanswered questions regarding the application of OCTs and SAMUs in digital substations. In addition, parts of the IEC instrument transformer standard are still being developed and have not yet been released. The product survey showed that there are several vendors offering OCTs presently. However, several of these OCTs do not support desirable and recommended features, such as PTP time synchronization, which may limit the selection of suitable products at the current time.

CCTs meet the requirements of the applications in present day transmission substations. However, in order to do so, several CT cores and a large number of copper cables are required. OCTs, on the other hand, can fulfill the requirements of transmission substation applications with just a single sensing element per phase, possibly two for redundancy. However, there is one exception. Since it has not yet been figured out how to perform accredited meter inspections in digital substations, which is a regulatory requirement, OCTs cannot be said to meet the requirements of electrical energy metering at the present time.

A possible solution to the above-mentioned issue is to apply CITs for electrical energy metering applications. However, this solution does not fulfill the digital substation concept. If this solution has to be employed, the full potential of digital substations will not be reached. The product survey showed that most of the present day commercial OCT solutions are based on an indoor placement of the MU in a protection and control panel. It can be questioned whether this solution actually fulfills the digital substation concept and if the full potential of digital substations will be realized if such solutions are employed.

Based on the findings in this thesis, it can be concluded that OCTs seems to be suitable for application in digital substations in the transmission network and can offer many important benefits compared to CCTs. However, there are several signs that the products and solutions are not completely mature yet. There are several investigations to be made, questions to be answered and issues to be solved before a migration from the present day conventional substations with CCTs to digital substations with OCTs can take place. In

this work real-life testing of digital substations to ensure that the different devices are interoperable and that the performance of the resulting system is as desired, is of great importance.

12.2 Future Work

Due to limitations in time and the absence of an actual OCT, some investigations were left for future work. OCT technology was the only NCCT technology considered in this thesis. This is the type of NCIT Statnett has installed in their pilot digital substation. However, it should be investigated whether there are other types of NCCTs and NCVTs commercially available which are suitable for digital substations in the transmission grid.

One point which has not been covered in this thesis is how to test OCTs and secondary IEDs in digital substations. It should be investigated how to perform testing in a digital substation and if there could be any potential problems here. The potential cost reductions of applying OCTs in digital substations should also be investigated in further detail. It was only briefly mentioned in this thesis that digital substations with OCTs allows costs to be saved in several areas. Estimates of the cost savings compared to the increased price of OCTs and other potential increased cost should be made in order to assess whether the total solution will be cost-effective.

Due to the absence of an actual OCT, experimental tests of such a sensor could not be performed. Thus, future work includes performing tests of an OCTs to corroborate the findings in this thesis. Further investigations in terms of the performance of protection functions when combining NCITs and SAMUs with different transient performances should also be performed.

Bibliography

[1] T. Buhagiar, J. P. Cayuela, A. Procopiou, and S. Richards, "Poste intelligent - The next generation smart substation for the French power grid", in *13th International Conference on Development in Power System Protection 2016 (DPSP)*, 2016, pp. 1–4.

[2] K. Hinkley and C. Mistry, "First digital substation in TransGrid – Australia: A journey, business case, lessons", in *The IET 14th International Conference on Developments in Power System Protection 2018 (DPSP)*, 2018, pp. 1–6.

[3] C. Patterson, P. Mohapatra, C. Fundulea, C. Popescu-Cirstucescu, and P. Newman, "Fitness - GB's pilot multi-vendor digital substation - Architecture and design philosophy", in *2017 PAC World Conference*, 2017, pp. 1–13.

[4] N. Hurzuk, S. Losnedal, S. Ingebrigtsen, H. H. Dietrichson, and R. S. J. Løken, *Digitale stasjoner i transmisjonsnettet*. [Online]. Available: `http://docplayer.me/48638751-Digitale-stasjoner-i-transmisjonsnettet.html` (visited on 08/28/2017).

[5] O. Kaspersen, *Innovativ teknologi*, 2017. [Online]. Available: `http://www.statnett.no/PageFiles/12902/Innovativ%5C%20Teknologi.pdf` (visited on 06/07/2018).

[6] S. Weiss, P. Graeve, and A. Andersson, "Benefits of converting conventional instrument transformer data into smart grid capable process data utilizing IEC 61850 merging unit", in *21st International Conference on Electricity Distribution*, 2011, pp. 1–4.

[7] *Network Protection & Automation Guide*, 5th ed. Alstom Grid, 2011.

[8] F. Rahmatian and J. N. Blake, "Applications of high-voltage fiber optic current sensors", in *2006 IEEE Power Engineering Society General Meeting*, 2006, pp. 1–6.

[9] I. U. Rian, "Digital substations in transmission networks", Specialization project, Norwegian University of Science and Technology, Trondheim, 2017.

[10] B. M. Buchholz and Z. Styczynski, "Modern technologies and the smart grid challenges in transmission networks", in *Smart Grids – Fundamentals and Technologies in Electricity Networks*. Springer, 2014, ch. 3, pp. 61–119.

[11] *Lov om produksjon, omforming, overføring, omsetning, fordeling og bruk av energi m.m. (energiloven)*, 1990. [Online]. Available: `https://lovdata.no/dokument/NL/lov/1990-06-29-50` (visited on 06/14/2018).

[12] R. Gore, H. Satheesh, M. Varier, and S. Valsan, "Analysis of an IEC 61850 based electric substation communication architecture", in *2016 7th International Con-*

ference on Intelligent Systems, Modelling and Simulation (ISMS), 2016, pp. 388–393.

[13] E. Padilla, *Substation Automation Systems: Design and Implementation*. Wiley, 2015.

[14] S. Borlase, M. C. Janssen, M. Pesin, and B. Wojszczyk, "Role of substations in smart grids", in *Electric Power Substations Engineering*, J. D. McDonald, Ed., 3rd ed. CRC Press, 2012, ch. 22, pp. 1–30.

[15] K. P. Brand *et al.*, "The introduction of IEC 61850 and its impact on protection and automation within substations", pp. 1–102, 2007.

[16] M. Golshani, G. A. Taylor, and I. Pisica, "Simulation of power system substation communications architecture based on IEC 61850 standard", in *2014 49th International Universities Power Engineering Conference (UPEC)*, 2014, pp. 1–6.

[17] H. Lei, C. Singh, and A. Sprintson, "Reliability modeling and analysis of IEC 61850 based substation protection systems", *IEEE Transactions on Smart Grid*, vol. 5, no. 5, pp. 2194–2202, 2014.

[18] S. Kunsman, S. Meier, and R. Hedding, "Protection and control system impacts from the digital world", in *2016 69th Annual Conference for Protective Relay Engineers (CPRE)*, 2016, pp. 1–13.

[19] J. W. Evans, "Interface between automation and the substation", in *Electric Power Substations Engineering*, J. D. McDonald, Ed., 3rd ed. CRC Press, 2012, ch. 6, pp. 1–29.

[20] S. H. Horowitz and A. G. Phadke, "Current and voltage transformers", in *Power System Relaying*, 4th ed. John Wiley and Sons, 2014, ch. 3, pp. 46–73.

[21] *Instrument transformers - Part 2: Additional requirements for current transformers*, IEC 61869-2:2012, 2012.

[22] E. Padilla, *Substation Automation Systems: Design and Implementation*. Wiley, 2015.

[23] D. H. Wilson, J. W. Wright, S. Richards, and P. Mohapatra, "Functionality, design and benefit analysis of end-to-end digital substation", in *13th International Conference on Development in Power System Protection 2016 (DPSP)*, 2016, pp. 1–5.

[24] J. W. Evans, "Interface between automation and the substation", in *Electric Power Substations Engineering*, J. D. McDonald, Ed., 3rd ed. CRC Press, 2012, ch. 6, pp. 1–29.

[25] J. Ekanayake, K. Liyanage, J. Wu, A. Yokoyama, and N. Jenkins, *Smart Grid: Technology and Applications*. Wiley, 2012.

[26] L. Hewitson, M. Brown, and R. Balakrishnan, "Instrument transformers", in *Practical Power System Protection*. Elsevier Science, 2005, ch. 6, pp. 45–69.

[27] S. Holst and J. Zakonjšek, "Transient behaviour of conventional current transformers and its impact on performance of conventional and process bus based protection systems", in *Protection, Automation & Control World (PAC World) Conference 2016*, 2016, pp. 1–8.

[28] G. Ziegler, *Numerical Differential Protection: Principles and Applications*. John Wiley & Sons, 2012.

[29] *Instrument transformers - Part 6: Additional general requirements for low-power instrument transformers*, IEC 61869-6:2016, 2016.

[30] *Application manual, transformer protection RET670 2.0, IEC*, ABB, 2016. [Online]. Available: `https://search-ext.abb.com/library/Download.aspx?DocumentID=1MRK504138-UEN&LanguageCode=en&DocumentPartId=&Action=Launch` (visited on 01/02/2018).

[31] J. D. P. Hrabluik, "Optical current sensors eliminate CT saturation", in *2002 IEEE Power Engineering Society Winter Meeting. Conference Proceedings*, vol. 2, 2002, pp. 1478–1481.

[32] K. P. Brand, C. Brunner, and I. D. Mesmaeker, "How to complete a substation automation system with an IEC 61850 process bus", *Electra*, no. 255, pp. 12–24, 2011.

[33] *Instrument transformers - Part 9: Digital interface for instrument transformers*, IEC 61869-9:2016, 2016.

[34] K. P. Brand *et al.*, "The introduction of IEC 61850 and its impact on protection and automation within substations", pp. 1–102, 2007.

[35] S. Kucuksari and G. G. Karady, "Experimental comparison of conventional and optical current transformers", *IEEE Transactions on Power Delivery*, vol. 25, no. 4, pp. 2455–2463, 2010.

[36] J. Schmid and K. Kunde, "Application of non conventional voltage and currents sensors in high voltage transmission and distribution systems", in *2011 IEEE International Conference on Smart Measurements of Future Grids (SMFG) Proceedings*, 2011, pp. 64–68.

[37] *Brocheure current transformers*, Arteche. [Online]. Available: `https://www.arteche.com/en/products/current-transformers` (visited on 04/22/2018).

[38] "IEEE guide for application of optical instrument transformers for protective relaying", *IEEE Std C37.241-2017*, pp. 1–50, 2018.

[39] P. Roccato, A. Sardi, G. Pasini, L. Peretto, and R. Tinarelli, "Traceability of MV low power instrument transformer LPIT", in *2013 IEEE International Workshop on Applied Measurements for Power Systems (AMPS)*, 2013, pp. 13–18.

[40] S. Richards *et al.*, "Feedback on in-service deployment of the fully digital substation", in *2014 CIGRE*, 2014.

[41] A. Apostolov, "Substation automation systems", in *Smart Grid Handbook*, C.-C. Liu, S. McArthur, and S. J. Lee, Eds. Wiley, 2016, vol. 1, ch. 20, pp. 333–356.

[42] K.-P. Brand and I. D. Mesmaeker, "Power system protection", in *Handbook of Electrical Power System Dynamics: Modeling, Stability, and Control*, M. Eremia and M. Shahidehpour, Eds. John Wiley & Sons Inc., 2013, ch. 12, pp. 737–785.

[43] A. Apostolov, "Efficient maintenance testing in digital substations based on IEC 61850 edition 2", *Protection and Control of Modern Power Systems*, vol. 2, no. 1, pp. 1–37, 2017.

[44] Q. Yang, D. Keckalo, D. Dolezilek, and E. Cenzon, "Testing IEC 61850 merging units", in *44th Annual Western Protective Relay Conference*, Spokane, Washington, 2017, pp. 1–9. [Online]. Available: `https://cdn.selinc.com/assets/Literature/Publications/Technical%5C%20Papers/6823_TestingIEC61850_QY_20170907_Web.pdf?v=20180123-085831` (visited on 02/02/2018).

[45] G. Rzepka, S. Wenke, and S. Walling, "Choose simplicity for a better digital substation design", in *2017 70th Annual Conference for Protective Relay Engineers (CPRE)*, 2017, pp. 1–9.

[46] *COSI-CT optical current transformer*, GE Grid Solutions, 2016. [Online]. Available: `https://www.gegridsolutions.com/app/Resources.aspx?prod=cosi&type=1` (visited on 02/22/2018).

[47] *Optical current transformers for air insulated substations*, Trench, 2016. [Online]. Available: `http://www.trenchgroup.com/en/Products-Solutions/Instrument-Transformers/Optical-Current-Transformers/Optical-Current-Transformers` (visited on 02/22/2018).

[48] *Arteche SDO OCT EN*, Arteche. [Online]. Available: `https://www.arteche.com/en/products/optical-current-transformer` (visited on 02/22/2018).

[49] *Fiber optics current sensor - Free standing (FOCS-FS)*, ABB, 2015. [Online]. Available: `https://search-ext.abb.com/library/Download.aspx?DocumentID=2GJA708628&LanguageCode=en&DocumentPartId=&Action=Launch` (visited on 02/22/2018).

[50] J. Wang, F. Viawan, and T. Werner, "Effects of sensor technology on differential protection", in *10th IET International Conference on Developments in Power System Protection (DPSP 2010). Managing the Change*, 2010, pp. 1–5.

[51] H. Lehpamer, "Introduction to power utility communications", in. Artech House, 2016, ch. 2 Communications Fundamentals.

[52] S. Meier, T. Werner, and C. Popescu-Cirstucescu, "Performance considerations in digital substations", in *13th International Conference on Development in Power System Protection 2016 (DPSP)*, 2016, pp. 1–9.

[53] S. Meier, *Webinar: We are bridging the gap. Enabling the ABB digital substation.* [Online]. Available: http://new.abb.com/network-management/webinars/2016/abbs-digital-substation-webinar (visited on 10/05/2017).

[54] *Communication networks and systems for power utility automation - Part 9-2: Specific communication service mapping (SCSM) - sampled values over ISO/IEC 8802-3*, IEC 61850-9-2:2011, 2011.

[55] F. Steinhauser, "Sampled values - History, status, and outlook", in *2017 PAC World Conference*, 2017, pp. 1–5.

[56] *Implementation guideline for digital interface to instrument transformers using IEC 61850-9-2*, UCA International Users Group, 2004.

[57] *Instrument transformers - Part 1: General requirements*, IEC 61869-1:2007, 2007.

[58] *TC 38 Stability date of publications*, International Electrotechnical Commission, 2018. [Online]. Available: http://www.iec.ch/dyn/www/f?p=103:21:2796706578222:::21:FSP_ORG_ID,FSP_LANG_ID:1241,25 (visited on 06/13/2018).

[59] *TC 38 Work programme*, International Electrotechnical Commission, 2018. [Online]. Available: http://www.iec.ch/dyn/www/f?p=103:23:2796706578222:::23:FSP_ORG_ID,FSP_LANG_ID:1241,25 (visited on 06/14/2018).

[60] V. Skendzic and D. Dolezilek, "New and emerging solutions for sampled value process bus IEC 61850-9-2 standard - an editor's perspective", in *Southern African Power System Protection & Automation Conference*, Johannesburg, South Africa, 2017, pp. 1–10. [Online]. Available: https://cdn.selinc.com/assets/Literature/Publications/Technical%5C%20Papers/6797_NewEmerging_DD_20170309_Web2.pdf?v=20171115-101441 (visited on 02/02/2018).

[61] *Instrument transformers - Part 8: Electronic current transformers*, IEC 60044-8:2002, 2002.

[62] *Forskrift om elektriske forsyningsanlegg*, 2005. [Online]. Available: https://lovdata.no/dokument/SF/forskrift/2005-12-20-1626 (visited on 06/12/2018).

[63] *Forskrift om leveringskvalitet i kraftsystemet*, 2004. [Online]. Available: https://lovdata.no/dokument/SF/forskrift/2004-11-30-1557 (visited on 06/12/2018).

[64] *Forskrift om forebyggende sikkerhet og beredskap i energiforsyningen (beredskapsforskriften)*, 2012. [Online]. Available: https://lovdata.no/dokument/SF/forskrift/2012-12-07-1157 (visited on 06/12/2018).

[65] *Forskrift om systemansvaret i kraftsystemet*, 2002. [Online]. Available: https://lovdata.no/dokument/SF/forskrift/2002-05-07-448 (visited on 06/12/2018).

[66] *Funksjonskrav i kraftsystemet*, 2012. [Online]. Available: http://www.statnett.no/Global/Dokumenter/Kraftsystemet/Systemansvar/FIKS%202012.pdf (visited on 06/12/2018).

[67] J. Skaar and T. Holtebekk, *Polarisert lys*, 2018. [Online]. Available: https://snl.no/polarisert_lys.

[68] S. Ziegler, R. C. Woodward, H. H. C. Iu, and L. J. Borle, "Current sensing techniques: A review", *IEEE Sensors Journal*, vol. 9, no. 4, pp. 354–376, 2009.

[69] A. K. Zvezdin and V. A. Kotov, *Modern Magnetooptics and Magnetooptical Materials*, J. M. D. Coey and D. R. Tilley, Eds., ser. Studies in Condensed Matter Physics. Institute of Physics Publishing, 1997.

[70] J. Tioh, R. J. Weber, and M. Mina, "Magneto-optical switches", in *Optical Switches: Materials and Design*, S. J. Chua and B. Li, Eds. Elsevier, 2010, ch. 4, pp. 97–135.

[71] *File:linearly polarized wave.svg*, Wikimedia Commons, 2010. [Online]. Available: `https://commons.wikimedia.org/wiki/File:Linearly_Polarized_Wave.svg` (visited on 06/22/2018).

[72] *File:circular.polarization.circularly.polarized.light with.components left.handed.svg*, Wikimedia Commons, 2010. [Online]. Available: `https://commons.wikimedia.org/wiki/File:Circular.Polarization.Circularly.Polarized.Light_With.Components_Left.Handed.svg` (visited on 06/22/2018).

[73] "Optical current transducers for power systems: A review", *IEEE Transactions on Power Delivery*, vol. 9, no. 4, pp. 1778–1788, 1994.

[74] M. H. Samimi, A. A. S. Akmal, and H. Mohseni, "Optical current transducers and error sources in them: A review", *IEEE Sensors Journal*, vol. 15, no. 9, pp. 4721–4728, 2015.

[75] A. J. Rogers, "Elements of polarization optics", in *Polarization in Optical Fibers*. Artech House, 2008, ch. 3, pp. 75–112.

[76] R. Wang, S. Xu, W. Li, and X. Wang, "Optical fiber current sensor research: Review and outlook", *Optical and Quantum Electronics*, vol. 48, no. 9, pp. 1–22, 2016. [Online]. Available: `https://link.springer.com/article/10.1007/s11082-016-0719-3` (visited on 04/17/2018).

[77] E. M. Esmail, N. I. Elkalashy, T. Kawady, and A. M. I. Taalab, "Experimental implementation of optical current transducers", in *2016 Eighteenth International Middle East Power Systems Conference (MEPCON)*, 2016, pp. 276–281.

[78] W. Wang, X. Wang, and J. Xia, "The nonreciprocal errors in fiber optic current sensors", *Optics & Laser Technology*, vol. 43, no. 8, pp. 1470–1474, 2011. [Online]. Available: `https://www.sciencedirect.com/science/article/pii/S0030399211001277` (visited on 04/25/2018).

[79] R. M. Silva, H. Martins, I. Nascimento, J. M. Baptista, A. L. Ribeiro, J. L. Santos, P. Jorge, and O. Frazão, "Optical current sensors for high power systems: A review", *Applied sciences*, vol. 2, no. 3, pp. 602–628, 2012. [Online]. Available: `http://www.mdpi.com/2076-3417/2/3/602/htm` (visited on 03/05/2018).

[80] F. Rahmatian, "Optical instrument transformers", *PAC World Magazine March 20018 Issue*, pp. 18–25, 2018.

[81] K. T. V. Grattan and Y. N. Ning, "Optical current sensor technology", in *Optical Fiber Sensor Technology: Applications and Systems*, L. S. Grattan and B. T. Meggitt, Eds., Springer, 1999, ch. 7, pp. 183–223.

[82] K. Bohnert, H. Brandle, M. G. Brunzel, P. Gabus, and P. Guggenbach, "Highly accurate fiber-optic dc current sensor for the electrowinning industry", *IEEE Transactions on Industry Applications*, vol. 43, no. 1, pp. 180–187, 2007.

[83] K. Bohnert, P. Gabus, J. Nehring, and H. Brandle, "Temperature and vibration insensitive fiber-optic current sensor", *Journal of Lightwave Technology*, vol. 20, no. 2, pp. 267–276, 2002.

[84] K. Bohnert, R. Thomas, and M. Mendik, "Light measures current", no. 1, pp. 12–17, 2014. [Online]. Available: `https://library.e.abb.com/public/0d948cedb40451cec1257ca900532dd0/12-17%5C%201m411_EN_72dpi.pdf` (visited on 04/22/2018).

[85] K. Bohnert, C. P. Hsu, L. Yang, A. Frank, G. M. Müller, and P. Gabus, "Fiber-optic current sensor tolerant to imperfections of polarization-maintaining fiber connectors", *Journal of Lightwave Technology*, vol. 36, no. 11, pp. 2161–2165, 2018.

[86] B. Li and L. Li, "An overview of the optical current sensor", in *2012 International Conference on Computer Science and Electronics Engineering*, vol. 3, 2012, pp. 202–206.

[87] P. Ripka, "Electric current sensors: A review", *Measurement Science and Technology*, vol. 21, no. 11, pp. 1–24, 2010. [Online]. Available: `http://iopscience.iop.org/article/10.1088/0957-0233/21/11/112001/meta` (visited on 03/05/2018).

[88] B. Lee, "Review of the present status of optical fiber sensors", *Optical Fiber Technology*, vol. 9, no. 2, pp. 57–79, 2003. [Online]. Available: `https://www.sciencedirect.com/science/article/pii/S1068520002005278` (visited on 04/25/2018).

[89] Y. Ding, Y. Dong, J. Zhu, B. Zheng, D. Zhang, and W. Hu, "Linear birefringence and imperfect quarter wave plate effects on optic-fiber current sensor", in *2011 Asia Communications and Photonics Conference and Exhibition (ACP)*, 2011, pp. 1–6.

[90] J. Blake, P. Tantaswadi, and R. T. de Carvalho, "In-line sagnac interferometer current sensor", *IEEE Transactions on Power Delivery*, vol. 11, no. 1, pp. 116–121, 1996.

[91] M. Lenner, W. Quan, G. Müller, L. Yang, A. Frank, and K. Bohnert, "Interferometric fiber-optic current sensor with inherent source wavelength shift compensation", in *2015 IEEE SENSORS*, 2015, pp. 1–4.

[92] *Instrument transformers - The use of instrument transformers for power quality measurement*, IEC TR 61869-103:2012, 2012.

[93] R. Thomas, A. Vujanic, D. Z. Xu, J. E. Sjödin, H. R. M. Salazar, M. Yang, and N. Powers, "Non-conventional instrument transformers enabling digital substations

for future grid", in *2016 IEEE/PES Transmission and Distribution Conference and Exposition (T D)*, 2016, pp. 1–5.

[94] M. Normandeau and J. Mahseredjian, "Evaluation of low-power instrument transformers for generator differential protection", *IEEE Transactions on Power Delivery*, vol. 33, no. 3, pp. 1143–1152, 2018.

[95] K. Bohnert, P. Gabus, J. Kostovic, and H. Brändle, "Optical fiber sensors for the electric power industry", *Optics and Lasers in Engineering*, vol. 43, no. 3-5, pp. 511–526, 2005.

[96] *Instrument transformers*, Trench, Trench Group. [Online]. Available: `http://www.trenchgroup.com/en/Products-Solutions/Instrument-Transformers/Instrument-Transformers` (visited on 04/22/2018).

[97] *Product guide, process bus I/O system SAM600 version 1.2*, ABB, 2017. [Online]. Available: `https://search-ext.abb.com/library/Download.aspx?DocumentID=1MRK511437-BEN&LanguageCode=en&DocumentPartId=&Action=Launch` (visited on 01/30/2018).

[98] *Reason MU320 digital substation merging unit*, GE Grid Solutions, 2017. [Online]. Available: `https://www.gegridsolutions.com/app/ViewFiles.aspx?prod=MU320&type=1` (visited on 04/22/2018).

[99] J. Jesus and A. Varghese, "Feeder differential protection in hybrid mode: Scheme performance with mix of -9-2le sampled values and analogue inputs", in *2017 International Conference on Modern Power Systems (MPS)*, 2017, pp. 1–5.

[100] C. A. Dutra, I. H. Cruz, T. A. Franzen, R. R. Matos, F. C. Neves, L. B. Oliveira, and G. Krefta, "Comparison of analogue measurements between merging units and conventional acquisition systems", in *12th IET International Conference on Developments in Power System Protection (DPSP 2014)*, 2014, pp. 1–5.

[101] A. Bonetti, *IEC 61850 standard and related iec committees as reference for relay protection applications*, 2018. [Online]. Available: `http://gnu.ets.kth.se/~nt/tmp/protaut/slides/ind_iec61850_standard_iec_committees_protection_applications.pdf` (visited on 06/13/2018).

[102] *Communication networks and systems for power utility automation - Part 5: Communication requirements for functions and device models*, IEC 61850-5:2013, 2013.

[103] *Communication networks and systems for power utility automation - Part 10: Conformance testing*, IEC 61850-10:2012, 2012.

[104] S. Hutterer, R. S. J. Løken, and M. Schicklgruber, "Digital substation pilot: Substation automation and protection system based on IEC 61850-9-2 process bus", in *2017 PAC World Conference*, 2017, pp. 1–7.

[105] D. M. E. Ingram, P. Schaub, D. A. Campbell, and R. R. Taylor, "Evaluation of precision time synchronisation methods for substation applications", in *2012 IEEE*

International Symposium on Precision Clock Synchronization for Measurement, Control and Communication Proceedings, 2012, pp. 1–6.

[106] V. Skendzic, I. Ender, and G. Zweigle, "IEC 61850-9-2 process bus and its impact on power system protection and control reliability", in *2007 9th Annual Western Power Delivery Automation Conference*, 2007, pp. 1–7.

[107] G. S. Antonova *et al.*, "Standard profile for use of IEEE std 1588-2008 Precision Time Protocol (PTP) in power system applications", in *2013 66th Annual Conference for Protective Relay Engineers*, 2013, pp. 322–336.

[108] X. Chen, H. Guo, and P. Crossley, "Interoperability performance assessment of multivendor IEC 61850 process bus", *IEEE Transactions on Power Delivery*, vol. 31, no. 4, pp. 1934–1944, 2016.

[109] X. Chen, H. Guo, and P. Crossley, "Performance testing of IEC 61850 based architecture for UK national grid standardised substation automation solutions", in *2015 IEEE Power Energy Society General Meeting*, 2015, pp. 1–5.

[110] J. Haude *et al.*, "Smart switchgear" using IEC standard 61850 - First experience gained with a pilot project in a 380/110 kV substation", in *2010 CIGRE*, 2010, pp. 1–8.

[111] C. R. del Castillo, J. F. Pozuelo, M. Goraj, R. Pereda, and A. Amezaga, "Redundancy challenges on IEC 61850 systems and migration paths for IEC 61850 substation communication networks", in *2012 CIGRE Paris Session*, 2012, pp. 1–14.

[112] D. M. E. Ingram, P. Schaub, R. R. Taylor, and D. A. Campbell, "System-level tests of transformer differential protection using an IEC 61850 process bus", *IEEE Transactions on Power Delivery*, vol. 29, no. 3, pp. 1382–1389, 2014.

[113] O. Aune, "Ikke-konvensjonelle måletransformatorer i digital stasjon", B.S. thesis, Norwegian University of Science and Technology, Gjøvik, 2017.

[114] *Communication networks and systems for power utility automation - Part 7-3: Basic communication structure - common data classes*, IEC 61850-7-3:2010, 2010.

[115] *Technical manual, transformer protection RET670 2.0, IEC*, ABB, 2016. [Online]. Available: `https://search-ext.abb.com/library/Download.aspx?DocumentID=1MRK504139-UEN&LanguageCode=en&DocumentPartId=&Action=Launch` (visited on 03/08/2018).

[116] R. Løken, M. W. Kristiansen, and S. Losnedal, "Expectations and specifications of IEC 61850 based digital substation automation system used by Statnett", in *2014 CIGRE*, 2014.

[117] Z. Bajramović, I. Turković, A. Mujezinović, A. Čaršimamović, and A. Muharemović, "Measures to reduce electromagnetic interferences on substation secondary circuits", in *Proceedings ELMAR-2012*, 2012, pp. 129–132.

[118] *OMICRON CMC 356 reference manual*, OMICRON electronics, 2014.

[119] *OMICRON getting started with OMICRON test universe 3.00*, OMICRON electronics, 2014.

[120] *Flyer SEL-2488 satellite-synchronized network clock*, Schweitzer Engineering Laboratories, 2014. [Online]. Available: https://cdn.selinc.com/assets/Literature/Product%5C%20Literature/Flyers/2488_PF00327.pdf?v=20170728-141139 (visited on 01/02/2018).

[121] *Product guide, transformer protection RET670 2.0, IEC*, ABB, 2016. [Online]. Available: https://search-ext.abb.com/library/Download.aspx?DocumentID=1MRK504141-BEN&LanguageCode=en&DocumentPartId=&Action=Launch (visited on 01/30/2018).

[122] R. Løken and S. Losnedal, "Multifunctional protection and control IEDs in future transmission systems", in *2017 PAC World Conference*, 2017, pp. 1–11.

Appendix A

E-Mail

A.1 Statnett

A.1.1 First E-Mail

Request:

Hei,

Sånn jeg har forstått det, benyttes det i dag godkjent utstyr for avregningsmåling i Statnetts stasjoner. I tillegg er det krav om at det må utføres en akkreditert målekjedekontroll av noen med godkjenning etter at utstyret er satt i drift.

For digital stasjon lurer jeg da på hvilket utstyr som kan benyttes, evt. hvor funksjonen avregningsmåling vil ligge? Foreligger det godkjent utstyr? Kan dette skape problemer for innføringen av digital stasjon med optiske strømtransformatorer i Statnett? Hvem kan utføre akkreditert målekjedekontroll for en digital stasjonsløsning?

Hvis det er slik at det ikke foreligger godkjent utsyr i dag, når forventes det at dette vil foreligge?

Ønsker gjerne rask tilbakemelding med hensyn til fullføring av oppgaven.

Med vennlig hilsen

Ingvill Rian

Reply:

Hei Ingvill,

Det stemmer at det i dag utføres akkreditert målekontroll for avregningsmåler etter at den er satt på drift av godkjent akkrediterings selskap.

Det er ein avregningsmåler som kan benyttes i kontrollanlegg med prosessbus som kan ta inn digitale målinger ved bruk av IEC 61850. Det er ikkje avklart korleis dei digitale målingene skal akkrediteres. Dette er eit spørsmål som diskuteres internasjonalt. Eg er usikker på når ei løysing er på plass, vi arbeider med problemstillinga i FoU Digital stasjon i Statnett.

Ei løysing kan være å bruke konvensjonelle måletransformatorer for avregningsmåling, men da tar vi ikkje i bruk teknikken heilt ut.

A.1.2 Second E-Mail

Hei,

Har du mulighet til å svare på disse spørsmålene i forbindelse med fullføring av masteroppgaven? Skulle gjerne hatt svar så raskt som mulig.

1. **Slik jeg har forstått det er Arteche's løsning for optisk strømtransformator basert på innendørs montasje av merging unit inne i kontrollrom sammen med vern- og kontroll-IED-er.**

    - **Ønsker Statnett å plassere den tilhørende elektronikken til de optiske strømtransformatorene ute i anlegget?**
      Det stemmer Arteche ønsker å plassere MU inne i kontrollrom, mens andre leverandører må plassere dem i skap i ute i anlegget.

    - **Har Statnett sett på løsninger i forhold til utendørs plassering av merging uniter i feltskap?**
      Statnett har planer om å ha en fleksibel løsning i forhold til plassering av MU, slik at de enten kan plasseres inne i kontrollrom eller ute i anlegget.

    - **Finnes det egnede skap med oppvarming?**
      Statnett ser på løsninger andre har valgt og skal i år utforme skap som har nødvendig oppvarming evt kjøling og EMP sikring for å plassere elektronikk ute i apparatanlegget.

2. **Bruk av vern i digital stasjon.**

   - **Støtter de vernene som Statnett benytter i dag prosessbuss, og kan de benyttes i en digital stasjon?**
     Det er mange leverandører som støtter prosessbus, begge leverandørene vi i dag bruker (ABB og Siemens) har vern som støtter prosessbus.

   - **Finnes det vern av alle typer som trengs i stasjoner, som støtter prosessbuss og som Statnett har godkjent? Eller vil Statnett måtte godkjenne nye vern for å kunne realisere en digital stasjon fullt ut?**
     Vernene som har prosessbus er nye versjoner som må godkjennes på nytt for de kan tas i bruk. Det er uklart om det finnes gode løsninger for samleskinnevern for større stasjoner, dette er en av sakene vi ser på i 2018.

3. **Har Statnett gjort noen vurderinger i forhold til hvilke krav vernene vil stille til de digitale målekretsene (optisk strømtransformator med tilhørende merging unit, stand-alone-merging unit og prosessbuss/fiberoptiske kabler) i forbindelse med prosjektet «Digital stasjon»?**

   - Det pågår arbeid i IEC TC95 AhWG3 som ser på krav som stilles til vern i forhold til krav som stilles til måletransformatorer. I dag er det ikke samme krav til transferkarakteristikken.
   - Statnett arbeider med hvilke krav som skal stilles.
   - Det diskuteres om typetest for godkjenning av nye produkt må inkluderer både MU/SAMU og vern fra aktuelle leverandører i tillegg til krav som stilles.

4. **Kunne jeg fått tilgang til teknisk dokumentasjon for Arteche's optiske strømtransformator, gjerne inkludert informasjon om hvilke tester som har blitt utført?**
   Dette må eg sjekke.

5. **Hvor stor datakapasitet (bit/s) har prosessbussnettverket i Statnetts pilotstasjon? Tenker man å benytte samme datakapasitet i en fremtidig digital stasjon?**
   Pilotstasjonen har 1 Gb prosessnettverk, det er og tenkt å bruke i framtida (vi har og mulighet for 5 Gb). Verna har stort sett 100 Mb tilkobling til nettverket.

6. **Bruk av fiber-optiske kabler i digital stasjon.**

   - **Hvilke erfaringer har Statnett gjort vedrørende bruk av fiber-optiske kabler i dagens anlegg?**

  - Vi har i piloten kun lagt fibernettverk lokalt i kontrollrommet.
  - Tilkobling til NCIT går på fiberoptisk forbindelse fra kontrollrom til apparatanlegg.
  - Det er behov for spesialkompetanse for å koble fibernettverk i Digital stasjon.

- **Har man erfart at det finnes støykilder eller andre problemer ved bruk av slike kabler?**
  Vi har ikkje hatt denne type erfaring, men skal plassere utstyr i feltskap i anlegg for å sjekke om det kan oppstå problem.

- **Hvilke konsekvenser vil bruk av fiber-optiske kabler i stedet for konvensjonelle kobberkabler få for kabelføringen og kabelleggingen i Statnetts stasjoner?**

  - Statnett vil ha behov for mindre kabelføring fra kontrollrom til apparatanlegg.
  - Det vurderes om vi endrer fra kabelkanaler til rør eller om vi legger ut små kabel kanaler.
  - Det vil trulig framleis være krav til to separate kanaler fra kontrollrom til apparatanlegg.
  - Vi ser for oss kostnadsreduksjon på kabling, kabelkanaler og moontasje.

Håper dette er til hjelp. Lykke til videre!

A.1.3 Third E-Mail

Hei,

Jeg har noen spørsmål angående konvensjonelle strømtransformatorer. Håper du kan svare så raskt som mulig med tanke på fullføring av masteroppgaven.

1. **Er det noen vedlikeholdsprosedyrer for de konvensjonelle strømtransformatorene i Statnetts stasjoner?**
   Ja. Det er månedlige visuelle inspeksjoner, avlesing av evt. instrumenter og sjekk av olje. Ikke særlig omfattende, men likevel noe som man da benytter litt tid på. Anta eksempelvis 30 min per inspeksjon per måned per strømtrafo.

2. **Hvor lang levetid har de konvensjonelle strømtransformatorene? Hvor ofte bytter Statnett dem ut?**
   Variabelt, men avhengig av leverandør osv typisk 20-50 år.

3. **Omtrent hvor mye koster et sett med tre konvensjonelle strømtransformatorer (f.eks. for systemspenning på 420 kV)?**
   Store variasjoner, men opptil 8500 Euro for en strømtrafo med tre vernkjerner og to målekjerner.

A.2 ABB

Hi

Your Questions for our FOCS optical ct with replies from our factory for this:

1. **What is the metering accuracy of FOCS-FS?**
   Class 0.2s for rated current above 400 A. For lower rated currents more prolonged integration time is required.

2. **Is FOCS-FS optimized for a specific application, such as metering or protection, e.g. in terms of number of fiber coil turns or type of sensor electronics? Or is a single FOCS-FS equally suited for both metering and protection applications?**
   Same sensor covers both metering and protection applications.

3. **Over which dynamic range are the metering and protection accuracy specifications of FOCS-FS maintained?**
   Metering 0.2S from rated currents 400A to 164kA, class 0.2 from 80A to 164kA, class 0.5 from 35A to 164kA. Protection 5P from rated currents 70A to 164kA.

4. **How good is the ability of FOCS-FS to reproduce rapid changes in the primary current?**
   The main limiting factor is the digital output protocol (IEC 61850-9-2LE). This limits for 50Hz the output bandwidth to 2kHz or 6.4kHz. Internally the FOCS is acquiring raw measurement data with more than 1MS/s, which means it will react to changes faster than 500kHz.

5. **What is the bandwidth of FOCS-FS? Does the opto-electronic module impose any limitations on the bandwidth of the digital output?**
   As said in the point 4, the bandwidth is determined by the standard for process bus protocol. Physical limitation of opto-electronic module is given by the length of the sensor head optical cable which influences the time of flight of light from the OE-unit to sensor head and back. This results in raw sampling rate of less than 2MS/s.

6. **How good is the ability of FOCS-FS to reproduce rapid changes in the primary frequency?**
   FOCS is measuring how much current has flown through the sensor head aperture during some short time of less than 1 microsecond. There is no direct influence of the primary current signal form (i.e. frequency variations) to the FOCS. Again is the final limit given with the output stream sampled values rate.

7. **Does the opto-electronic module support other methods for time synchronization than PPS?**
   No.

8. **What is the expected lifetime of FOCS-FS?**
   Expected lifetime of opto-electronic units is comparable to the one for IEDs (15 years), lifetime of optical sensor is 30+ years.

9. **Do you supply other non-conventional current transformers, or any non-conventional voltage transformers?**
   ABB does not have optical voltage transformers with IEC61850-9-2 output. For GIS application, there are capacitive voltage sensors with such output.

Let us know if you need any more information.

A.3 Arteche

A.3.1 First E-Mail

Dear Ingvill,

Thanks for your e-mail.

Most of your questions cover 2 main topics:

a) Questions 2,3 and 4 are related to the sample rate. Internally, we work with 192kHz sampling rate. However, the output we provide (sampled values) is filtered so the output is compliant with the recommendations of the IEC61869-9 standard.

b) Questions 1 and 7 are related to the accuracy and dimensioning of the OCT. There are 2 basic principles here (see the attached document for more details) that explain why the dynamic range is virtually unlimited:

   i. You can see the measurement error as electronic noise → The lower the signal

the more difficult to measure accurately
But, it is possible to increase the signal to noise ratio by adding fiber turns at the sensing coil, so we can ensure accuracy at low currents by adding more fiber turns.

ii. The response of the OCT is very linear and it does not saturate → High currents are not an issue (from the point of view of accuracy)

You can find more detailed explanations on the attached document.

Please find my answers to each question below in red.

Should you need further clarifications, please do not hesitate to contact us.

1. **Over which dynamic range are the metering and protection accuracy specifications of SDO OCT maintained?**
   It is virtually unlimited. Designs for Cl0.2 accuracy are possible for any given current levels.

2. **How good is the ability of SDO OCT to reproduce rapid changes in the primary current?**
   The performance is very good. This is related to the sample rate that is selected. We have implemented the sample rates that the IEC61869-9 standard defines for digital instrument transformers.

3. **Does the SDO MU impose any limitations on the bandwidth of the digital output?**
   No. The only constraint is the standard for the digital output (IEC61869-9), the MU does not impose any additional constraints.

4. **How good is the ability of SDO OCT to reproduce rapid changes in the primary frequency?**
   This is related to the sample rate. Internally we 192kHz sample rate and the output (sampled values) are as per the above mentioned standard. Please also see the above answers.

5. **What is the maximum permissible length of the fiber optic cables connecting the SDO ICT to the SDO MU?**
   No limitation for digital substation applications. For some special applications, we have installations with distances as high as 20km

6. **What is the expected lifetime of SDO OCT?**

Tricky question. There is no specific aging test that we conducted so far so I cannot commit to a given period of time. However, there is no maintenance requirement in the OCT, so its useful life should be at least as long as the useful life of equivalent conventional CTs. This is applicable for the primary part, the Merging Unit is an IED and it has a useful life that is equivalent to that of conventional digital protection IED-s.

7. **Is SDO OCT optimized for a specific application, such as metering or protection, e.g. in terms of number of fiber coil turns or type of sensor electronics? Or is a single SDO OCT equally suited for both metering and protection applications?**
   A single device covers both metering and protections applications. The response of the OCT is very linear and there is no saturation, so at very high currents, we can keep an excellent accuracy class (way better than protection accuracy requirements). Please see the attached document for more details on this.

8. **Do you supply other non-conventional current transformers other than SDO OCT, or any non-conventional voltage transformers?**
   As of today, for HV applications we supply Capacitive VTs. For lower voltages (up to 36kV) we are also supplying resistive dividers and Rogowski coils.

A.3.2 Second E-Mail

Dear Ingvill,

Please find below our answers.

1. **What is the weight of SDO OCT (e.g. with a system voltage rating of 420 kV)? How does this compare to the weight of a conventional current transformer with the same system voltage rating?**
   It is much lighter than a conventional CT. The sensor head is 15kg and it can be used for any voltage level. For 420kV, I estimate that the total weight would be approx. 160kg.

2. **How much does SDO OCT cost (sensor heads and SDO MU, respectively)? How does this compare to the cost of a comparable conventional current transformer?**
   You can consider approx. 45k€ for a complete set of 3 CT-s and 1 MU. Once the product is industrialized, we expect the optical CT to be more cost-effective than a conventional one for voltages above 245kV.

3. **What is the operating voltage range of SDO OCT (e.g. with a system voltage rating of 420 kV)? Can a SDO OCT with a system voltage rating of 420 kV be operated at 300 kV?**
   Unlimited, the voltage level doesn't influence on the operation of the OCT. It is just a matter of selecting the proper insulator. So yes, a 420kV device can be used for 300kV.

4. **What is the processing delay time of SDO MU?**
   The "delay time" is less than 1,58 ms.

5. **Does SDO MU support PRP and HSR network redundancy protocols?**
   Yes

6. **According to the SDO OCT brochure, "the rotation of the polarization state of the light is measured interferometrically". What type of configuration does the SDO OCT employ (Sagnac loop interferometer, reflective interferometer, other)?**
   It is a 3x3 Sagnac interferometer

7. **Does the accuracy of SDO OCT change over the given operating temperature range (-40°C to +85°C)? Have any measures been taken in order to reduce the sensitivity of SDO OCT to temperature variations? Does SDO OCT employ temperature compensation?**
   No, we guarantee accuracy over the whole temperature range. We employ temperature compensation by sensing the temperature of the sensor-fiber.

8. **Is the accuracy of SDO OCT sensitive to vibrations and stray magnetic fields? Have any measures been taken in order to reduce the sensitivity of SDO OCT to vibrations and stray magnetic fields?**
   The design is immune to vibrations and stray magnetic fields.

9. **Does SDO OCT require any maintenance? In that case, what are the maintenance procedures and how often do they have to be performed?**
   No specific maintenance is required.

10. **How is the procedure of replacing sensor heads and SDO MU? If a single sensor head fails, is it possible to only replace this sensor head or does all of the sensor heads and the SDO MU have to be replaced?**
    It is possible to replace any given sensor head or any given MU without on-site calibration.

11. **What type of tests have SDO OCT been subjected to?**
    IEC 60044-8.

12. **Does SDO OCT pose any requirements for the surrounding systems in a digital substation (fiber-optic process bus, protection IEDs and measuring IEDs) in order to perform satisfactory?**
    No special requirements other than being connected to the process bus using 2 x 100 Base FX Ethernet interface with LC type connectors and Multimode fiber optics. We support both IEC61850-9-2LE and IEC61869-9 Sampled Values.

13. **Lastly, I would like to ask permission to reuse the figure which displays the SDO ICT head and insulator on page 4 of the Arteche SDO OCT brochure, in my thesis.**
    You can do it with the only requirement of mentioning ARTECHE.

A.4 GE Grid Solutions

Hi Ingvill,

I am happy to respond to your questions related to our COSI-CT .

Please observe that we have a broad portfolio of non-conventional CTs & VTs and in communication with Statnett we have expressed our interest in addition to the COSI-CT to also pre-qualify our CMO/VTO/CTO range. See attached pdf's for details.

Back to your questions , find my replay in red below.

1. **What is the rated dynamic current of COSI-CT?**
   The COSI-CT has been tested up to 80 kA rms for 1 s and 210 kA pk (fully offset).

2. **How good is the ability of COSI-CT to reproduce rapid changes in the primary current?**
   Very good. dI/dt exceeds 70 A/µs.

3. **Does the electronic module of COSI-CT impose any limitations on the bandwidth of the digital output?**
   The digital output is filtered to avoid anti-aliasing in the digital output. The cut-off frequency is programmable and is set based on the digital output sampling rate. For 4800 Hz, we set the cut-off frequency to 1.5 kHz.

4. **How good is the ability of COSI-CT to reproduce rapid changes in the**

primary frequency?
For protection it is very good. There are no limitation. For very precise revenue metering applications the output is filtered, so there is a slower response to changes in the power system frequency.

5. **Is COSI-CT optimized for a specific application, such as metering or protection, e.g. in terms of number of fiber coil turns or type of sensor electronics? Or is a single COSI-CT equally suited for both metering and protection applications?**
The number of fiber turns does affect the accuracy to some extent – especially for very precise measurements such as revenue metering. Having said that, in general we use a single fiber with a standard number of turns for both metering and protection. One sensor can provide 0.15 % accuracy from <1 % to 200 % of the rated primary current and IEC 5P accuracy up to 210 kApk. If the rated primary current exceeds 3000 A, we reduce the number of fiber turns to improve the metering accuracy as we start to get into the non-linear portion of CT transfer function above 3000 A with our standard number of fiber turns.

6. **What is the maximum permissible length of the fiber optic cables connecting the sensor head of the COSI-CT to its electronic modules? Should the electronic modules be installed in the in the switchyard or indoor in a protection and control panel?**
1000 m. For the COSI-CT, this limitation comes from the modulator cable (which is a copper cable that controls the sensor's phase modulator, i.e. the fiber optic cable isn't the limiting factor).

7. **Which time synchronization methods does the electronic module of COSI-CT support?**
Today we support 1PPS and IRIG-B. IEEE 1588 PTP is planned for not-to-distant future.

8. **Can the electronic module of COSI-CT interface conventional current and voltage transformers, or is a stand-alone merging unit required for this purpose?**
The COSI-MU (COSI-CT Electronics) has a 3-phase conventional secondary input for digitizing VT signals. No CT inputs today.

9. **What is the expected lifetime of COSI-CT?**
The COSI-CT is designed for 30+ years. The limiting factor is the silicon sheds on the insulator. The electronics are designed for 25 years, but in practise the actual

life is lower (more like 15 years). We recommend planning to replace the electronics once during the life of the COSI-CT (in general we recommend replacing the CT electronics when the IEDs are replaced).

I hope our reply is according to your expectations. Feel free to contact me in case of questions.

Appendix B

Formulas

B.1 Supply Grid

The short-circuit impedance of the supply grid was calculated by the use of Equation (B.1),

$$Z_{SC} = \frac{{U_N}^2}{S_{SC}} \tag{B.1}$$

where U_N is the nominal voltage of the supply grid and S_{SC} is the short-circuit capacity. Based on Equation (B.2) and the assumption given by Equation (B.3), Equation (B.4) can be derived,

$${Z_{SC}}^2 = {R_+}^2 + {X_+}^2 \tag{B.2}$$

$$\frac{X_+}{R_+} = 10 \tag{B.3}$$

$$X_+ = \sqrt{\frac{{Z_{SC}}^2}{1.01}} \tag{B.4}$$

where Z_{SC} is the short-circuit impedance of the supply grid, R_+ is the short-circuit positive sequence resistance and X_+ is the short-circuit positive sequence reactance. The assumptions given by Equation (B.5), Equation (B.6) and Equation (B.7) were used to calculate the positive and zero sequence resistance and reactance of the supply grid at different short-circuit capacities. The resulting values are given in Table B.1

$$R_+ = 0.1 \cdot X_+ \tag{B.5}$$

$$X_0 = 3 \cdot X_+ \tag{B.6}$$

$$R_0 = 3 \cdot R_+ \tag{B.7}$$

R_+ is the short-circuit positive sequence resistance of the supply grid, X_+ is the short-circuit positive sequence reactance, R_+ is the short-circuit zero sequence resistance and X_+ is the short-circuit zero sequence reactance.

Table B.1: Supply grid data at different short-circuit capacities.

Short-Circuit Capacity [MVA]	$\mathbf{R_0}$ **[Ω]**	$\mathbf{X_0}$ **[Ω]**	$\mathbf{R_+}$ **[Ω]**	$\mathbf{X_+}$ **[Ω]**
10 000	5.265	52.65	1.755	17.55
6 800	7.743	77.43	2.581	25.81
3 300	15.957	159.57	5.319	53.19

B.2 Current Transformers

The rated primary currents of the CT on the HV side of the power transformer and the CT on the LV side of the power transformer were calculated by the use of Equation (B.8) and Equation (B.9), respectively,

$$I_{PN,HV} = \frac{S_N}{U_{HVN}} \tag{B.8}$$

$$I_{PN,LV} = \frac{S_N}{U_{LVN}} \tag{B.9}$$

where S_N is the rated power of the power transformer, U_{HVN} is the rated voltage of the HV winding and U_{LVN} is the rated voltage of the LV winding.

B.3 Load

The resistance of the load at different short-circuit capacities was calculated by the use of Equation (B.10),

$$R_{load} = \frac{U_{LV}^2}{S_{SC}} \tag{B.10}$$

where U_{LV} is the rated voltage of the LV winding of the power transformer and S_{SC} is the short-circuit capacity of the supply grid. The resulting resistances are given in Table B.2.

Table B.2: Resistance of the load at different short-circuit capacities.

Short-Circuit Capacity [MVA]	**R [Ω]**
10 000	55.37
6 800	54.86
3 300	52.94

Appendix C

MATLAB Scripts

C.1 Fundamental Frequency Phase Current

```
%% DFT, fundamental frequency

close all;
clear all;
clc;

R1 = 1;
C1 = 0;

B = csvread('simulation473.CSV', R1, C1);

t = B(763:4763,1);
CT1 = B(763:4763,2);
CT2 = B(763:4763,3);
CT3 = B(763:4763,4);
MU1 = B(763:4763,5);
MU2 = B(763:4763,6);
MU3 = B(763:4763,7);

t = t - 190.5;

for n = 1:80
    cosDFT(n) = cos(2*pi*n/80);
    sinDFT(n) = sin(2*pi*n/80);
end; clear n;

real_CT = sqrt(2) / 80 * filter(sinDFT, 1, CT1);
imag_CT = sqrt(2) / 80 * filter(cosDFT, 1, CT1);
real_MU = sqrt(2) / 80 * filter(sinDFT, 1, MU1);
imag_MU = sqrt(2) / 80 * filter(cosDFT, 1, MU1);

```

```
32 abs_CT = (real_CT.^2 + imag_CT.^2).^(1/2) / 1000;
33 abs_MU = (real_MU.^2 + imag_MU.^2).^(1/2) / 1000;
34
35 figure;
36 plot(t, abs_MU, 'linewidth', 1.5);
37 hold on;
38 plot(t, abs_CT, 'linewidth', 1.5);
39 xlabel('Time [ms]');
40 ylabel('Primary Current [kA_{RMS}]');
41 xlim([0 1000]);
42 set(gca,'FontSize', 18);
43 legend('I_{rec\_samu\_fundamental}', 'I_{rec\_analog\_fundamental}');
```

C.2 Fundamental Frequency Differential Current

```
%% DFT, fundamental frequency differential current

close all;
clear all;
clc;

R1 = 1;
C1 = 0;

B = csvread('simulation467.CSV', R1, C1);

t = B(763:4763,1);
CT1 = B(763:4763,2);
CT2 = B(763:4763,3);
CT3 = B(763:4763,4);
MU1 = B(763:4763,5) / 1312*412;
MU2 = B(763:4763,6) / 1312*412;
MU3 = B(763:4763,7) / 1312*412;

t = t - 190.5;

for n = 1:80
    cosDFT(n) = cos(2*pi*n/80);
    sinDFT(n) = sin(2*pi*n/80);
end; clear n;

real_CT = sqrt(2) / 80 * filter(sinDFT, 1, CT1);
imag_CT = sqrt(2) / 80 * filter(cosDFT, 1, CT1);
real_MU = sqrt(2) / 80 * filter(sinDFT, 1, MU1);
imag_MU = sqrt(2) / 80 * filter(cosDFT, 1, MU1);

real = real_CT + real_MU;
imag = imag_CT + imag_MU;

abs = (real.^2 + imag.^2).^(1/2);

figure;
plot(t, abs, 'linewidth', 1.5);
xlabel('Time [ms]');
ylabel('Primary Current [A_{RMS}]');
legend('I_{rec\_diff\_fundamental}');
xlim([0 1000]);
set(gca,'FontSize', 18);
```

C.3 Second Harmonic Component

```
%% DFT, 2nd harmonic

close all;
clear all;
clc;

R1 = 1;
C1 = 0;

B = csvread('simulation403.CSV', R1, C1);

t = B(763:4763,1);
CT1 = B(763:4763,2);
CT2 = B(763:4763,3);
CT3 = B(763:4763,4);
MU1 = B(763:4763,5);
MU2 = B(763:4763,6);
MU3 = B(763:4763,7);

t = t - 190.75;

for n = 1:80
    cosDFT(n) = cos(2*2*pi*n/80);
    sinDFT(n) = sin(2*2*pi*n/80);
end; clear n;

real_CT = sqrt(2) / 80 * filter(sinDFT, 1, CT1);
imag_CT = sqrt(2) / 80 * filter(cosDFT, 1, CT1);
real_MU = sqrt(2) / 80 * filter(sinDFT, 1, MU1);
imag_MU = sqrt(2) / 80 * filter(cosDFT, 1, MU1);

abs_CT = (real_CT.^2 + imag_CT.^2).^(1/2);
abs_MU = (real_MU.^2 + imag_MU.^2).^(1/2);

figure;
plot(t, abs_MU, 'linewidth', 1.5);
hold on;
plot(t, abs_CT, 'linewidth', 1.5);
xlabel('Time [ms]');
ylabel('Primary Current [A_{RMS}]');
xlim([0 1000]);
set(gca,'FontSize', 18);
legend('I_{rec\_samu\_2nd\_harmonic}', 'I_{rec\_analog\_2nd\_harmonic}');
```